

AD625952

Quarterly report:

FOUNDATIONAL RESEARCH PROJECTS

JULY-SEPTEMBER 1965

CLEARINGHOUSE FOR FEDERAL SCIENTIFIC AND TECHNICAL INFORMATION		
Microcopy	Microfilm	
\$ 3.00	\$ 0.75	96ms as
ARCHIVE COPY		

Code 1

DDC  
 JAN 13 1966  
 DDC-IRA B

Distribution of this document is unlimited.



NAVAL ORDNANCE LABORATORY CORONA

CORONA, CALIFORNIA

X

## CONTENTS

	<u>Page</u>
<b>HIGH TEMPERATURE POLYMER PROGRAM</b>	
Condensation Reactions of Hexaphenyldichlorophosphonitrile Tetramer With Diols and Diamines, by D. L. Herring, C. M. Douglas, and A. J. Bilbo . . . . .	1
A Study of the Thermal Decomposition of Trans-2,6-Diazidohexaphenylcyclophosphonitrile Tetramer and Further Studies on the Solvent Polymerization of the Tetramer With Bisphosphines, by C. M. Sharts . . . . .	19
<b>INFRARED ATOMIC SPECTRA</b>	
The First Spectrum of Mercury in the 3.2- to 4.0-Micron Region, by C. J. Humphreys and E. Paul, Jr. . . . .	27
Note on Cesium I, by C. J. Humphreys and E. Paul, Jr. . . . .	35
<b>PLASMA PHYSICS</b>	
Production of High Power Pulses by Magnetic Field Compression, by R. L. Conger, J. H. Johnson, L. T. Long, and J. A. Parks . . . . .	37
<b>SEMICONDUCTOR PHYSICS</b>	
Accurate Measurement of Small Rotary Dispersion, by C. J. Gabriel and H. Piller . . . . .	55
Ellipticity in Multiply Reflected Faraday Rotation, by C. J. Gabriel and H. Piller . . . . .	62
Optical Constants of Germanium in Spectral Regions From 0.5 to 3.0 eV, by R. F. Potter . . . . .	69
<b>SOLID STATE SPECTROSCOPY</b>	
Crystal Field Effects for $Ce^{3+}$ and $Yb^{3+}$ in the Garnets, by G. F. Herrmann, J. J. Pearson, K. A. Wickersheim, and R. A. Buchanan . . . . .	87

# HIGH TEMPERATURE POLYMER PROGRAM

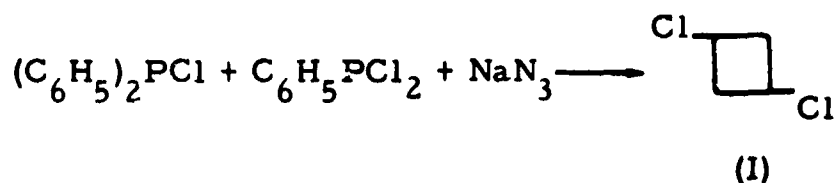
## CONDENSATION REACTIONS OF HEXAPHENYL- DICHLOROPHOSPHONITRILE TETRAMER WITH DIOLS AND DIAMINES

by

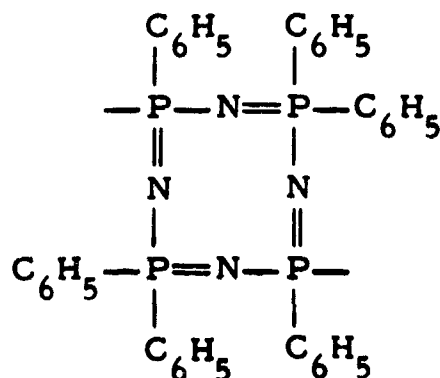
D. L. Herring, C. M. Douglas, and A. J. Bilbo  
Chemistry Division

### INTRODUCTION

The synthesis of hexaphenyldichlorophosphonitrile tetramer, compound (I), by the reaction



where  $\square$  represents

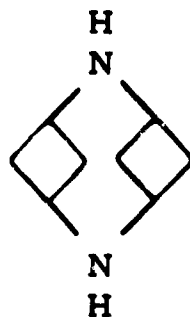


has been described in an earlier report.<sup>1</sup> In addition to the diethoxy- and diphenoxy-derivatives that were also reported, further substitution reactions have been carried out and the dipiperidino-, diamino-, and bis(dimethylamino)-hexaphenylphosphonitrile tetramers—compounds (II), (III), and (IV), respectively—have been prepared.

<sup>1</sup>D. L. Herring and C. M. Douglas, NAVWEPS Report 8226, Quarterly Report: Foundational Research Projects, October-December 1964, p. 5.

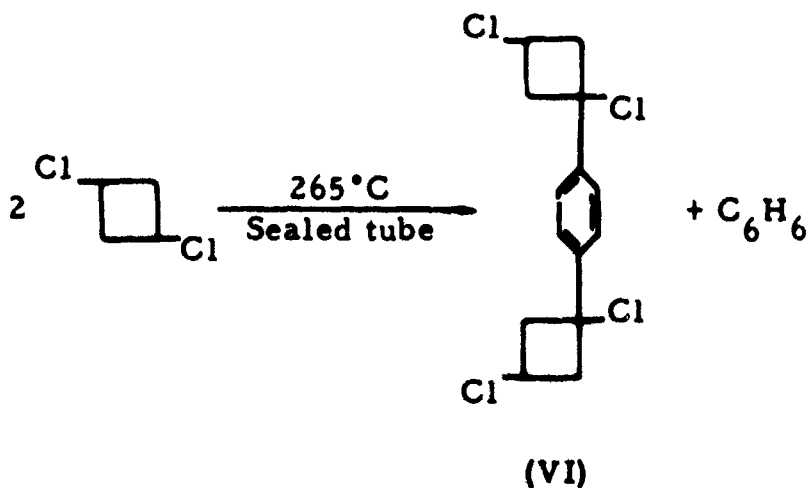
## DISCUSSION

Upon pyrolysis, compound (III) condenses, with the elimination of ammonia, to form a low molecular weight species which is probably dimeric:



Heating compound (I) at 265°C in a sealed tube results in the formation of a glassy material (m.p. 70-80°C). By fractional crystallization, the crude product can be separated into the isomers of hexaphenyl-dichlorophosphonitrile tetramer. Compound (I), m.p. 303-304°C, is recovered in 30% yield, and the remainder, compound (V), melts at 185-187°C.

The thermal rearrangement of compound (I) was accompanied by the formation of a very small quantity of benzene, that is, 1 mmole of benzene per 278 mmoles of compound (I). It can be postulated that the benzene was formed by condensation of 2 molecules of (I), thus:



Some support for the above explanation is given by consideration of the properties of the polymeric products obtained from the condensation of the isomer mix and biphenol. The melting points were above 300°C and benzene insolubility was observed. These are properties of cross-linked material and would be expected if compound (VI) was present in the mixture of isomers.

It is believed that the higher-melting isomer has the trans configuration and that compound (V) has the cis configuration. Compound (V), when treated with  $\text{LiN}_3$  in refluxing acetonitrile, yields a mixture of cis- and trans-diazido tetramers, as does compound (I). A careful study of the dipole moments of low- and high-melting diazido tetramers has proven them to be the cis and trans forms, respectively.<sup>2</sup>

Compound (I) represents a useful starting material for the preparation of polymers in which the phosphonitrile ring system can be linked in a systematic linear fashion by means of other difunctional compounds such as diols.



For the polymerization studies, compound (I) was recrystallized twice from toluene, dried at  $150^\circ\text{C}$  for 24 hours, and stored in evacuated tubes. Biphenol, which was supplied by Eastman Organic, was sublimed twice. It was then finally sublimed, and only the middle 80% was retained.

The ratio of (I) to biphenol was varied from 1:1.2 to 1:0.95 to determine the effect of any inert impurities that might be present in the starting materials. This imbalance in the stoichiometry had no appreciable influence either on the range of molecular weights (10,000 to 12,000) or in the softening points ( $185$ - $220^\circ\text{C}$ ). In all cases, the evolution of hydrogen chloride gas was over 95% of theoretical. However, elemental analysis of most of the polymeric resins showed no chlorine.

A temperature of  $200$ - $220^\circ\text{C}$  was required for the initiation of the melt reaction, which proceeded very slowly at this temperature, but continuation was aided by the removal of the hydrogen chloride generated. Although it was convenient to carry out the polymerizations at reduced pressure, it was noted that at  $220^\circ\text{C}$  biphenol sublimed out of the reaction zone. When the bath temperature was raised, additional diol was lost, making a total loss up to 2%. Carrying out the polymerization under nitrogen or in sealed tubes that were relieved of HCl pressure periodically did not improve the results.

It was anticipated that use of the lower-melting isomer, compound (V), with biphenol would give a mixture which would react at such a low temperature that loss of the diol would not occur. However, even though

<sup>2</sup>C. M. Sharts and D. Gentry, unpublished results.

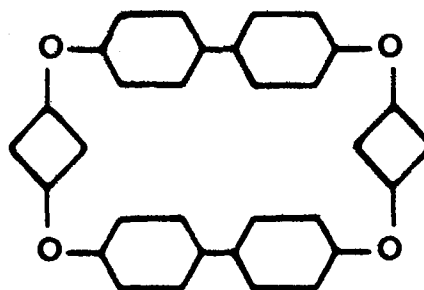
the reaction mixture was held at the melting point of (V), no gas was evolved and prolonged heating caused the sublimation of the diol.

As pointed out earlier, the unseparated mixture of the phosphonitrilic isomers melts at 70-80°C. The polymerization of this mixture with biphenol yielded a resinous material which softened slightly at 320°C but did not melt. It was insoluble in most organic solvents and was swollen by benzene. No molecular weight measurements could be made.

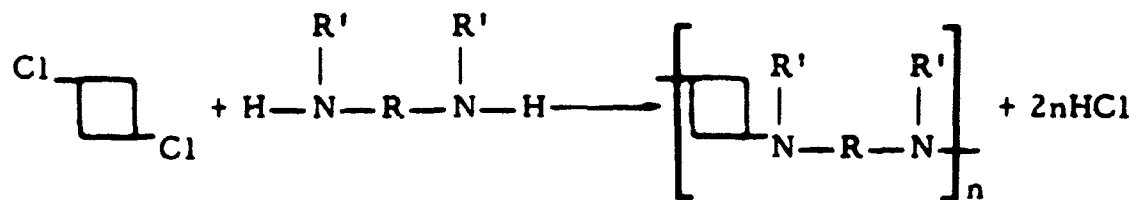
Methods for circumventing the loss of the diol from the reaction zone have also included the use of the disodium salt of biphenol. Results from one preliminary experiment have been encouraging in that a resin which did not melt at 320°C was isolated. Again, however, insolubility of this product prevented the molecular weight determination.

Solution polymerizations were carried out in refluxing anisole, diphenyl ether, petrolatum, and acetonitrile containing quinoline. Hydrogen chloride was slowly generated over a six-week period in the anisole reaction. After removal of the solvent, further heating of the product in vacuum not only yielded additional HCl, but resulted in the sublimation of unreacted diol. The polymer was a low molecular weight species (5200) containing no chlorine as end groups. The reaction in the higher boiling solvent, diphenyl ether, proceeded more rapidly, but did not near completion after a week of refluxing. About 75% of the theoretical amount of HCl was obtained. A mixture of (I) and biphenol suspended in boiling petrolatum yielded only a small fraction of the expected HCl. An equimolar mixture of (I) and biphenol did not react in refluxing acetonitrile with or without the presence of an acid acceptor such as quinoline.

The compound (I)-biphenol polymer can be fractionated, by use of a benzene-heptane mixture, into a material having a molecular weight of 18,000. The melting range of this fraction was not substantially higher than the original polymer with a molecular weight of ~12,000. Separation of the polymer species gave, as the most soluble portion, a crystalline material whose molecular weight and elemental analysis correspond very closely with that calculated for the dimer:



Compound (I) couples with diamines according to the following equation:



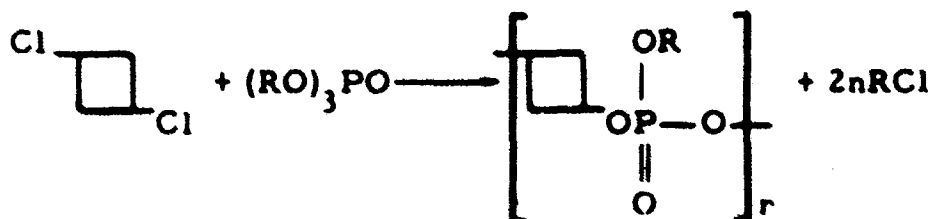
where  $\text{R}' = \text{H}$  or  $\text{C}_6\text{H}_5$

$\text{R} = \text{biphenylene}$

In this condensation, it is possible that some of the hydrogen chloride reacts with the amine to form the hydrochloride. Since no sublimation was noted, any amine hydrochloride produced initially was probably decomposed at the elevated reaction temperature. It is interesting that although the gas evolution indicates that the reaction was only 83% complete, the resinous product contains no chlorine and the elemental analysis is very close to that calculated for the polymer shown in the brackets above (where  $n$  is large).

When  $\text{R}'$  was phenyl, the coupling proceeded less satisfactorily. A temperature  $100^\circ\text{C}$  higher was required to initiate the reaction, and although somewhat more  $\text{HCl}$  was generated, the product was a low-melting, low molecular weight material containing 0.5% residual chlorine.

Compound (I) reacted with trialkyl phosphates in the following manner:



In the case of ethyl phosphate, evolution of ethyl chloride indicated that the reaction was 95% complete. The product was a low-melting resin which was insoluble in benzene.

In view of the relatively high temperatures that must be employed to effect the tetramer dichloride-diol condensations, it appeared that it would be advantageous to prepare the tetramer dibromide, which might be reactive at a lower temperature. Replacement of chloride by azide groups takes place readily when the tetramer dichloride and excess lithium azide are allowed to react in boiling acetonitrile.<sup>3</sup> It therefore

<sup>3</sup> NAVWEPS Report 8226, p. 23.

seemed that lithium bromide, which is very soluble in acetonitrile, might engage in the same type of replacement reaction. Despite prolonged contact between lithium bromide and tetramer dichloride in refluxing acetonitrile, no reaction occurred and the tetramer dichloride was recovered unchanged.

## EXPERIMENTAL

### Preparation of Hexaphenyldipiperidino-phosponitrile Tetramer (II)

Hexaphenyldichlorophosponitrile tetramer (3.0 g) was dissolved in 100 ml of refluxing chlorobenzene, and an excess (10 cc) of piperidine was added. Upon cooling, a precipitate of piperidine hydrochloride was formed and was removed by filtration. The chlorobenzene solution was concentrated to 50 ml, yielding the crude product. The dipiperidino-derivative was recrystallized from benzene to give 2.0 g of white crystalline material melting at 290-292°C. The infrared spectrum is shown in Figure 1.

Anal. Calc. for  $C_{46}H_{50}P_4N_6$ : C, 68.1; H, 6.2; P, 15.3; N, 10.4;  
mol. wt. 810.

Found: C, 68.1; H, 6.4; P, 15.1; N, 10.5;  
mol. wt. 832.

### Preparation of Hexaphenyldiamino-phosponitrile Tetramer (III)

A slurry containing 20.0 g of (I) in 500 ml of chloroform was treated with gaseous ammonia for 6 hours. The reaction mixture was then filtered to remove ammonium chloride. Evaporation of the chloroform yielded the crude product, which recrystallized from heptane as long white needles, m.p. 205-207°C. Its infrared spectrum is shown in Figure 2.

Anal. Calc. for  $C_{36}H_{34}P_4N_6$ : C, 64.1; H, 5.0; P, 18.4; N, 12.5;  
mol. wt. 674.

Found: C, 64.0; H, 4.9; P, 18.1; N, 12.6;  
mol. wt. 668.

### Pyrolysis of Hexaphenyldiaminophosponitrile Tetramer

A sample of 5.0 g (0.007 mole) of compound (III) was heated in vacuum at 25-360°C for 12 hours. During the heating cycle 0.006 mole of ammonia was generated, along with a small amount of benzene. Both volatile

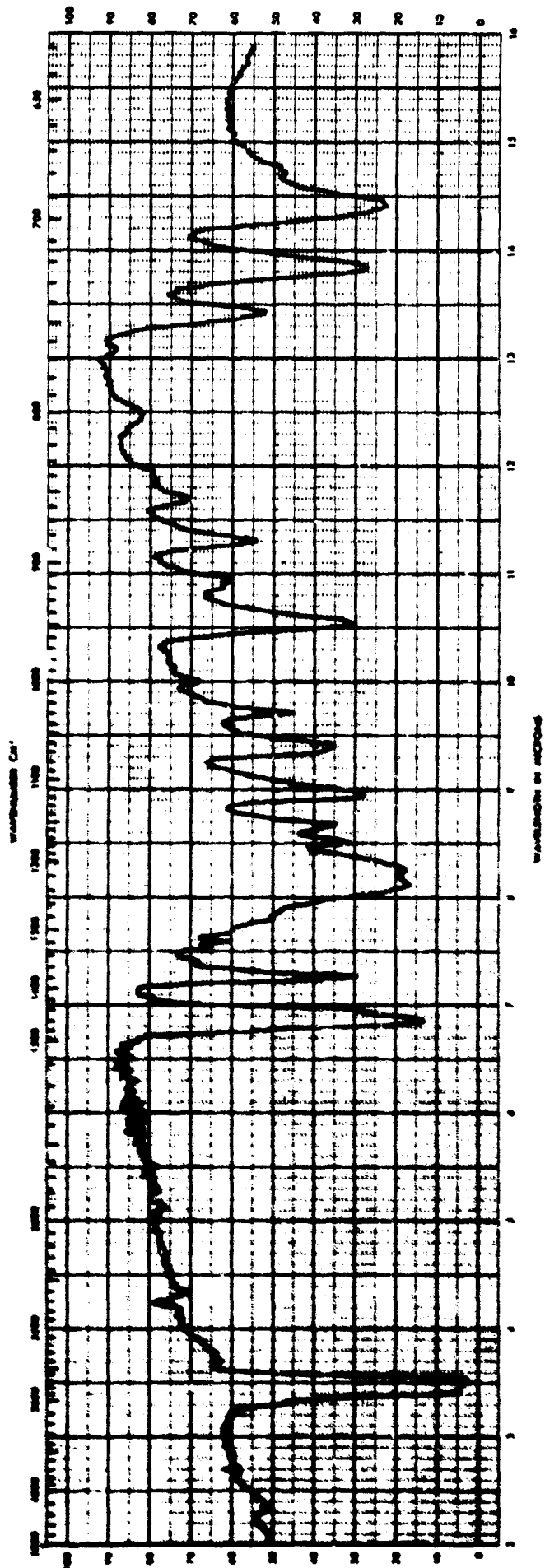


FIGURE 1. Infrared Spectrum of Hexaphenyldipiperidinophosphonitrile Tetramer, Compound (II)

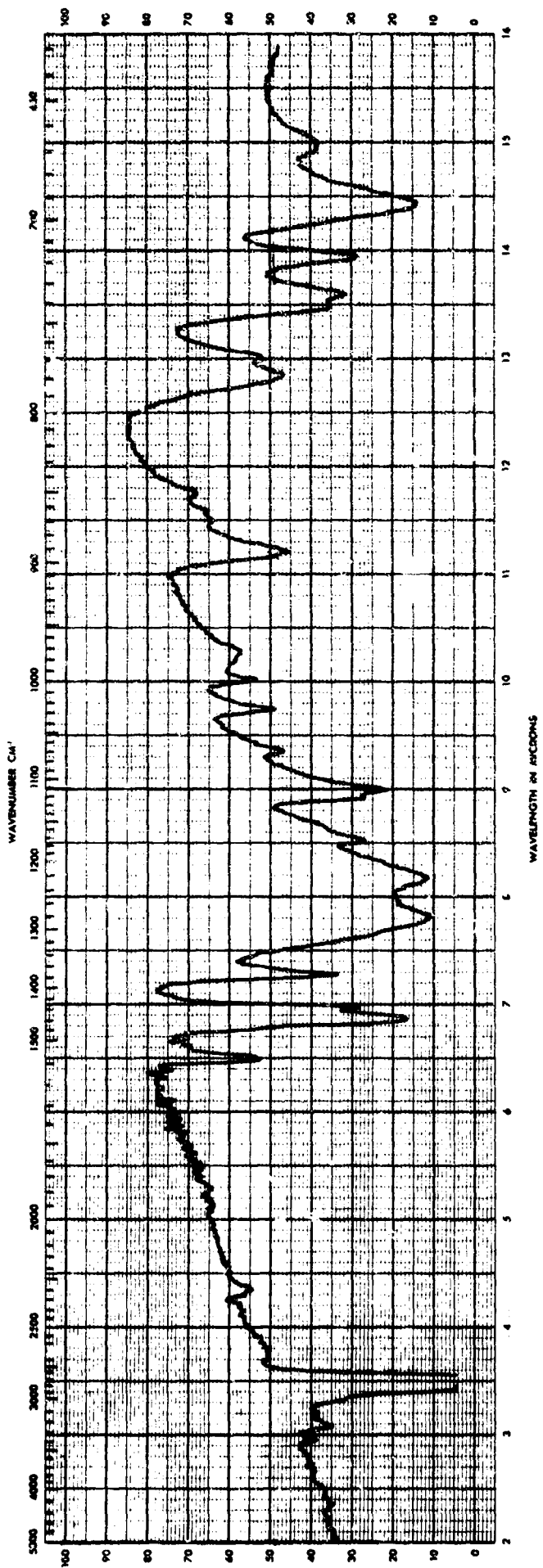


FIGURE 2. Infrared Spectrum of Hexaphenyldiaminophosphonitrile Tetramer, Compound (III)

products were identified by infrared analysis. The residue was a tan resin softening over the range 160-185°C.

Anal. Calc. for  $C_{36}H_{31}P_4N_5$ : C, 65.8; H, 4.7; P, 18.9; N, 10.7;  
mol. wt. per unit 657.

Found: C, 65.6; H, 4.8; P, 18.9; N, 10.8;  
mol. wt. 1320.

#### Preparation of Hexaphenylbis(dimethylamino)- phosponitrile Tetramer (IV)

Gaseous dimethylamine was combined with a slurry of 250 ml of chloroform and 14.0 g of (I). The reaction mixture was stirred vigorously during the addition of  $(CH_3)_2NH$ . After 1 hour, the reaction was complete, as indicated by the disappearance of  $(C_6H_5)_6Cl_2P_4N_4$ . The chloroform solution was completely clear. The solvent was then evaporated and the solids were extracted with benzene to separate the dimethylamine hydrochloride. The benzene solution was concentrated, and when it had cooled the hexaphenylbis(dimethylamino)phosponitrile was recovered as white needles, m.p. 189-190°C. The infrared spectrum is shown in Figure 3.

Anal. Calc. for  $C_{40}H_{42}P_4N_6$ : C, 65.8; H, 5.8; P, 17.0; N, 11.5;  
mol. wt. 730.

Found: C, 66.0; H, 6.0; P, 16.7; N, 11.6;  
mol. wt. 723.

#### Thermal Arrangement of Hexaphenyldichloro- phosponitrile Tetramer (I)

A 30-g sample of (I), which had been recrystallized twice from toluene, was sealed in an evacuated glass ampoule and heated in an oven at 265°C for 48 hours. After cooling, the ampoule was opened into a vacuum line and the volatile material was condensed into a measuring system. Benzene, 3.4 cc STP (0.151 mmole), was collected and identified by its infrared spectrum. The non-volatile material, m.p. 70-80°C, was then extracted with benzene, and the insoluble portion (about 25%) was identified by its infrared spectrum and melting point (298-300°C) as the starting material. The benzene was evaporated and the residue was twice recrystallized from heptane. It yielded an isomer, (V), m.p. 185-187°C, with the infrared spectrum shown in Figure 4.

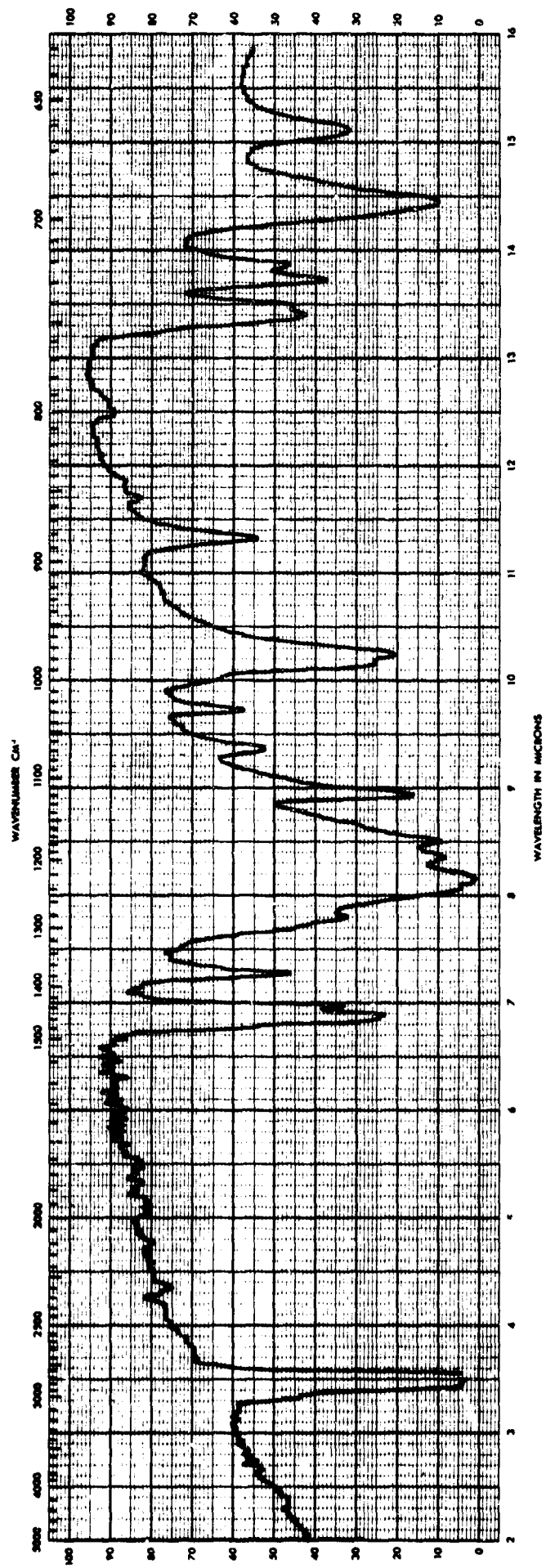


FIGURE 3. Infrared Spectrum of Hexaphenylbis(dimethylamino)phosphonitrile Tetramer, Compound (IV)

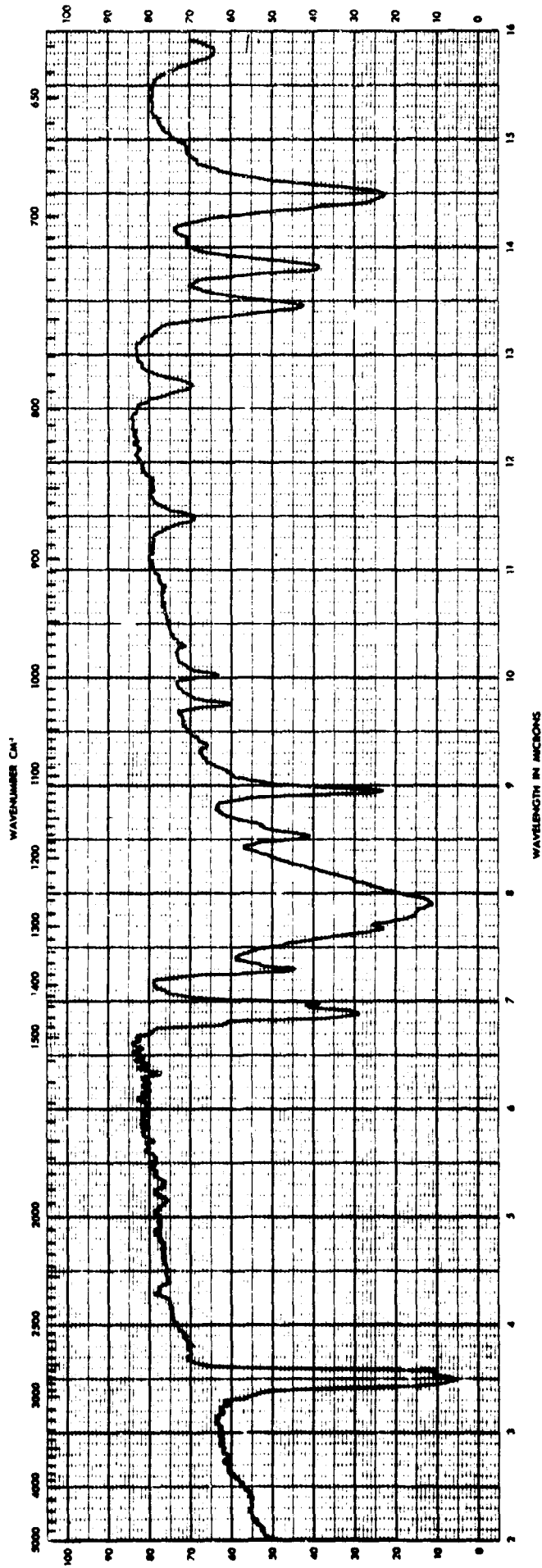


FIGURE 4. Infrared Spectrum of Isomer of Hexaphenyldichlorophosphonitrile Tetramer, Compound (V)

### Reaction of Compound (V) with Lithium Azide\*

Two separate experiments were carried out. In the first experiment, 2.0 g of (V) was permitted to react with 3.0 g of lithium azide in 50 ml of refluxing acetonitrile. After 24 hours, solids were filtered off and solvents removed until only 20 ml of solution remained. A first crop of 0.18 g of crystals was obtained, m.p. 178-212°C, which was identified by infrared spectroscopy as trans-2,6-diazidocyclophosphonitrile. A second crop of the same diazide, amounting to 0.10 g, was obtained, making a total of 0.28 g (about 15% of theory) of diazide. No additional solid could be obtained from the mother liquor of the crystallizations. The viscous glass had an infrared spectrum which suggested the glass was a mixture of cis- and trans-2,6-diazidocyclophosphonitrile. In addition, the bands of a hydroxyl group were observed.

When the experiment was repeated, the same results were obtained. An analysis of the reaction product that could not be crystallized showed it to be free of chlorine.

Anal. Calc. for  $C_{36}H_{30}P_4N_{10}$ : C, 59.51; H, 4.16; N, 19.28; P, 17.05.  
Found: C, 60.36; H, 4.49; N, 19.35; P, 15.89.

### Polymerization of Hexaphenyldichlorophosphonitrile Tetramer and Biphenol

#### MELT REACTIONS

A mixture of 7.1363 g (0.01 mole) of compound (I) and 2.0507 g (0.011 mole) of biphenol was heated in an evacuated ampoule. Evolution of hydrogen chloride began at 220-225°C, although the mixture was not fused at this temperature. Over the course of 10 hours, the bath temperature was gradually increased to 400°C. The small amount of material which had sublimed into the neck of the ampoule during the heating cycle was recovered, weighed (0.1145 g), and identified as biphenol by its infrared spectrum. The total amount of HCl generated was 96.7% of the calculated amount. The polymeric product was a transparent glass melting over the range 185-220°C and having a molecular weight of 11,360.

A summary of information on the melt polymerizations involving tetramer dichloride and biphenol is shown in Table I.

---

\* This reaction was conducted by C. M. Sharts.

TABLE 1. Polymerization of Tetramer Dichloride and Biphenol

Molar Ratio of Tet. Dichloride and Biphenol	Species of Tetramer Dichloride Used	Percent of HCl Obtained	Mol. Wt. of Polymer	Melting Range, °C
1.0 : 0.95	Compound (I)	71	6,420	165-175
1.0 : 1.0	Compound (I)	92.7	10,000	170-200
1.0 : 1.1	Compound (I)	96.7	11,360	185-220
1.0 : 1.2	Compound (I)	98.4	12,000	165-185
1.0 : 1.0	Low-melting isomer, (V), 185-187°C	97.0	14,500	180-240
1.0 : 1.0	Mixture of isomers	98.5	Insoluble	> 300
1.0 : 0.95	Mixture of isomers	96.2	Insoluble	> 300

Reaction of Compound (I) with Biphenol in a Sealed Tube. An intimate mixture of 0.579 g (0.813 mmole) of compound (I) and 0.2088 g (1.12 mmole) of biphenol was loaded into a 50-cc reaction tube. After being evacuated, the tube was sealed off and heated in an oven at 265°C for 8 hours. The tube neck was broken by a tube breaker attached to the vacuum line and HCl gas was condensed into a measuring system. The amount of HCl calculated for 0.813 mmole of (I) was 36.4 cc STP; found, 15.7 cc STP, or 43%. The tube neck was cleaned and sealed off under vacuum a second time and heated at 265°C for 48 hours. Only 1.5 cc STP of HCl was found. The experiment was abandoned after several more cycles of heating and venting of gas yielded negligible amounts of hydrogen chloride.

Preparation of the Disodium Salt of Biphenol, NaO——ONa. Twenty-five grams (0.13 mole) of biphenol was dissolved in 200 ml of 3.9 molar sodium hydroxide. The addition of 800 ml of acetone to the solution resulted in the precipitation of the disodium biphenolate. The product was recrystallized twice from 400-ml portions of ethanol, then dried in vacuum at 180°C.

Anal. Calc. for  $C_{12}H_8O_2Na_2$ : C, 62.6; H, 3.5; O, 13.9; Na, 20.0.

Found: C, 62.2; H, 3.7; O, 13.6; Na, 20.2.

Reaction of Compound (I) and Disodium Biphenolate. In the drybox, a mixture of 5.0217 g (0.007 mole) of compound (I) and 1.6219 g (0.007

mole) of sodium biphenolate was loaded into a 150-ml, round-bottomed flask containing stainless steel balls. The flask was then attached to a Rinco Evaporator, slowly rotated under vacuum, and heated to 310°C over a period of 24 hours. After the dark brown reaction mixture was extracted with boiling benzene, the benzene-soluble portion was dried in vacuum; its melting range was 150-165°C.

Anal. Calc. for  $C_{48}H_{38}P_4N_4O_2$ : C, 69.7; H, 4.6; P, 15.0; N, 6.8;  
O, 3.9.

Found: C, 69.2; H, 4.7; P, 15.0; N, 6.4;  
O, 3.5; Na, 0.77; Cl, 1.2.

The benzene-insoluble fraction was extracted with boiling water, then washed with ethanol and ether, and dried. This material softened slightly at 300°C but did not melt.

### SOLUTION POLYMERIZATION

Reaction of Compound (I) and Biphenol in Anisole. Compound (I) (14.26 g, 0.02 mole) and 3.72 g (0.02 mole) of biphenol were dissolved in 500 ml of anisole, b.p. 152-154°C. The solution was refluxed under nitrogen. After an induction period of about 3 hours, the evolution of hydrogen chloride began. Heating was continued for 6 weeks until no additional HCl was detected. The anisole was then evaporated and the solid product was heated in vacuum at 300°C for about 8 hours. During this heating cycle, a small amount of hydrogen chloride was generated and a few milligrams of unreacted diol was sublimed; both of these compounds were identified by infrared spectra. The polymeric product was a brittle brown glass softening over the range 140-180°C.

Anal. Calc. for  $C_{48}H_{38}P_4N_4O_2$ : C, 69.7; H, 4.6; P, 15.0; N, 6.8;  
O, 3.9; mol. wt. per unit, 826.

Found: C, 70.0; H, 4.9; P, 14.8; N, 6.6;  
O, 4.2; Cl, 0; mol. wt. 5200.

Reaction of Compound (I) and Biphenol in Diphenyl Ether. A mixture of 7.13 g (0.01 mole) of compound (I) and 1.90 g (0.0102 mole) of biphenol, together with 50 ml of diphenyl ether and a magnetic stirrer bar, was placed in a cylindrical tube (40 × 250 mm) which had been carefully dried and filled with dry N<sub>2</sub> gas. The tube was equipped with a removable head which carried a water condenser, stopcock, and joint for attachment to the vacuum line. The apparatus was connected to a vacuum line which had incorporated into it a manostat and a manometer that was open to the atmosphere. The system and reaction apparatus were filled with dry N<sub>2</sub> at atmospheric pressure and the manostat was set to maintain this pressure.

An oil bath heated with a hot plate-magnetic stirrer combination was used to bring the stirred reaction mixture to the reflux temperature of diphenyl ether, 258-259°C. As pressure in excess of 1 atmosphere developed because of increasing diphenyl ether vapor pressure and evolution of HCl gas, the manostat released gas, which passed through several liquid-nitrogen-cooled traps and thence through the pumps. After the material had refluxed for 8 hours, the apparatus was cooled and evacuated. Volatile components were caught in the above-mentioned traps. After fractionation of the volatiles, 252.8 cc STP (56.4%) of HCl gas was collected. The amount of HCl calculated for 0.01 mole of (I) was 444 cc STP. The above treatment was repeated and continued for 6 days but the total HCl evolved amounted to only 347 cc STP, or 77.6% of theory.

The reaction mixture was not worked up because of the low yield of HCl, which indicates a poor condensation reaction.

Attempted Reaction of (I) and Biphenol in Petrolatum. An equimolar mixture of compound (I) and biphenol suspended in distilled petrolatum was heated and stirred at 275°C in the apparatus described above. Only a small fraction of the theoretical yield of HCl gas was obtained.

Attempted Reaction of Compound (I) and Biphenol in Acetonitrile with Quinoline as Acid Acceptor. In the drybox, 2 g of an equimolar mixture of compound (I) and biphenol was added to a flask containing 250 cc of dry acetonitrile and 1.3 g (0.01 mole) of freshly distilled quinoline. After the mixture was refluxed for 48 hours and filtered, 1.53 g (95.6%) of compound (I) was recovered unchanged. Identification was made by infrared spectrum.

#### Fractionation of Compound (I)-Biphenol Polymer

The polymer sample used for this preliminary fractionation was prepared by the melt reaction described earlier (page 12). The molecular weight, determined osmometrically, was 11,360. Benzene was used as the solvent and n-heptane as the non-solvent. A summary of the data obtained from the fractionation of a 3.9474-g sample is shown in Table 2.

The fourth fraction was a crystalline material with an elemental analysis corresponding closely to that calculated for  $C_{48}H_{38}P_4N_4O_2$ . The infrared spectrum (Figure 5) was characterized by absorption bands much sharper than those encountered in the tetramer dichloride-biphenol polymers.

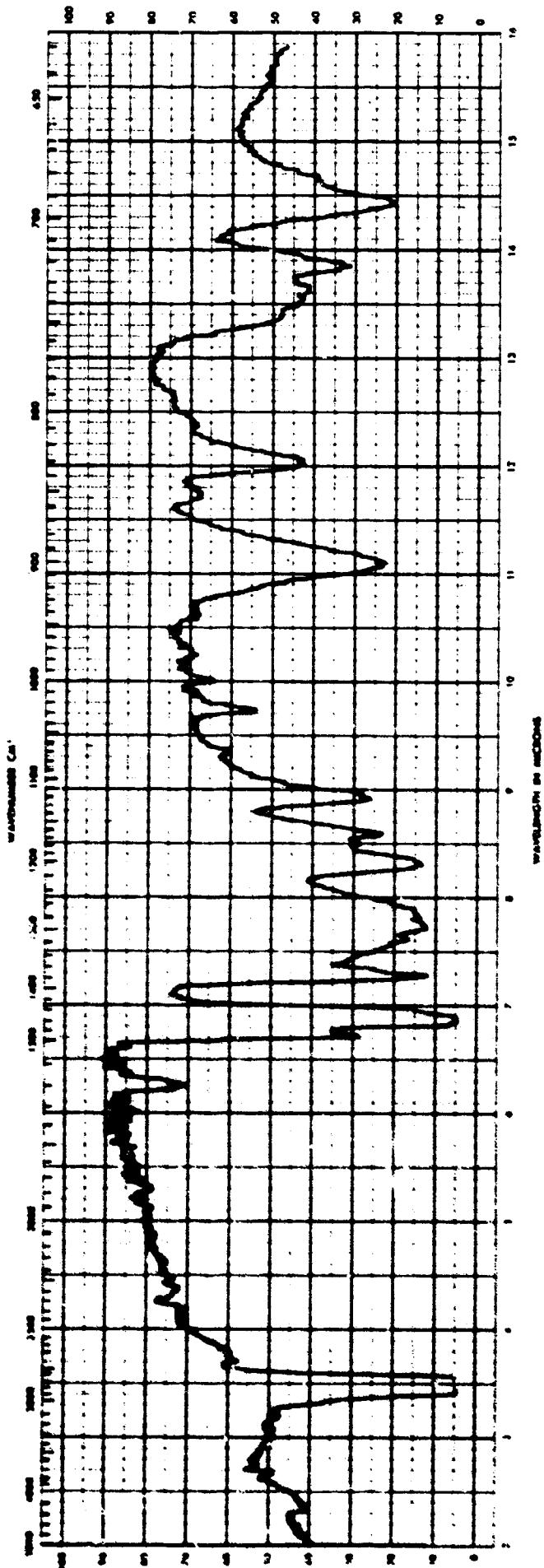


FIGURE 5. Infrared Spectrum of Sample Fraction of Compound (I)-Biphenol Polymer

TABLE 2. Results of Fractionation of  
Compound (I)-Biphenol Polymer

Weight of Fraction, g	Percent of Total	Melting Range, °C	Molecular Weight
2.2089	56	160-185	18,100
1.0195	26	160-170	9,100
0.2840	7	145-160	5,800
~0.1	~3	308-310	1,600

Polymerization of Hexaphenyldichlorophospho-  
nitrile Tetramer with Diamines

Benzidine. A mixture of 2.86 g (0.004 mole) of compound (I) and 0.73 g (0.004 mole) of benzidine was heated in vacuum to 300°C for 11 hours. During the heating cycle, 83% of the calculated amount of hydrogen chloride was liberated. The product was a brown glass which gradually softened over the range 205-250°C and swelled in benzene but did not dissolve.

Anal. Calc. for  $C_{48}H_{40}P_4N_6$ : C, 69.9; H, 4.8; P, 15.1; N, 10.2.

Found: C, 69.5; H, 5.2; P, 15.2; N, 10.4; Cl, 0.

N,N'-Diphenylbenzidine. A mixture of 3.36 g (0.01 mole) of N,N'-diphenylbenzidine and 7.13 g (0.01 mole) of compound (I) was heated in an evacuated ampoule. No gas evolution occurred until about 275°C, and the reaction became vigorous only at 300°C. The reaction temperature was held at 360°C for 6 hours. About 90% of the calculated amount of hydrogen chloride was evolved.

Anal. Calc. for  $C_{60}H_{48}P_4N_6$ : C, 73.8; H, 4.9; P, 12.7; N, 8.6;  
mol. wt. per unit 976.

Found: C, 71.4; H, 4.8; P, 14.2; N, 8.9;  
Cl, 0.5; mol. wt. 2090.

Reaction of Compound (I) with Trialkylphosphates

A mixture of 2.14 g (0.003 mole) of compound (I) and 0.60 g (0.003 mole) of triethylphosphate was heated in vacuum. Gas evolution began around 150°C and the mixture changed to a transparent liquid. Heating was continued for 10 hours; the temperature was gradually raised to

300°C. The volatile product (95% of theory) was identified by infrared analysis as ethyl chloride. The residue, a light yellow resin, melted at 125-145°C.

Anal. Calc. for  $C_{38}H_{35}P_5N_4O_4$ : C, 59.5; H, 4.6; P, 20.2; N, 7.3;  
O, 8.4.

Found: C, 59.3; H, 4.6; P, 19.6; N, 7.5;  
O, 8.8; Cl, 0.

Similar results were obtained with both tributylphosphate and tripropylphosphate.

Attempted Reaction of Compound (I)  
with LiBr in Acetonitrile

In the drybox, a 1-necked, round-bottomed flask, equipped with a magnetic stirrer and condenser, was loaded with 10 g (0.015 mole) of compound (I), 20 g (0.17 mole) of LiBr (dried in vacuum at 200°C for 18 hours), and 500 ml of acetonitrile, which had been distilled from  $P_2O_5$ .

After 63 hours at the reflux temperature of  $CH_3CN$ , the reaction mixture was filtered free of solids. Compound (I), 9.8 g, was recovered unchanged as revealed by infrared spectrum.

A STUDY OF THE THERMAL DECOMPOSITION OF TRANS-  
2,6-DIAZIDOHENXAPHENYLCYCLOPHOSPHONITRILE  
TETRAMER AND FURTHER STUDIES ON THE  
SOLVENT POLYMERIZATION OF THE  
TETRAMER WITH BISPHTOSPHINES

by

C. M. Sharts  
Chemistry Division

## INTRODUCTION

The polymerization of trans-2,6-diazidocyclophosphonitrile tetramer with the bisphosphines 1,4-bis(diphenylphosphino)butane and 4,4'-bis(diphenylphosphino)biphenyl to give polymers of medium chain length was reported earlier.<sup>4</sup>

Also reported was the thermal decomposition of trans-2,6-diazidocyclophosphonitrile tetramer. This thermal decomposition of the diazide tetramer causes considerable concern for the possibility of eventually obtaining high molecular weight polymers from the trans-diazide with bisphosphines. A decomposition of only a very small percentage of the starting diazide can cause premature ending of polymer chains linked through —P=N— linkages.

## DISCUSSION

An investigation has been made of the melt-decomposition of trans-2,6-diazidocyclophosphonitrile tetramer.<sup>5</sup> The decomposition was studied with a thermal balance and the reaction was followed by means of the weight loss caused by nitrogen evolution. The decomposition, shown in Table 3, is first order over the range 220-260°C. The activation energy for the decomposition was 37 Kcal/mole.

Since the polymerizations are normally carried out in solution, a study was made of the decomposition of 2,6-diazidocyclophosphonitrile tetramer at 213°C in dibutylphthalate solvent, in a calibrated vacuum system. The amount of data collected for several runs was voluminous. Although final calculations to the three significant figures justified by the data have not been completed, preliminary calculations to one and two significant figures have been made and the following conclusions reached:

---

<sup>4</sup> NAVWEPS Report 8226, Quarterly Report: Foundational Research Projects, October-December 1964, p. 16.

<sup>5</sup> C. M. Sharts, D. R. Gentry, and A. Bilbo, unpublished results.

TABLE 3. First Order Decomposition of trans-2,6-Diazidocyclophosphonitrile Tetramer

Sample size, g	Temperature, °C	K, min <sup>-1</sup>
0.314	220	$1.6 \times 10^{-2}$
0.410	240	$7.7 \times 10^{-2}$
0.312	240	$6.9 \times 10^{-2}$
0.144	260	$28 \times 10^{-2}$

The decomposition is first order in dibutylphthalate solution with a half-life at 213°C of  $31 \pm 2$  min, which corresponds to a rate constant  $K_1^{213} = 2.2 \times 10^{-2} \text{ min}^{-1}$ . This first-order constant at 213°C is slightly greater than the rate constant for the melt decomposition at 220°C ( $K_1^{220} = 1.6 \times 10^{-2} \text{ min}^{-1}$ ). The slight discrepancy can be attributed to the difference in medium. The close agreement between  $K_1^{213}$  for solution decomposition and  $K_1^{220}$  for melt decomposition is encouraging enough to permit the discussion which follows.

It seems reasonable to assign an activation energy to the solution decomposition of diazide identical with the activation energy for melt decomposition. An extrapolation of a  $\ln K$  ( $K$  = rate constant) vs  $1/T$  from  $K_1^{213}$  for diazide decomposition with an assumed activation energy of 37 Kcal/mole will permit an estimation of the rate of decomposition of diazide at lower temperatures. The results of such a plot are shown in Table 4.

The last column of Table 4 is the significant one for consideration of the temperature of polymerization of trans-2,6-diazidocyclophosphonitrile tetramer. It represents the time required to decompose 0.1% of the diazide present. For the chlorobenzene solution polymerization reported earlier,<sup>6</sup> a typical time for 96% polymerization was on the order of 250 minutes. At the 132°C temperature, the time for 0.1% decomposition is around 40 minutes. In other words, the polymerization in chlorobenzene will of necessity compete with an amount of decomposition which, although insignificant for normal organic reactions, is very important for polymerizations.

Before going further, it is important to recall the long extrapolation that has been made to get the times for 0.1% decomposition. Table 4

<sup>6</sup> NAVWEPS Report 8226, op cit.

TABLE 4. Extrapolated Rate Constants and Half-Lives at Lower Temperatures for Decomposition of 2,6-Diazidocyclophosphonitrile Tetramer in Dibutylphthalate

Temperature, °C	K extrapolated, min <sup>-1</sup>	Relative rate	t <sub>1/2</sub> min	t <sub>1/1000</sub> min
213	2.2 × 10 <sup>-2</sup>	2.2 × 10 <sup>4</sup>	31	0.045
202	1.0 × 10 <sup>-2</sup>	1.0 × 10 <sup>4</sup>	69	0.10
186	2.2 × 10 <sup>-3</sup>	2.2 × 10 <sup>3</sup>	310	0.45
175	1.0 × 10 <sup>-3</sup>	1.0 × 10 <sup>3</sup>	690	1.0
152	2.2 × 10 <sup>-4</sup>	2.2 × 10 <sup>2</sup>	3,100	4.5
137	1.0 × 10 <sup>-4</sup>	1.0 × 10 <sup>2</sup>	6,900	10
130	2.2 × 10 <sup>-5</sup>	2.2 × 10	31,000	45
118	1.0 × 10 <sup>-5</sup>	1.0 × 10		100
111	2.2 × 10 <sup>-6</sup>	2.2	310,000	450
99	1.0 × 10 <sup>-6</sup>	1.0		1000

can be wrong by an order of magnitude. Regardless of the absolute accuracy of the table, the results clearly show that lowering the temperature will be extremely advantageous in preventing thermal decomposition of the diazidophosphonitrile tetramer. For polymerizations whose rate of reaction is such that 3-4 hours are required, it would be highly desirable for temperatures to remain below 115°C.

A number of polymerizations were carried out in solvents and the results of the runs are shown in Table 5. Of these, only Run V will be given detailed treatment in the Experimental part of this report.

Runs III and IV are noteworthy in that polymers of molecular weights 9100 and 8900 were obtained for the diazide tetramer and bisphosphine in the solvents dibutylphthalate and xylene, respectively. Also significant in Run III was the low temperature used, 110-115°C. The polymer was white when isolated.

TABLE 5. Polymerization of Diazaide Tetramer and Bisphosphines in Solvents

P. n. No.	Diazaide, g (mmole)	Bisphosphine, <sup>a</sup> g (mmole)	Solvent	Temperature, °C	Reaction time	Analytical data
I <sup>b</sup>	0.4429 (0.6145)	0.2639 (0.6145)	Dibutyl-phthalate, 10 ml	132	98%, 3 hr 100%, 24 hr Cured at 183°	Theor. C, 70.06; H, 5.33; N, 7.66 Found: C, 70.26; H, 5.69; N, 7.36 Mol. wt. 7000 (All solvent may not have been removed)
II <sup>c</sup>	0.4424 (0.6086)	0.2611 (0.6122)	Dibutyl-phthalate, 25 ml	100-120	Overnight	Mol. wt. 3350 Solvent believed present in sample
III <sup>d</sup>	0.6100 (0.8395)	0.3583 (0.8395)	Dibutyl-phthalate, 52 ml	110-115 160-170 185	Overnight 4 hr Removal of solvent	1.615 mmole N <sub>2</sub> (Theor. 1.679) 96.2% N <sub>2</sub> obtained Mol. wt. 9100
IV <sup>e</sup>	0.5921 (0.8149)	0.3479 (0.8149)	Xylene, 25 ml	137	Overnight	Quantitative yield (0.90 g) of polymer. Mol. wt. 8900
V	1.0885 (1.498)	0.7827 (1.498)	Dibutyl-phthalate, 50 ml	95-110	Overnight	Pending

<sup>a</sup> 1,4-bis(diphenylphosphino)butane was used in all except Run V, in which 4,4'-bis(diphenylphosphino)biphenyl was used.

<sup>b</sup> Decomposition of end groups probably resulted at 183°C. Initially, the polymer was white; after 183°C treatment, it was yellow.

<sup>c</sup> After 4 hours the polymer precipitated out of solution as a beautiful white solid. The preliminary results led to the next run.

<sup>d</sup> The polymer was white until heated to 185°C. About 0.9 g was obtained—a near-quantitative yield.

<sup>e</sup> Xylene worked well. Toluene should be used, or possibly heptane.

The most promising polymeric material of Run V (sample 1076-42B-End) was subjected to thermal gravimetric analyses\* in both helium and air (Figures 6 and 7) and found to be stable to 400°C. Decomposition was slow between 400° and 450°C but quite rapid between 450° and 600°C where nearly 50% of the weight loss occurred. A DTA thermogram (Figure 8) on the sample was in very close agreement with the TGA results.

Thus it can be concluded that polymers from 2,6-diazidocyclophosphonitrile tetramer and bisphosphines remain highly promising as temperature-stable material. Future polymerization studies will be directed to polymerizations occurring at 90-100°C. Heptane, toluene, isopropyl alcohol, and a suitable ester will be investigated as solvents for polymerization.

## EXPERIMENTAL

### Low Temperature Polymerization of trans-2,6-Diazidocyclophosphonitrile Tetramer and 4,4'-bis(diphenylphosphino)biphenyl in Dibutylphthalate Solvent, Run V

Diazide tetramer (1.0885 g, 1.498 mmole), bisphosphine (0.7827 g, 1.498 mmole), and 60 ml of dibutylphthalate were placed in a flask which was then evacuated to degas solvent and reactants. After extended (1 hour) degassing, the contents of the flask was heated slowly. Nitrogen evolution was observed at 95°C. The temperature was maintained overnight between 95° and 110°C and during the night, white polymer precipitated. The solvent was slightly discolored to a pale yellow. About 0.11 g of diazide was added to the flask. Dibutylphthalate was then distilled off under reduced pressure. Care was taken not to exceed 160°C pot temperature at any time. The polymer residue should have been all azide-terminated at this time. The reaction flask was maintained at 160°C for several hours to assure complete reaction of all phosphine end groups. Most of the polymeric solid dissolved when it was treated with 50 ml of hot benzene. The benzene-insoluble polymer, amounting to about 0.2 g, was labelled "Sample A" and set aside to dry. Upon the addition of 100 ml of heptane to the benzene solution, polymer precipitated which was labelled "Sample B." The material in the benzene-heptane solution was recovered as an oil and labelled "Sample C." Samples A, B, and C were each dissolved in *o*-dichlorobenzene and 0.1 g of triphenylphosphine was added to each. The endcapping reaction was carried out overnight and the heptane was added to the hot *o*-dichlorobenzene solutions. Endcapped polymers were obtained which had the final designations 1076-42A End, 1076-42B End, and 1076-42C End. Analyses and molecular weight determinations of these samples are pending.

---

\*The thermal gravimetric analyses (TGA) were made on a Stanton Model H.T. thermal balance. The differential thermal analyses (DTA) were obtained on a Du Pont 900 DTA.

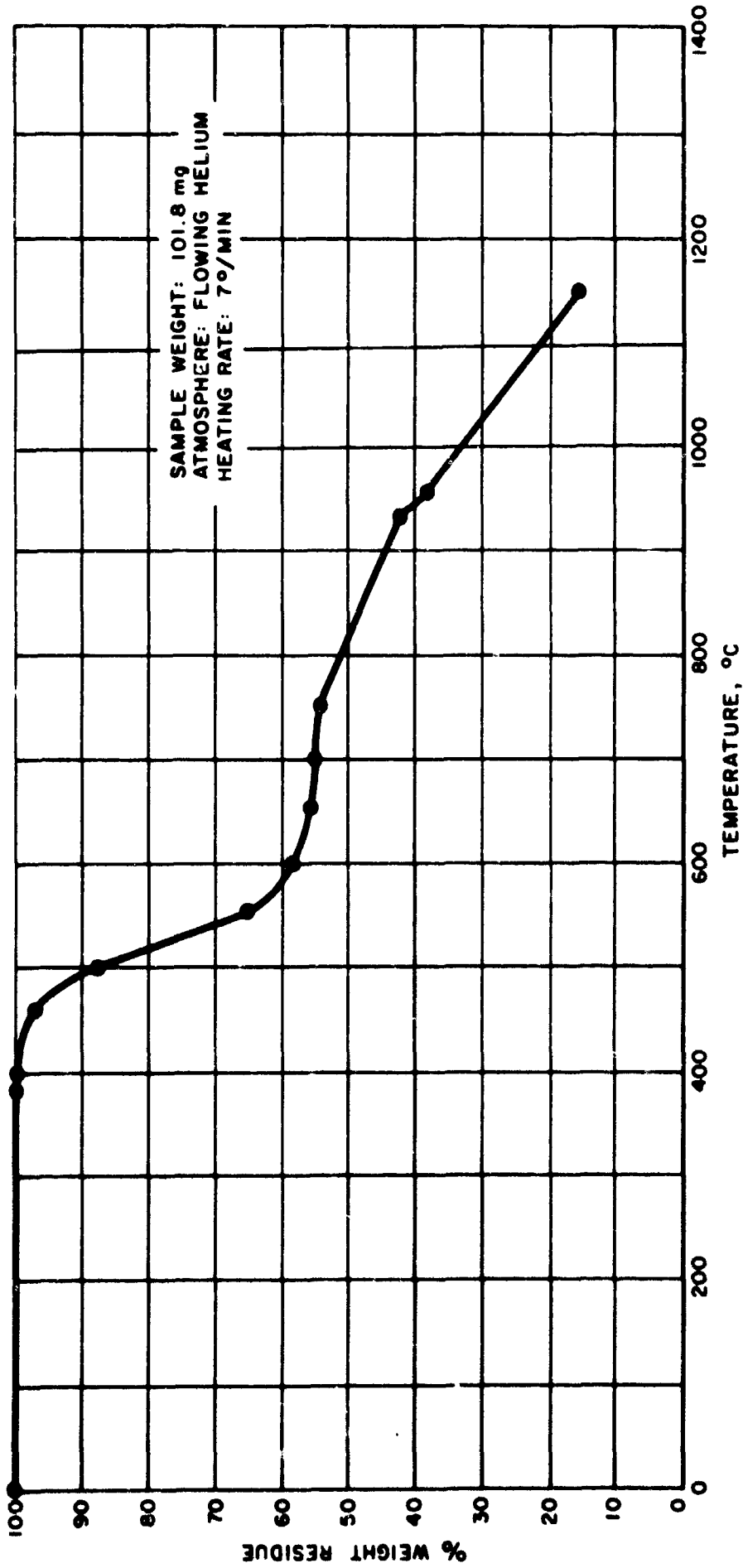


FIGURE 6. Thermal Gravimetric Analysis of Sample 1076-42B-End in Helium

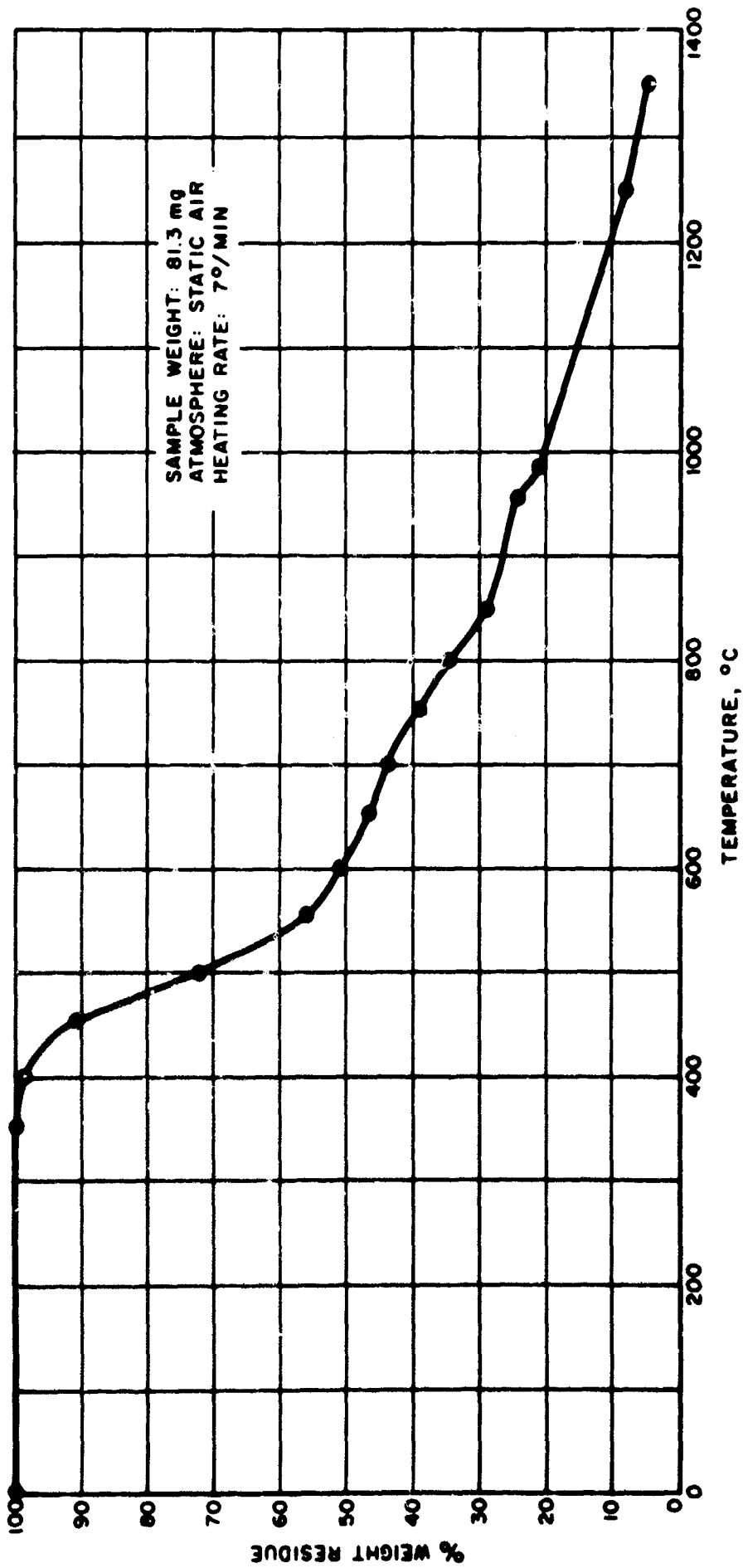


FIGURE 7. Thermal Gravimetric Analysis of Sample 1076-42B-End in Air

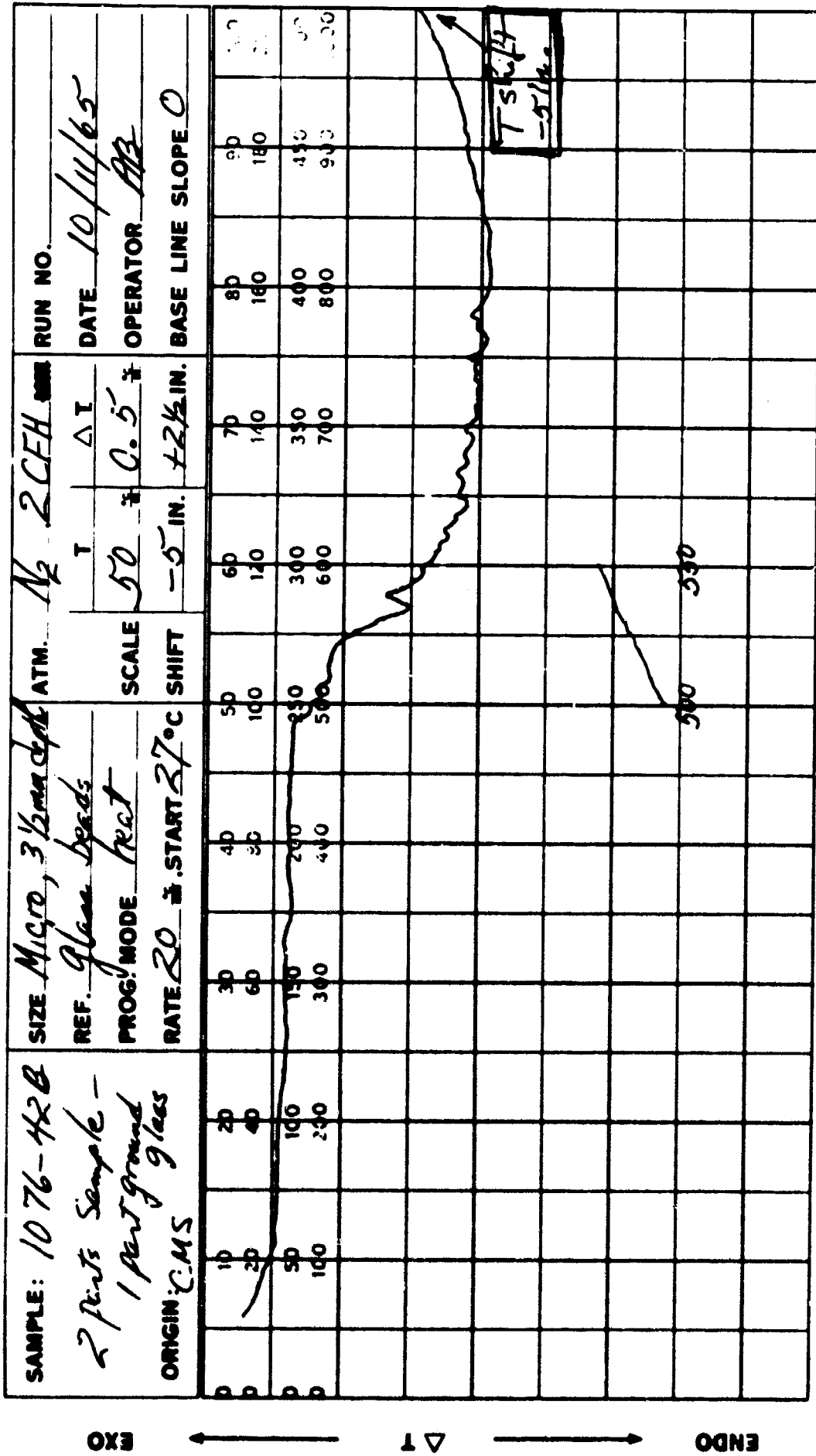


FIGURE 8. Differential Thermal Analysis of Sample 1076-42B-End in Nitrogen

# INFRARED ATOMIC SPECTRA

## THE FIRST SPECTRUM OF MERCURY IN THE 3.2- TO 4.0-MICRON REGION

by

C. J. Humphreys and E. Paul, Jr.  
Research Department

### INTRODUCTION

The spectrum of neutral mercury, Hg I, is one of the best-described and analyzed among atomic emission spectra. It was also one of the first to be studied, being included in the investigations of Kayser and Runge and of Rydberg before the turn of the century. The results of these early investigations are included and referenced in the monograph by Paschen and Götze,<sup>1</sup> as are also Paschen's own observations in the extra-photographic infrared region.

One of the authors of this section published a paper in 1953,<sup>2</sup> reporting and discussing observations of Hg I made somewhat earlier at the National Bureau of Standards and covering the region between 1.3 and 2.0 microns accessible to observation with an ambient-temperature lead sulfide detector. References to the then available literature on the analysis of Hg I were included. Most of the lines reported in that paper had already been observed during the Paschen era. The principal new experimental contribution was the resolution of the satellite lines of the  $6d^3D-5f^3F^o$  multiplet.

The mercury level system is similar to that of the other homologous elements, zinc and cadmium, but, as might be expected in the instance of an element of so great an atomic mass, there is considerable departure from LS coupling. Figure 1 is a Grotrian diagram showing the portions of the energy level scheme that are required for discussion of the material obtained in the experiments herein reported. Further discussion will be given of the observed transitions illustrated in the figure. The normal configuration  $d^{10}s^2$  accounts for the lowest term  $^1S_0$ . Excitation of an electron from  $s^2$  to a succession of s, p, d,

---

<sup>1</sup>F. Paschen and R. Götze, Seriengesetze der Linienspektren, Berlin: Springer, 1922.

<sup>2</sup>C. J. Humphreys, J. Opt. Soc. Am., Vol. 43, p. 1027 (1953).

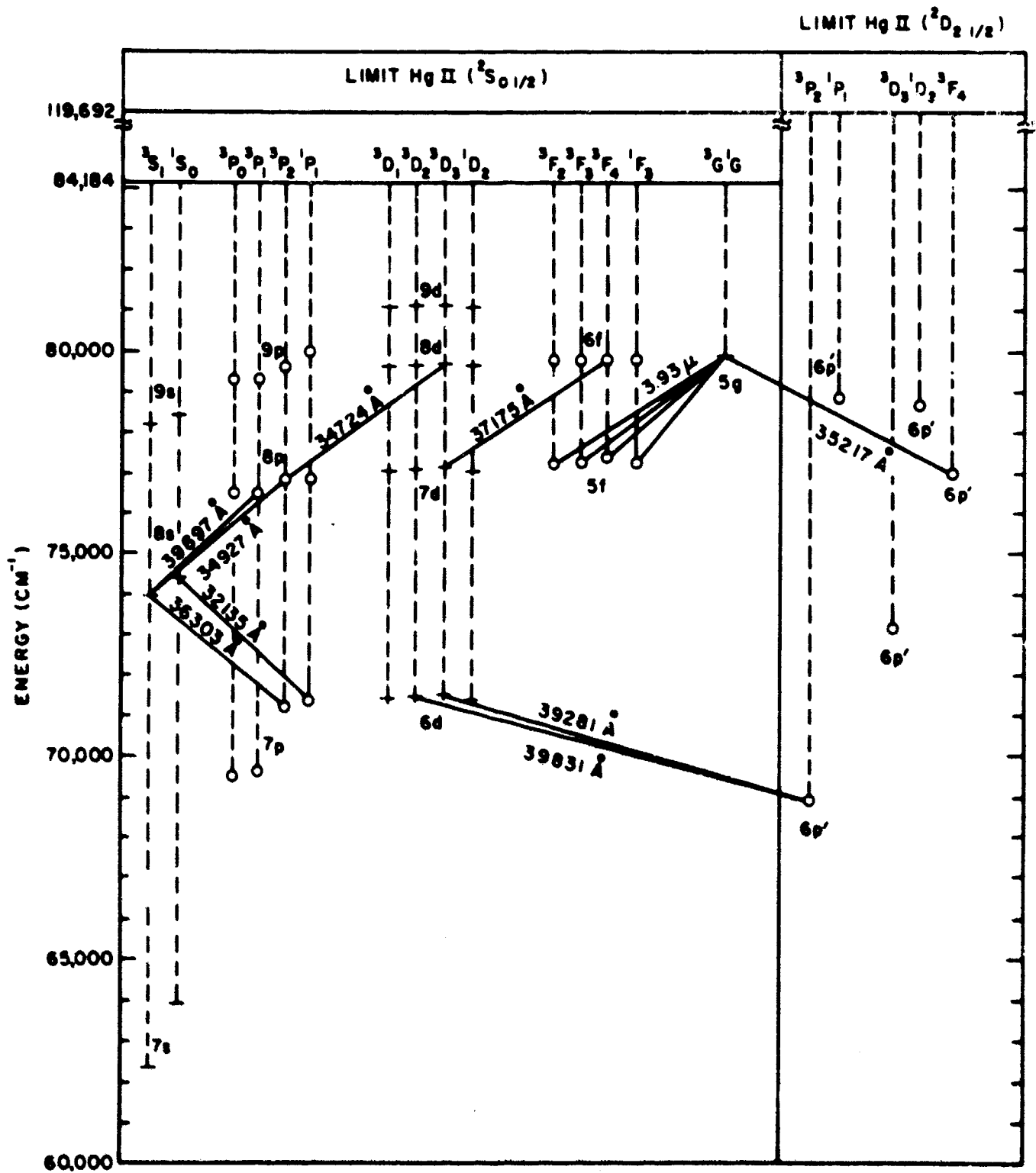


FIGURE 1. Partial Energy-Level Diagram of Hg I. Circles represent odd levels and horizontal lines even levels. Some of the more intense transitions beyond 3 microns are indicated.

f, or g states gives rise to long series of triplet and singlet levels, all of which converge to the  $d^{10}s^2S_{0\frac{1}{2}}$  normal state of the mercury ion. This simple pattern is broken by the appearance of levels from the configuration resulting from binding an electron to the  $d^9s^2$  configuration of the ion. The  $d^9s^2$  configuration accounts for an inverted  $^2D$  term in the ion spectrum. Owing to extremely large spin-orbit interaction in the ion, the ion doublet separation is very large, amounting to  $15038 \text{ cm}^{-1}$ . All of the Hg I levels in this family that lead to high-energy transitions arise from the configuration  $d^9s^2 \cdot p$  and converge to the lower doublet limit  $^2D_{2\frac{1}{2}}$ . Such known levels, conventionally designated by a prime, are  $6p^1P_2'$ ,  $6p^1D_3'$ ,  $6p^1F_4'$ ,  $6p^1D_2'$ , and  $6p^1P_1'$ . Levels associated with the upper level of the inverted  $^2D$ , although known, are not of significance in connection with the material introduced into this report. The levels of the  $d^9s^2(^2D_{2\frac{1}{2}})np$  family are intermingled with those built upon  $d^{10}s(^2S)$ . As a result, the mercury spectrum is characterized by numerous perturbations between levels of the same parity and j-value. The most conspicuous example is the perturbation of  $5f^3F_4^o$  by  $6p^1F_4^o$ , which leads to extremely irregular intervals in the  $5f^3F$  multiplet. This situation was discussed in the earlier paper,<sup>3</sup> but it is also significant for the identification and evaluation of the complex level  $5gG$ , which is one of the items with which this report is concerned.

Recent observations of the mercury spectrum have been to a great extent features of various laser programs. The observations described and discussed here were stimulated by receipt of an advance copy of a paper by Bockastén, Garavaglia, Lengyel, and Lundholm that appeared subsequently in the Journal of the Optical Society of America.<sup>4</sup> That paper reported laser lines in Hg I in the interval between 1 and 2.5 microns. Discussion was included, however, of several laser transitions reported by other observers at wavelengths greater than 2.5 microns. Included among these was a feature at  $3.932 \mu$  first observed in spontaneous emission by Paschen<sup>5</sup> and classified by him ambiguously as  $6p^1P_2^o - 6d^3D_3$  or  $5fF^o - 5gG$ . On the basis of this background material, it appeared desirable to try to determine the origin of the feature by observing it with higher resolution than had been employed heretofore. Preliminary results of this study were reported at the Philadelphia meeting of the Optical Society of America, October 1965.<sup>6</sup> Subsequent to submission of the abstract, the problem was discussed with Dr.

<sup>3</sup> Ibid.

<sup>4</sup> K. Bockastén, M. Garavaglia, B. A. Lengyel, and T. Lundholm, J. Opt. Soc. Am., Vol. 55, p. 1051 (1965).

<sup>5</sup> F. Paschen, Ann. Physik, Vol. 6, p. 47 (1930).

<sup>6</sup> C. J. Humphreys and E. Paul, Jr., J. Opt. Soc. Am., Vol. 55, p. 1572 A (1965).

Bockastén in Sweden and with K. C. M. Learner of the Imperial College, South Kensington. Dr. Learner was interested in the possibility of observing the transition  $6p^13F_4^o-5gG$ , assuming, of course, that the  $5gG$  complex had been found. The expected location was at about  $3.522 \mu$ . In brief, the investigation demonstrated that the ambiguously classified feature at  $3.932 \mu$  consisted of four resolved components, three of which represented a portion of the  $5fF-5gG$  multiplet, the fourth and strongest being  $6p^13P_2^o-6d^3D_3$ . The transition  $6p^13F_4^o-5gG$  was also observed as a moderately intense line. Significant details are reported below.

## EXPERIMENTS AND ANALYSIS

Observations of the infrared spectrum of mercury were made by means of a  $^{198}\text{Hg}$  microwave-excited electrodeless source and the same grating spectrometer (mounting a 7500-lines-per-inch grating) used in all recently reported experiments. Although the problems of immediate interest involved only the region between  $3.5$  and  $4.0 \mu$ , the entire range from  $1.8$  to a little beyond  $4.0 \mu$  was covered. A section of chart with identified features covering the region between  $3.9$  and  $4.0 \mu$  is reproduced as Figure 2. The group of four lines at the short wavelength end of this figure is identified with the ambiguously classified feature at  $3.93 \mu$ . The wavelength of the line  $6p^13P_2^o-6d^3D_3$  originating in  $^{198}\text{Hg I}$  is calculable from levels derived from interferometric measurements.<sup>7,8</sup> Measurement of the positions of the other three lines of this group, together with that of the transition identified as  $5f^3F_4^o-5gG$ , permits evaluation of the complex of energy levels described as  $5gG$ . Agreement between determinations of this value,  $79783.85 \text{ cm}^{-1}$ , from the four available transitions is close enough to estimate the precision at  $\pm 0.02 \text{ cm}^{-1}$ . It is noted at this point that the separation, amounting to about  $50 \text{ cm}^{-1}$ , of the level  $5f^3F_4^o$  from the group of closely spaced levels,  $5f^3F_2^o$ ,  $5f^3F_3^o$ , and  $5f^1F_3^o$ , is anomalous, probably being caused by a perturbation between  $5f^3F_4^o$  and  $6p^13F_4^o$ . Inspection of higher-series  $f$ -levels reveals no such anomaly. Keeping in mind the fact that the  $f$ -levels should show very small intervals, it is not unexpected that the  $5gG$  levels should be completely unresolved within the limits of available instrumental capabilities.

The levels of  $^{198}\text{Hg I}$  that are involved either directly or indirectly in the determination of  $5gG$  are compiled in Table 1. A description of the spectrum between  $3.2 \mu$  and the upper wavelength limit of the observations is compiled and presented as Table 2. Unfortunately, not all

<sup>7</sup> K. Burns and K. B. Adams, J. Opt. Soc. Am., Vol. 42, p. 56 (1952).

<sup>8</sup> C. J. Humphreys and E. Paul, Jr., J. Physique, Vol. 19, p. 424 (1958); Trans. I. A. U., Vol. 11 A, p. 77 (1962).

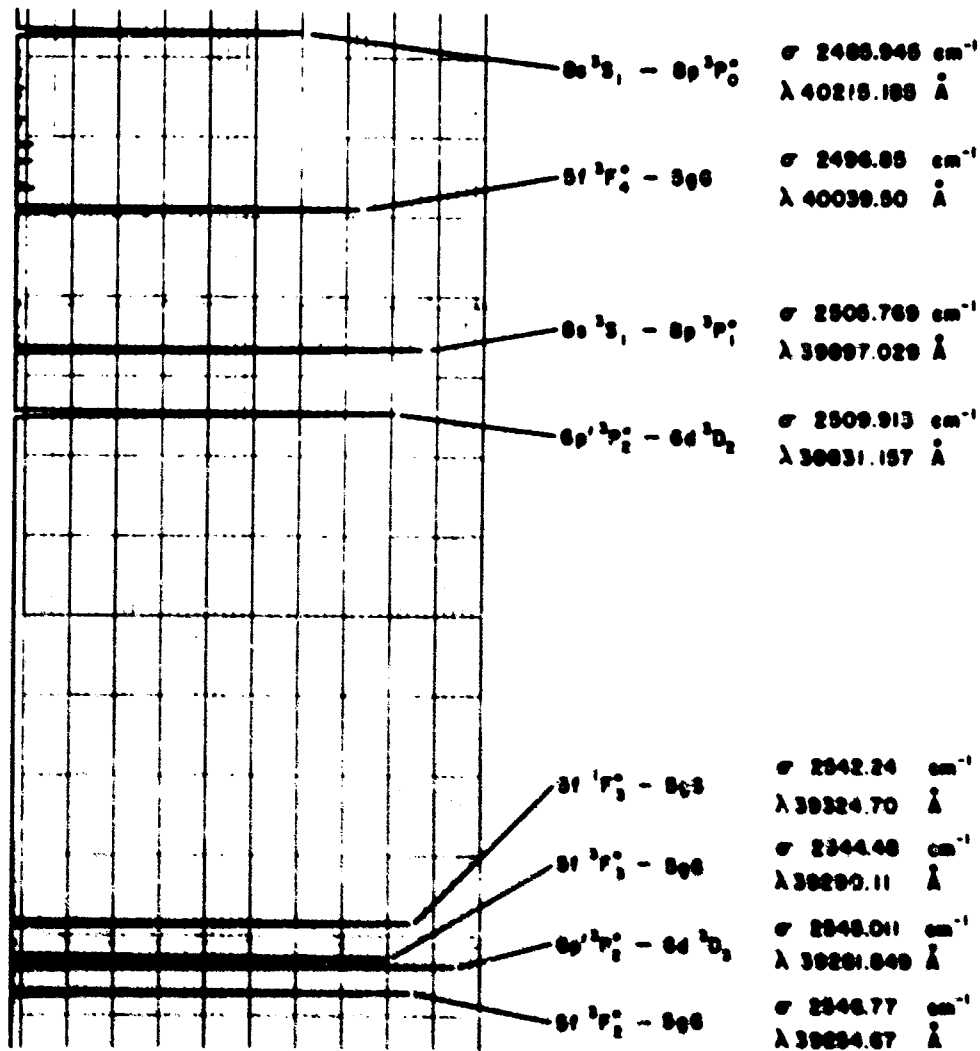


FIGURE 2.  $^{198}\text{Hg I}$ , 4-Micron Region—Section of Chart Record With Identifications

TABLE 1. Selected Levels in  $^{198}\text{Hg I}$

Designation	Level value, $\text{cm}^{-1}$ *
$6p^1 3P_2^\circ$	68886.445
$6d^1 D_2$	71333.334
$6d^3 D_1$	71336.299
$6d^3 D_2$	71396.368
$6d^3 D_3$	71431.466
$5f^3 F_2^\circ$	77237.016
$5f^3 F_3^\circ$	77239.344
$5f^1 F_3^\circ$	77241.656
$5f^3 F_4^\circ$	77287.027
5gG	79783.85 $\pm$ 0.02

\* The value of 5gG is based on current observations; all others are derived from interferometric measurements by Burns and Adams and by Humphreys and Paul.

TABLE 2. Description of  $^{198}\text{Hg I}$  and  $\text{Hg I}$ , Natural  
(3.2-4 Micron Region)

Estimated intensity	$\lambda$ , air, Å	$\sigma$ , vac., $\text{cm}^{-1}$	Transition
6000	32135.674	3110.958	$7p^1 P_1^{\circ} - 8s^1 S_0$
250	34724.16	2879.05	$8p^3 P_2^{\circ} - 8d^3 D_3$
30	34872.98	2866.77	$8p^3 P_2^{\circ} - 8d^3 D_2$
5000	34927.78	2862.27	$8s^3 S_1 - 8p^3 P_2^{\circ}$
200	* 35217.5	2838.7	$6p^3 F_4^{\circ} - 5gG$
150	† 35736.18	2797.522	$8p^1 P_1^{\circ} - 8d^1 D_2$
7000	36303.07	2753.84	$7p^3 P_2^{\circ} - 8s^3 S_1$
200	{ † 37286.6	2681.2	$7d^1 D_2 - 6f^1 F_3^{\circ}$
	{ † 37290.7	2680.9	$7d^1 D_2 - 6f^3 F_3^{\circ}$
160	† 37308.8	2679.6	$7d^1 D_2 - 6f^3 F_2^{\circ}$
100	37475.98	2667.65	$7p^1 P_1^{\circ} - 8s^3 S_1$
300	† 37596.5	2659.1	$7d^3 D_1 - 6f^3 F_2^{\circ}$
80	{ † 37905.8	2637.4	$7d^3 D_2 - 6f^1 F_3^{\circ}$
	{ † 37910.1	2637.1	$7d^3 D_2 - 6f^3 F_3^{\circ}$
200	† 37928.8	2635.8	$7d^3 D_2 - 6f^3 F_2^{\circ}$
800	† 37175.0	2618.8	$7d^3 D_3 - 6f^3 F_4^{\circ}$
600	* 39254.67	2546.77	$5f^3 F_2^{\circ} - 5gG$
5000	39281.849	2545.011	$6p^3 P_2^{\circ} - 6d^3 D_3$
1500	* 39290.11	2544.48	$5f^3 F_3^{\circ} - 5gG$

(Footnote at end of table)

TABLE 2 (Contd.)

Estimated intensity	$\lambda$ , air, Å	$\sigma$ , vac., cm <sup>-1</sup>	Transition
1000	* 39324.70	2542.24	5f <sup>1</sup> F <sub>3</sub> <sup>o</sup> - 5gG
300	39831.157	2509.913	6p <sup>1</sup> P <sub>2</sub> <sup>o</sup> - 6d <sup>3</sup> D <sub>2</sub>
900	† 39897.029	2505.769	8s <sup>3</sup> S <sub>1</sub> - 8p <sup>3</sup> P <sub>1</sub> <sup>o</sup>
700	* 40039.50	2496.85	5f <sup>3</sup> F <sub>4</sub> <sup>o</sup> - 5gG
200	† 40215.185	2485.945	8s <sup>3</sup> S <sub>1</sub> - 8p <sup>3</sup> P <sub>0</sub> <sup>o</sup>
400	† 40661.242	2458.674	8s <sup>1</sup> S <sub>0</sub> - 8p <sup>1</sup> P <sub>1</sub> <sup>o</sup>
50	40857.246	2446.879	6p <sup>1</sup> P <sub>2</sub> <sup>o</sup> - 6d <sup>1</sup> D <sub>2</sub>

Note: Unmarked wavelengths are calculated from <sup>198</sup>Hg levels.  
 \* Measured wavelengths, <sup>198</sup>Hg source.  
 † Calculated from levels of natural Hg.

observed transitions can be evaluated from available energy levels obtained from observations on <sup>198</sup>Hg I. In such instances calculated wavelengths are those of natural mercury obtained from levels listed in "Atomic Energy Levels."<sup>9</sup> Apology is made for publishing this mixed list, but it was the best that could be done since <sup>198</sup>Hg was used as the source.

## CONCLUSION

The interpretation of a feature (namely,  $\lambda$  3.93  $\mu$ ) obtained in spontaneous emission and also observed as a laser transition leaves an obvious question open. If laser emission were observed with sufficient resolving power, would both categories of transitions observed in spontaneous emission also appear, or to what extent would the entire spontaneously emitted spectrum be reproduced? To answer these questions it is highly desirable that further observations with lasers coupled with high-resolution equipment be undertaken.

<sup>9</sup>C. E. Moore, "Atomic Energy Levels," Circular of the National Bureau of Standards 467, Vol. III, p. 192 (1958).

## NOTE ON CESIUM I

by

C. J. Humphreys and E. Paul, Jr.  
Research Department

The first spectrum of cesium is noteworthy because of the relatively small interval separating the  $^2P$  and  $^2D$  terms comprising the first excited levels above the normal  $^2S$  state. Owing to the relative simplicity of the spectrum with the energy distributed over a small number of transitions, combinations of such low terms are expected to be intense. Accordingly, the multiplet of three lines comprising the permitted transitions between the levels of the listed terms, classically described as the diffuse doublet, is not only located relatively far out in the infrared but is probably the most intense group of atomic emission lines to be found in the given region. Based on the best available level values, which require further discussion, the wavelengths of the three lines are as follows:

$6p^2P_{0\frac{1}{2}}^{\circ} - 5d^2D_{1\frac{1}{2}}$	30103.355 Å, air
$6p^2P_{1\frac{1}{2}}^{\circ} - 5d^2D_{2\frac{1}{2}}$	34900.137 Å, air
$6p^2P_{1\frac{1}{2}}^{\circ} - 5d^2D_{1\frac{1}{2}}$	36131.089 Å, air

The cesium levels are characterized by a hyperfine structure splitting, but this splitting is too small to be observed by direct observation except in the instances of  $^2S_{0\frac{1}{2}}$  and  $^2P_{0\frac{1}{2}}^{\circ}$ .

Because of its intensity, location, and essentially single character, the strongest line of the group,  $\lambda 3.49 \mu$ , has appeared to be a good candidate for precise evaluation as a wavelength standard. During the summer of 1964, when the infrared spectrum of  $^{136}\text{Xe}$  was being measured interferometrically in preparation for the Hamburg meeting of the International Astronomical Union, an attempt was made to intercompare Cs,  $\lambda 3.49 \mu$ , with several  $^{136}\text{Xe}$  lines in the same region. At that time the preliminary wavelength of Cs,  $\lambda 3.49 \mu$ , was calculated from levels published by H. Kleiman.<sup>10</sup> Several recordings were made using an étalon of 30 mm. Because it was not found possible to establish the whole order of interference for the Cs patterns, the attempt failed, suggesting that the provisional wavelength was in error. Subsequently, Eriksson, Johansson,

<sup>10</sup>H. Kleiman, J. Opt. Soc. Am., Vol. 52, p. 441 (1962).

and Norlén<sup>11</sup> remeasured the cesium spectrum and obtained revised values of the  $6p^2P$  levels, indicating that a portion of Kleiman's level determinations had been in error. On the basis of this new information, the wavelength of  $\lambda 3.49 \mu$  was recalculated. The old records were then re-examined. It was found that intercomparison of three  $^{136}\text{Xe}$  lines, namely, 35070.2520, 33666.6991, and 32739.2788 Å, led to agreement with the calculated value for the Cs wavelength 34900.137 Å, within one in the thousandths place. Actually, the reductions led to the following uncorrected values listed opposite the appropriate  $^{136}\text{Xe}$  line:

$^{136}\text{Xe}$	Cs
35070.2520 Å	34900.1380 Å
33666.6991 Å	34900.1366 Å
32739.2788 Å	34900.1365 Å

This agreement constitutes a verification of the correctness of the observations by Eriksson, Johansson, and Norlén. To complete the record, the following tabulation is given of the levels used in the calculation of diffuse doublet lines in Cs I:

$6p^2P_{0\frac{1}{2}}^\circ$	11178.2697	Center of gravity, E, J, and N
$6p^2P_{1\frac{1}{2}}^\circ$	11732.3079	Center of gravity, E, J, and N
$5d^2D_{1\frac{1}{2}}$	14499.253	Center of gravity, Kleiman
$5d^2D_{2\frac{1}{2}}$	14596.845	Center of gravity, Kleiman

Additional intercomparisons making use of longer interference paths are desirable. These should include the other cesium lines of the p-d multiplet as well as still others in the same region.

<sup>11</sup> K. B. Eriksson, I. Johansson, and G. Norlén, Arkiv för Fysik, Vol. 28, p. 233 (1964).

## PLASMA PHYSICS

### PRODUCTION OF HIGH POWER PULSES BY MAGNETIC FIELD COMPRESSION

by

R. L. Conger, J. H. Johnson, L. T. Long, and J. A. Parks  
Electricity and Magnetism Division

#### INTRODUCTION

The object of this research is to investigate the possibility of constructing a small device that, with energy provided from a chemical explosive, could produce  $10^4$  joule pulses of electricity at  $10^9$  watts.

A transient field of the order of 100 kG, lasting for a few hundred microseconds, can be produced by discharging a capacitor bank into a strongly constructed solenoid of a few turns. Higher fields cannot be obtained because the forces produced by the magnetic field destroy the solenoid. However, fields of over a million gauss can be produced by using high explosives<sup>1</sup> to implode a one-turn coil in the form of a cylinder. If the implosion takes place in a time small compared to the decay time of current in the cylinder, the total flux will be conserved and the magnetic field will be inversely proportional to the decreasing volume of the cylinder. Cold rolled copper and stainless steel have a high enough conductivity for field compressors of this type. Although the cylinders are usually circular, they can be of other shapes.

Since the energy in the magnetic field is given by the integral<sup>2</sup>

$$\mathcal{E} = \frac{1}{2} \int \mu H^2 dV$$

and the field is roughly inversely proportional to the volume, the energy in the field compressor is also inversely proportional to the volume and therefore is increased in the implosion. This increase comes from the chemical energy of the explosive. If the initial field before the implosion

---

<sup>1</sup>R. S. Caird, W. B. Garn, D. B. Thomson, and C. M. Fowler, J. Appl. Phys., Vol. 35, p. 781 (1964).

<sup>2</sup>J. A. Stratton, Electromagnetic Theory, International Series in Pure and Applied Physics. New York: McGraw-Hill, 1941, p. 124.

is sufficiently high, 10 percent or more of the energy in the explosive can be transferred to the magnetic field energy. At the limit of the implosion, the magnetic pressure exceeds the pressure produced by the explosive and the field starts to expand again. Since the current in the compressor is proportional to the magnetic field, this current is also inversely proportional to the volume of the compressor.

Although the magnetic field compressor converts the chemical energy of the explosive to electrical energy with high efficiency, getting this energy out can be difficult. The conductance of the field compressor plus any constant load applied during the compression must be sufficiently high so that the decay time of the magnetic field is much longer than the time of the implosion. More efficient conversion of the chemical energy is obtained if the field is compressed with little or no energy removed, and then, after the field is compressed, the current is switched to the load. There are several possible ways of accomplishing this. One method is to place a strip of tungsten in the circuit of the field compressor, or some similar material which has a high conductivity when cold but has a small enough mass so that it is heated to a high temperature by the high current in the compressor and strip. As it heats up, the resistance of the strip increases, thus switching the current to the load.

Since the total magnetic flux in this device is conserved, it is not possible to cascade field compressors to produce larger and larger fields; however, it is possible to obtain energy from each stage of a cascaded field compressor as the field is allowed to expand into the next stage. The first step in developing such a cascaded compressor would be to develop a single stage in which energy could be removed efficiently.

## THEORY OF MAGNETIC FIELD COMPRESSION

Magnetic field compression calculations can be based on the integral form of Maxwell's equation:

$$\int \nabla \times \mathbf{E} \cdot d\mathbf{a} = -\frac{d}{dt} \int \mathbf{B} \cdot d\mathbf{a} \times 10^{-8} \quad (1)$$

where  $\mathbf{E}$  is the electric field,  $\mathbf{B}$  is the magnetic field,  $t$  is the time, and cgs units are used.

From a vector identity and Ohm's law,

$$\int \nabla \times \mathbf{E} \cdot d\mathbf{a} = \oint \mathbf{E} \cdot d\mathbf{l} = iR \quad (2)$$

where  $R$  is the resistance of the cylinder in which the field is being compressed and  $i$  is the current.

The field compressor could be constructed as shown in Figure 1. The explosive would cause the short to advance to the right at the detonation velocity  $v$ .

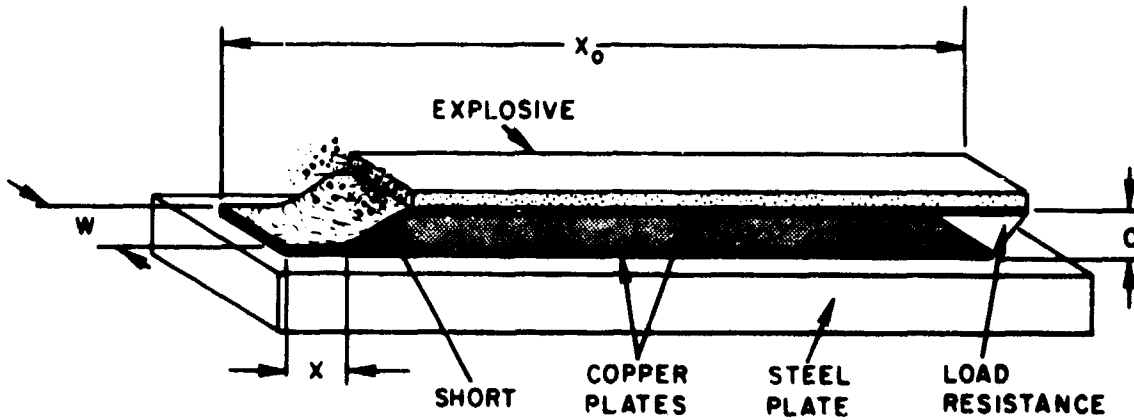


FIGURE 1. Flat Magnetic Field Compressor

For this geometry equations (1) and (2) give the differential equation

$$-a(X_0 - X) \frac{dB}{dt} + aB \frac{dX}{dt} = iR \times 10^8 \quad (3)$$

If edge corrections are neglected

$$B = \frac{2\pi i}{5w} \quad (4)$$

and thus

$$\frac{5wR dt \times 10^8}{2\pi a(X_0 - X)} = \frac{dX}{X_0 - X} - \frac{dB}{B} \quad (5)$$

The advancing shock wave from the explosive drives the conductors of Figure 1 together at a velocity  $v$ , so that  $X = vt$ . Substitution of this value for  $X$  in equation (5), followed by integration, gives

$$B = B_0 \left(1 - \frac{X}{X_0}\right)^{\beta-1} \quad (6)$$

where

$$\beta = \frac{5wR \times 10^8}{2\pi av} \quad (7)$$

If  $R = 0$ , then  $B$  is inversely proportional to  $1 - X/X_0$ , and the field is inversely proportional to the volume between the plates; but for  $R$  finite some of the magnetic field leaks through the conductor. If  $\beta \geq 1$ , no field compression takes place.

Since  $B$  is proportional to  $i$ , equation (6) can be written in terms of current to give

$$i = i_0 \left(1 - \frac{X}{X_0}\right)^{\beta-1} \quad (8)$$

For  $\beta \gg 1$  and  $X \ll X_0$ , the logarithm of equation (8) gives

$$\ln \frac{i}{i_0} \cong \beta \ln \left(1 - \frac{X}{X_0}\right) \cong -\frac{\beta X}{X_0} = -\frac{\beta vt}{X_0} \quad (9)$$

or

$$i = i_0 e^{-\beta vt/X_0} \quad (10)$$

The inductance of the field compressor shown in Figure 1 is given by

$$L = \frac{2\pi a(X_0 - X) \times 10^{-8}}{5w} \quad (11)$$

if edge connections are neglected. From equations (7) and (11)

$$\beta = \frac{RX_0}{L_0 v} \quad (12)$$

where  $L_0$  is the value of  $L$  when  $X = 0$ . For  $X \ll X_0$  and by the use of equation (12), equation (10) can be written as

$$i \cong i_0 e^{-Rt/L} \quad (13)$$

which is the usual equation for the decay of current in an inductance. Field compression must take place in a time that is small compared to the  $L/R$  time constant of the field compressor.

When  $\beta$  is expressed in terms of equation (12), equation (6) can be applied to geometries other than the one shown in Figure 1. In particular, it can be applied to a helical coil with a metal tube mounted axially inside the coil. In a field compressor of this form, the field is compressed between the coil and the tube as the tube is expanded explosively starting at one end. Since this type of field compressor can have a much higher inductance than the one shown in Figure 1, the impedance can also be much higher.

When the resistance  $R$  of the field compressor is constant, the energy transferred to it is given by the integral

$$\mathcal{E} = \int_0^t i^2 R d\tau = i_0^2 R \int_0^t \left(1 - \frac{v\tau}{X_0}\right)^{2\beta-2} d\tau \quad (14)$$

This integral can be maximized by differentiating with respect to  $R$  and setting the result equal to 0. If this is done it is found that  $W$  is a maximum when  $\beta = \frac{1}{2}$ . For this value of  $\beta$ , equation (14) becomes

$$\mathcal{E} = \frac{i_0^2 R X_0}{v} \ln n \quad (15)$$

where  $n$  is the compression ratio or  $X_0/(X_0 - X)$ .

From equation (12), with  $\beta = \frac{1}{2}$

$$R = \frac{L_0 v}{2X_0} \quad (16)$$

Substitution of (16) into equation (15) gives

$$\mathcal{E} = \frac{1}{2} i_0^2 L_0 \ln n \quad (17)$$

Since the initial energy before compression is  $\frac{1}{2}i_0^2 L_0$ , the energy increase ratio is  $lnn$ . However, the term  $lnn$  does not increase very rapidly with  $n$ . More efficient transfer of energy from the explosive to the load can be obtained by making the load resistor of a sheet of tungsten or tantalum thin enough to heat up during the compression, thereby increasing the resistance and transferring energy to the load.

When  $R$  is not constant, equation (14) cannot be evaluated analytically. Two methods were used to evaluate this equation with  $R$  as a variable. One method was the use of an analog computer; the other was a desk calculation that consisted of dividing the compression into a number of small increments and letting  $R$  be a constant in each increment. The successive values of  $R$  were calculated from the energy transferred to  $R$  in the preceding increment. Both methods gave the same result, with the desk calculation serving as a check on the computer calculation. Only the computer calculations will be discussed in this report, since they are probably the more accurate of the two.

It is desired to maximize the energy delivered to the load. The equation for this energy is

$$\mathcal{E} = \int_0^{t_1} i^2 R dt \quad (18)$$

where  $i$  and  $R$  are variables. The term  $R$  has an upper limit determined by the melting point of the material used for the load. For tungsten  $R_{\max} = 12 R_0$ , and for tantalum  $R_{\max} = 9 R_0$ , where  $R_0$  is the initial resistance of the load. The compression ratio determines  $t_1$ , which, for the computer calculations, is  $0.95 X_0/v$ .

The variables  $i$  and  $R$  are determined by the pair of differential equations

$$\left(\frac{X_0}{v} - t\right) \frac{di}{dt} = \left(\frac{R}{L} + 1\right) i \quad (19)$$

and

$$i^2 R = \frac{C}{\alpha R_0} \cdot \frac{dR}{dt} \quad (20)$$

Equation (19) is derived from equation (3), and equation (20) represents the change in  $R$  caused by its heating. Here  $X_0$ ,  $v$ ,  $L$ ,  $\alpha$ , and  $R_0$  are constants,  $C$  is the heat capacity of the load, and  $\alpha$  is the temperature coefficient of resistance in the equation

$$R = R_0(1 + \alpha T) \quad (21)$$

where T is temperature.

For these calculations, the constants had the following values:

$$X_0 = 25 \text{ cm}$$

$$v = 7 \times 10^5 \text{ cm/sec}$$

$$\dot{L} = 4.4 \times 10^{-3} \text{ h/sec}$$

$$\alpha = 0.0045 \text{ ohm/}^\circ\text{C for tungsten}$$

$$\alpha = 0.0035 \text{ ohm/}^\circ\text{C for tantalum}$$

$$t_1 = 3.392 \times 10^{-5} \text{ sec}$$

$$i_0 = 6 \times 10^4 \text{ amp}$$

The computer was used to find a value of  $C/\alpha R_0$  for a given  $R_0$  such that  $R = R_{\max}$  at  $t = 3.392 \times 10^{-5}$  sec. When this constraint was met, the value of E for that value of  $C/\alpha R_0$  was recorded. Figure 2 presents  $\mathcal{E}$  as a function of  $R_0/\dot{L}$  for the case of  $R_{\max} = 12 R_0$ , and E as a function of  $R_0/\dot{L}$  for  $R_{\max} = 9 R_0$  is presented in Figure 3.

These figures show that E is a maximum when

$$\frac{R_0}{\dot{L}} \approx 0.1 \quad (22)$$

From equations (18) and (20)

$$\mathcal{E} = \frac{C \Delta R}{\alpha R_0} \quad (23)$$

For tungsten, with  $R_{\max} = 12 R_0$ ,  $\Delta R = 11 R_0$ , and

$$C = \frac{\alpha \mathcal{E}}{11} \quad (24)$$

For tantalum, with  $R_{\max} = 9 R_0$ ,  $\Delta R = 8 R_0$ , and

$$C = \frac{\alpha \mathcal{E}}{8} \quad (25)$$

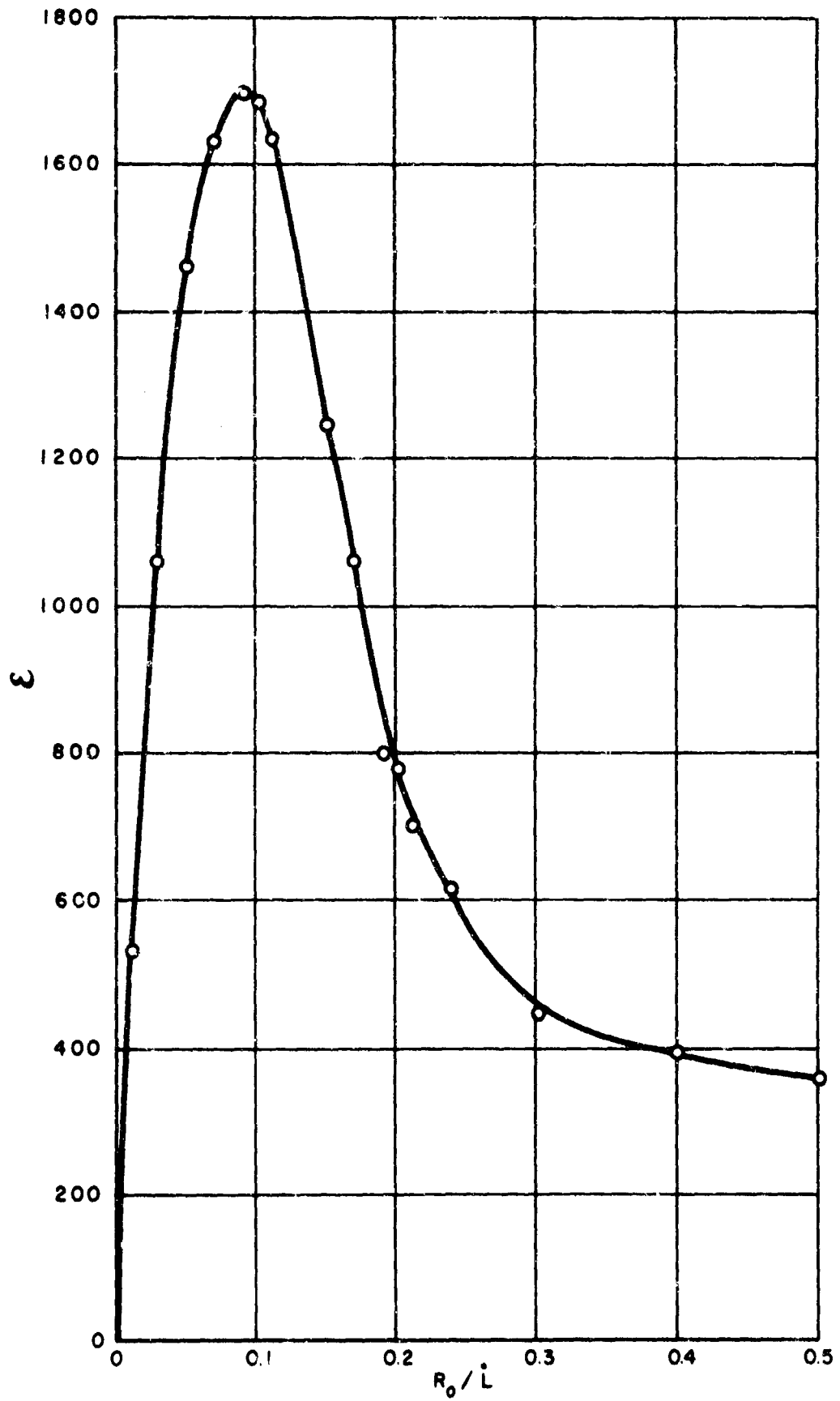


FIGURE 2. Variation of  $\epsilon$  With  $R_0/L$  for  $R_{\max} = 12 R_0$

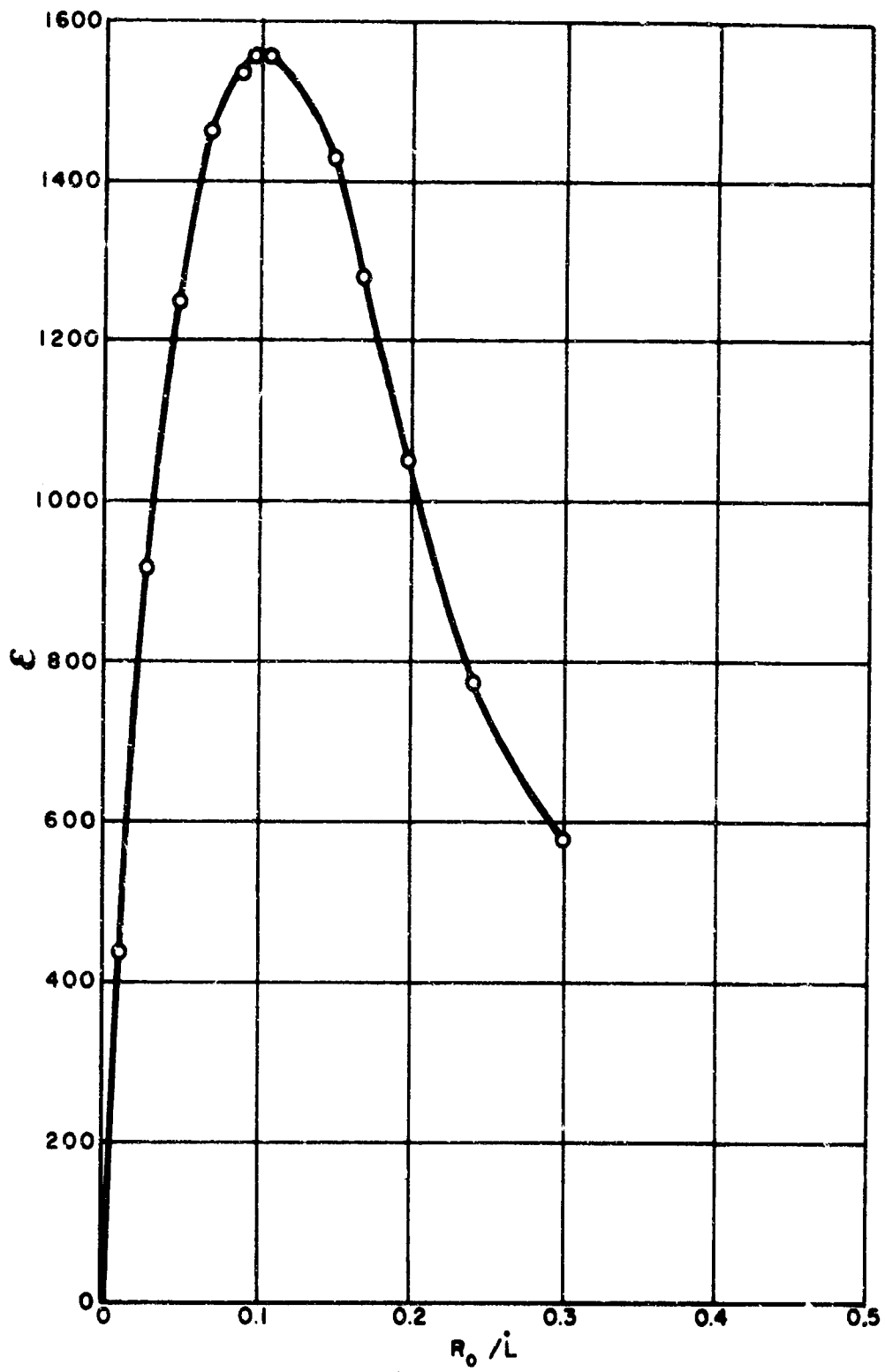


FIGURE 3. Variation of  $\mathcal{E}$  With  $R_0 / \dot{L}$  for  $R_{\max} = 9 R_0$

The energy  $\mathcal{E}$  in equations (24) and (25) is the maximum value of the curves of Figures 2 and 3, respectively. From the values of  $R_0$  from equation (22), and  $C$  from equation (24) or (25), the required shape of the load can be determined.

Figure 4 shows the computer mechanization diagram for this problem.

## MAGNETIC FIELD COMPRESSION TESTS

Figure 5 shows the magnetic field compressor before the 0.25 in. thick penta-erythritol tetranitrate (PETN) explosive was glued to the top of the upper copper plate, which is 0.75 in. above the lower plate. A steel plate 1 in. thick above the explosive partially confines the explosive and therefore increases the detonation pressure on the upper copper plate. The three RG-9B/U coaxial cables attached at the right are connected to a 480- $\mu$ f capacitor bank 30 ft away, which produces the initial field. An exploding-bridge-wire (EBW) type detonator at the top of the wooden assembly on the right initiates a 17.2 cm length of explosive cord, which in turn initiates the PETN explosive after a 36.5- $\mu$ sec delay. This delay allows the magnetic field in the compressor to reach its maximum initial value before the detonation wave progressing down the explosive forces the upper copper plate against the lower one. The wedge on the lower plate at the right end of the compressor allows contact to be made between the upper and lower copper plates when the detonation wave has traveled 5.5 cm. Both plates are 15 in. long, 1.5 in. wide, and 0.070 in. thick. As the compression progresses, current is forced through the load, which is a 0.007 in. tantalum strip at the left side behind the resistors. The tantalum strip is placed at an angle of 30 deg so that there will be less dead space at the end of the compression when the detonation wave reaches the left end of the upper plate. The steel block on which the lower plate is mounted is sufficiently large to withstand the force of the explosion. This block becomes dented and the lower copper strip is firmly welded to the steel after the explosion.

Figure 6 is a block diagram of the apparatus. The Mk 88 electronic firing switch supplied two simultaneous pulses, each of about 1000 v, from a 1- $\mu$ f capacitor. One pulse fired the EBW detonator; the other drove the primary of an air core transformer. This transformer, with about a 20-to-1-turns ratio, stepped up the voltage of the pulse from the Mk 88 firing switch sufficiently to trigger the spark gap switch; thus the EBW detonator and the spark gap switch were fired simultaneously.

The tantalum strip load formed the resistance  $R_2$  of one arm of the bridge shown in Figure 7. The resistive voltage drop across the tantalum strip is approximately equal to the inductive voltage drop produced by  $L$  across the same strip. A section of the upper copper plate,

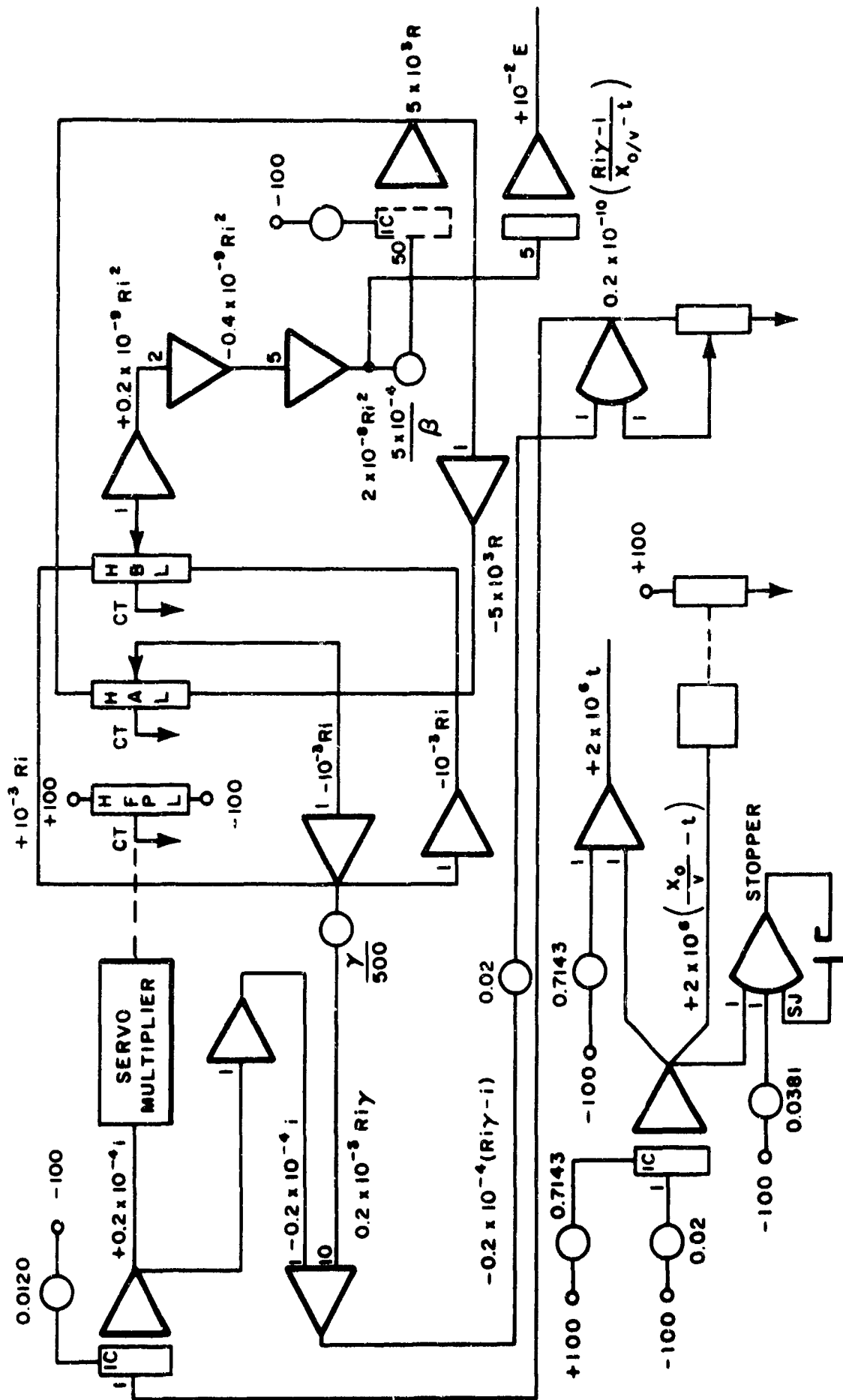


FIGURE 4. Analog Computer Mechanization Diagram

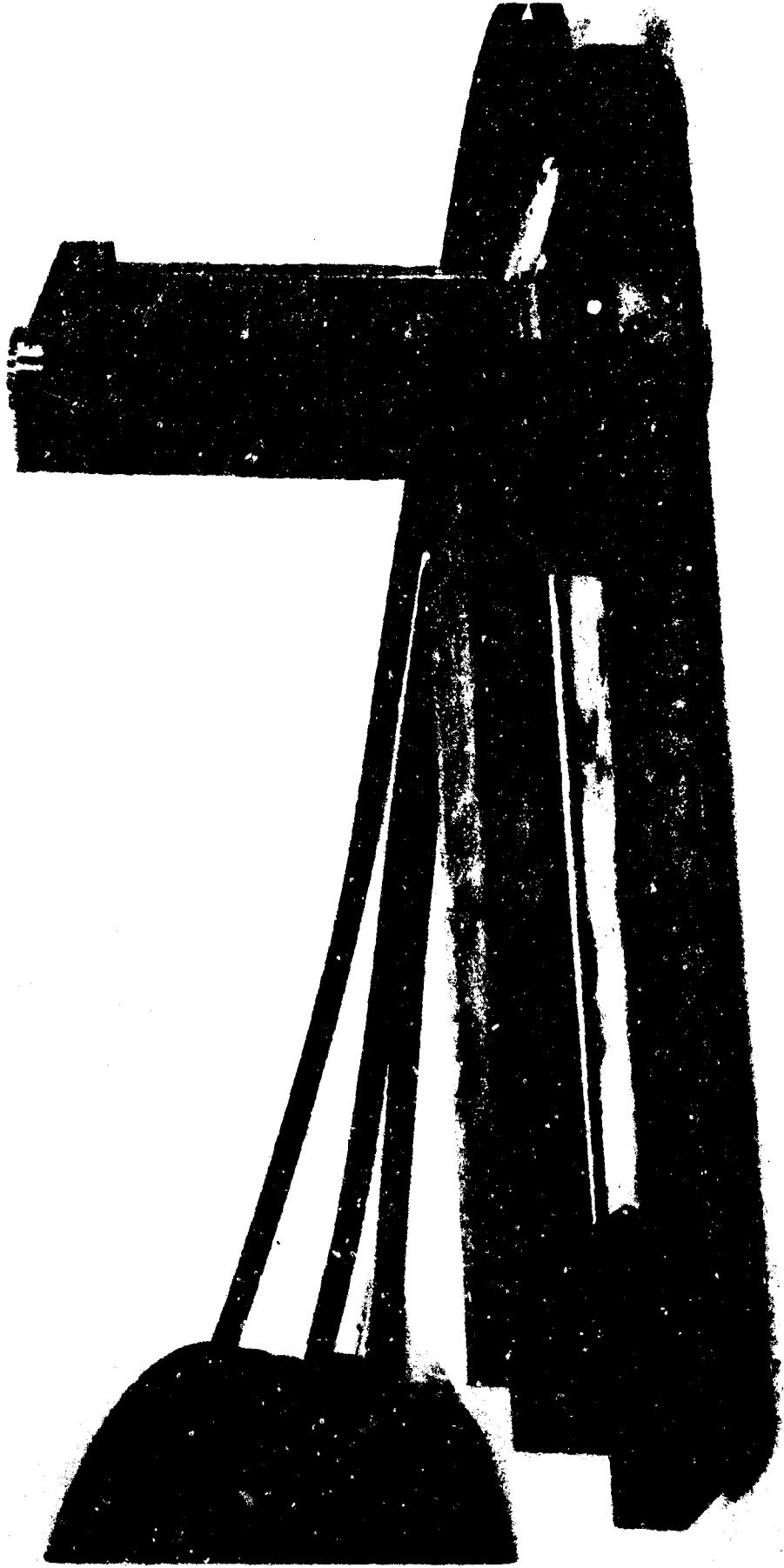


FIGURE 5. Magnetic Field Compressor

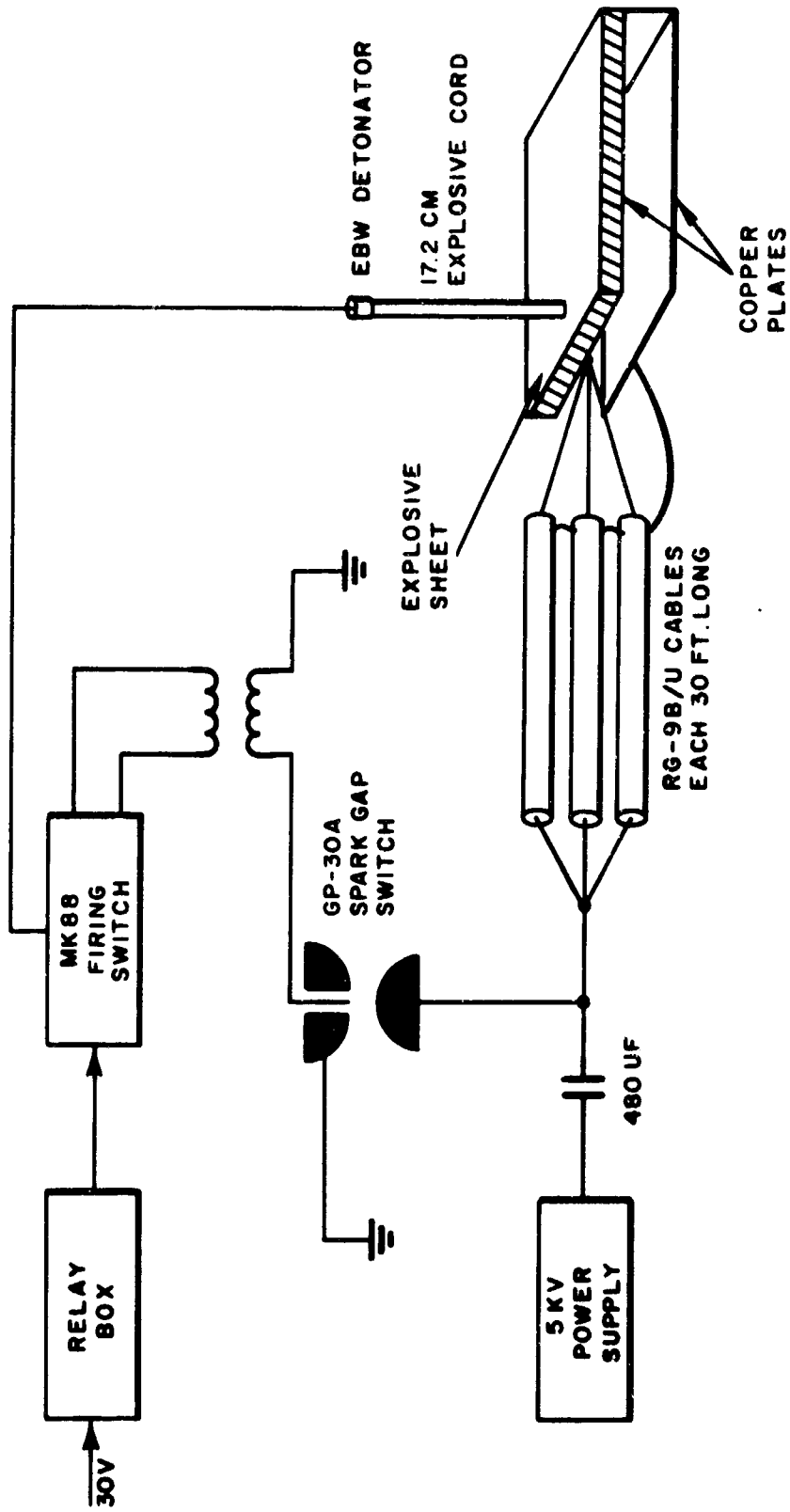


FIGURE 6. Block Diagram of Magnetic Field Compressor

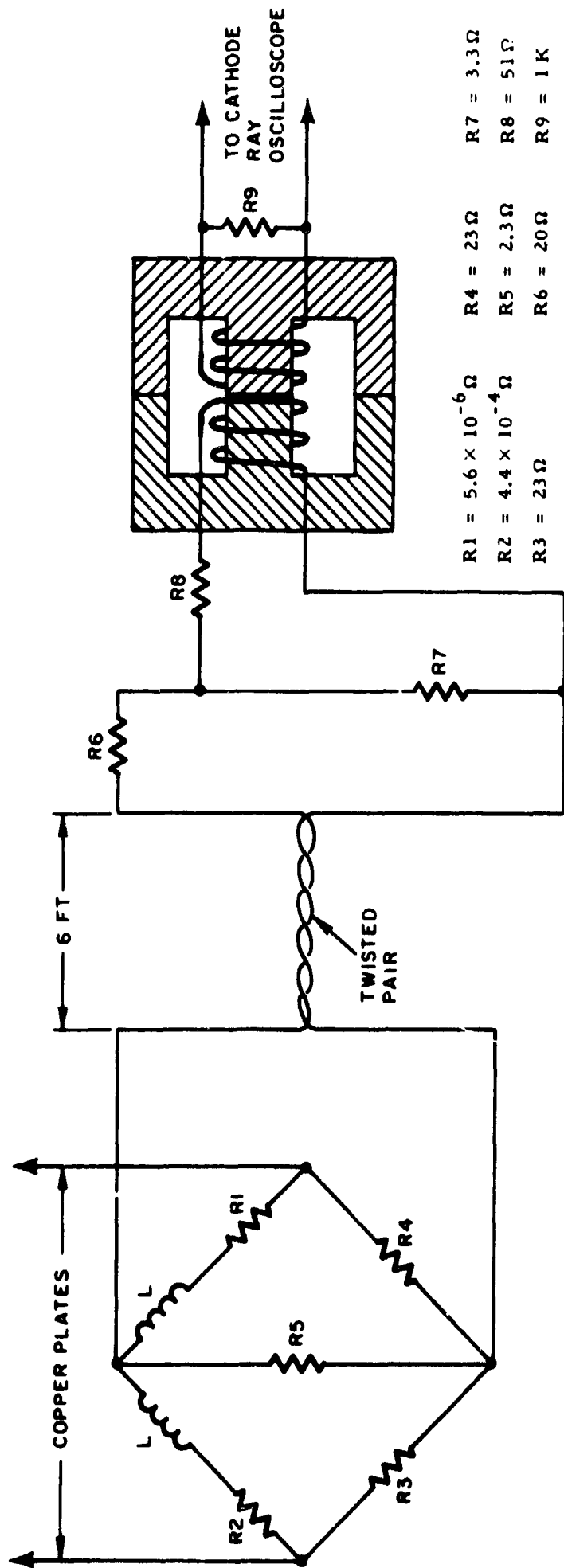


FIGURE 7. Power Output Circuit

sufficiently long to produce an inductance equal to that of the inductance of the tantalum strip, formed another arm of the bridge R1 and L. The other parts of the bridge were resistors (see Figure 5) shown schematically in Figure 7. The output of the bridge was conducted by a twisted pair of wires to an attenuator and pulse transformer placed about 6 ft from the field compressor and outside the firing chamber. The pulse transformer was necessary to prevent the large ground currents flowing in the flux compressor from upsetting the operation of the oscilloscopes used for recording the voltage developed in the bridge of the field compressor.

The pulse transformer was constructed from two ferrite cores, each in the form of a letter E. Copper wire was wound on the center arm of the E's and the two sections were then clamped together with electric tape. The transformer had a 1-to-1-turns ratio. A test of the transformer showed that it would pass a 100- $\mu$ sec pulse without significant distortion as long as the input pulse was not more than 5 v. A voltage divider was therefore connected to the input of the pulse transformer to keep the voltage below this level.

Oscilloscopes and a high voltage power supply for charging the capacitor bank were placed in a firing shack and connected to the capacitor bank and field compressor by 100 ft of high voltage coaxial cable.

To test the apparatus, the capacitor bank was first charged to 3000 v and then, without a detonator, the firing circuit was armed and fired, thus triggering the spark gap switch and the oscilloscopes. The result is shown in Figure 8, which is a photograph of an oscilloscope trace. A detonator was placed on the field compressor and the capacitor bank was again charged to 3000 v. This time when the firing switch was closed, the spark gap switch discharged the capacitors into the field compressor and the PETN sheet explosive forced the two copper plates together. The oscilloscope trace of this test is shown in Figure 9. The maximum current was about 2.8 times that obtained without the explosive charge. Current increase stopped about 34  $\mu$ sec after field compression began. The detonation wave in the PETN sheet travels about 7 mm/ $\mu$ sec, and field compression stopped after the detonation wave had advanced about 9.4 in. Why the field compression stopped then is not known.

Figure 10 is a photograph taken of the compressor after the test. The figure shows that the upper and lower copper strips were still continuous, although there was a tear in the upper strip. The upper strip had become welded to the lower strip along the edges, and it also exhibited bulges as if some fluid had been trapped under it. Calculations indicate that the magnetic field pressure was only a few hundred pounds per centimeter of compressor length.

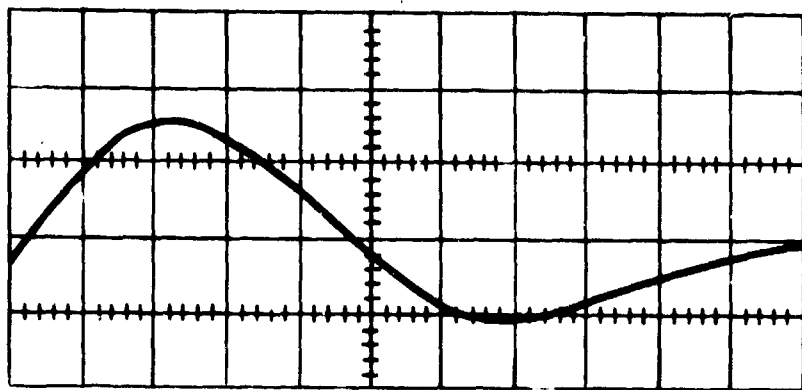


FIGURE 8. Field Compressor Output Without Explosive. (Time scale: 20  $\mu$ sec/cm)

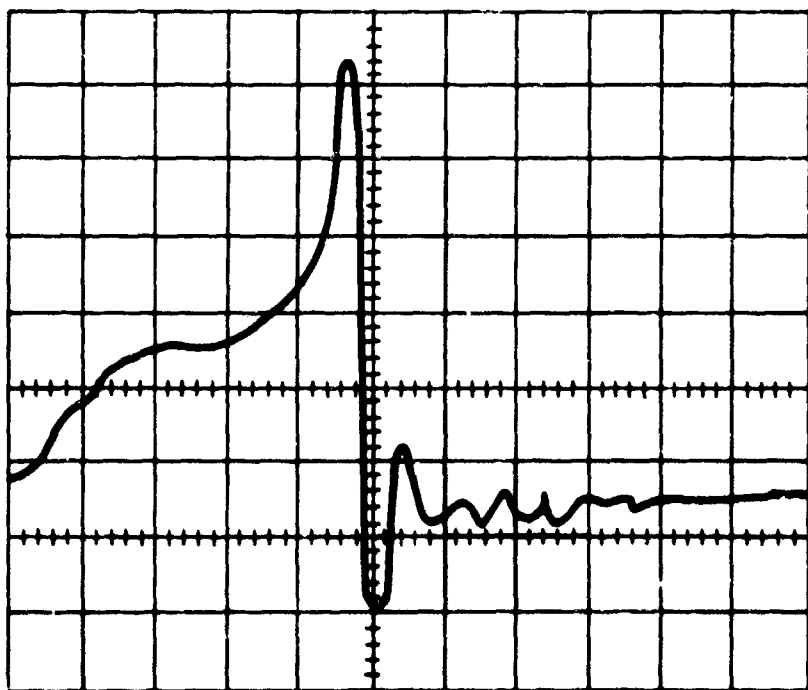


FIGURE 9. Field Compressor Output With Explosive. (Time scale: 20  $\mu$ sec/cm)



**FIGURE 10. Effects of Explosion on Compressor**

After 9.4 in. of compression, not enough energy would have been transferred to the tantalum strip to heat it sufficiently to increase its resistance significantly, and so  $\beta$  of equation (8) must have remained near its initial value of 0.1. From equation (8), with  $X = 9.4$ ,  $X_0 = 15$ , and  $\beta = 0.1$

$$\frac{i}{i_0} = \left(1 - \frac{9.4}{15}\right)^{-0.9} = 2.41$$

which is close to the measured value of 2.8. The size of the tantalum strip was based on a compression ratio of 20. If further experiments show that a compression ratio this large cannot be obtained, the resistance of the tantalum strip load should be increased.

# SEMICONDUCTOR PHYSICS

## ACCURATE MEASUREMENT OF SMALL ROTARY DISPERSION

by

C. J. Gabriel and H. Piller  
Infrared Division

### INTRODUCTION

The study of interband Faraday rotation in semiconductors requires the transmission of electromagnetic energy through highly absorbing materials. In order to have sufficient transmitted energy to make the measurements, often samples must be used having thicknesses of the order of  $1/\eta$ , where  $\eta$  is the absorption coefficient. The rotations induced by such thin samples can be less than one minute. This report discusses how the addition of phase-sensitive detection to an apparatus described in a previous report<sup>1</sup> allows the measurement of small rotations.

### MODIFICATION OF THE APPARATUS

Priefly, the apparatus consists of a high-pressure xenon arc, focusing optics, a 510-cps light chopper, monochromator, Glan-Thompson polarizer, sample cell, Wollaston prism beam splitter, two photodetectors, a bridge circuit, and suitable amplifiers. Details of the apparatus were given previously.<sup>2</sup>

The modification was made by replacing the Hewlett-Packard Model 415A amplifier by a Princeton Applied Research Model JB-5 lock-in amplifier. Because the gain of the PAR JB-5 is somewhat less than the gain of the HP 415A, a Tektronix 122 preamplifier was used. Since the Tektronix 122 is double-ended, the coupling transformer was eliminated and capacitive coupling was used instead. A parallel LC circuit tuned to the chopping frequency was placed at the input of the preamplifier; its purpose was to decrease the loading effect on the tuned stages

---

<sup>1</sup>C. J. Gabriel, V. A. Patton, and H. Piller, NAVWEPS Report 8226, Quarterly Report: Foundational Research Projects, October-December 1964, p. 69.

<sup>2</sup>Ibid.

of the lock-in amplifier by the pickup of 60-cps voltage from the line. The reference for this amplifier was obtained by mounting a flashlight lamp and solar cell on opposite sides of the chopper disc. The voltage obtained from the solar cell was sufficient to drive the reference channel of the lock-in amplifier.

Three advantages result from the use of the phase-sensitive amplifier:

1. An improvement is obtained in signal-to-noise ratio because of the narrow bandpass of the lock-in amplifier. This effect, being well known,<sup>3</sup> will not be discussed here.
2. A bipolar signal is obtained. The sign of the signal indicates which detector is more strongly irradiated, thus making the balancing of the bridge easier and indicating the sign of the rotation.
3. A more linear response is obtained. This allows the accurate measurement of small rotation, regardless of phase imbalance of the bridge network. This point will be discussed in detail.

## THEORY OF MEASUREMENT

Assume that the signal voltages from the photodetector are out of phase by the angle  $\phi$  and that  $\phi$  is independent of the signal amplitudes  $v_1$  and  $v_2$ . Let the phase  $\Phi$  of the reference signal be measured from the bisector of the phase difference  $\phi$ . (See Figure 1.) The components of the difference signal  $v_s$  and the sum signal  $V$  that are in phase with the reference are then given, respectively, by the expressions

$$v_s(a + \theta) = (v_1 - v_2) \cos \Phi \cos \frac{\phi}{2} - (v_1 + v_2) \sin \Phi \sin \frac{\phi}{2} \quad (1)$$

$$V(a + \theta) = (v_1 + v_2) \cos \Phi \cos \frac{\phi}{2} - (v_1 - v_2) \sin \Phi \sin \frac{\phi}{2} \quad (2)$$

where the signal amplitudes are given by the expressions

$$v_1 = IK_1 \sigma_1 k_1 \cos^2(a + \theta) \quad (3)$$

$$v_2 = IK_2 \sigma_2 k_2 \sin^2(a + \theta) \quad (4)$$

<sup>3</sup>R. H. Dicke, Rev. Sci. Instr., Vol. 17, p. 268 (1947).

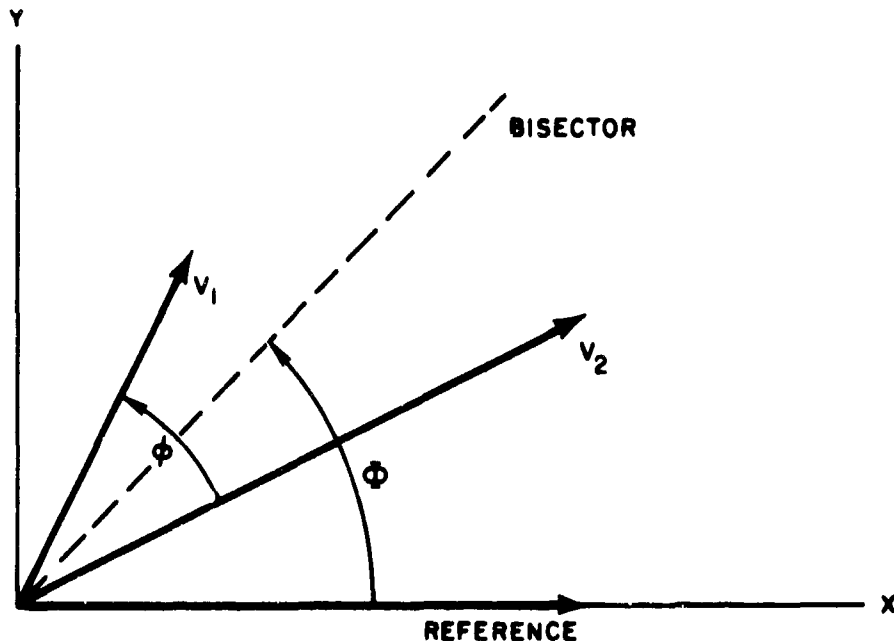


FIGURE 1. Relative Phases of the Signal Voltages  $v_1$ ,  $v_2$ , and the Reference Channel

in which  $I$  is the source intensity,  $K_1$  and  $K_2$  are factors depending on the bridge parameters,  $\sigma_1$  and  $\sigma_2$  are factors depending on the detector responses,  $k_1$  and  $k_2$  are factors to take into account differences in absorption in the two beams,  $\alpha$  is the angle between the planes of polarization of the polarizer and analyzer, and  $\theta$  is the rotation of the plane of polarization caused by rotary dispersion in the sample.

The expressions (1) and (2) for  $v_s$  and  $V$  should be compared with the corresponding expressions for the amplitudes of  $v_s$  and  $V$  that are obtained if phase-sensitive detection is not used:

$$v_s = (v_1 - v_2) \left[ 1 + \frac{2v_1 v_2}{(v_1 - v_2)^2} (1 - \cos \phi) \right]^{\frac{1}{2}} \quad (5)$$

$$V = (v_1 + v_2) \left[ 1 - \frac{2v_1 v_2}{(v_1 + v_2)^2} (1 - \cos \phi) \right]^{\frac{1}{2}} \quad (6)$$

It is evident that equation (1) is linear in  $\theta$  in the region where  $v_1 \approx v_2$ , whereas equation (5) is not. If  $V$  were obtained by measuring  $v_1$  and  $v_2$  separately, by covering each detector, then equation (6) would become

$V = v_1 + v_2$ . It is assumed that  $V$  is determined from a single measurement.

For values of  $\theta$  less than 5 degrees, an expansion to second order in  $\theta$  can be used.

$$v_s(\alpha + \theta) \approx -I\Omega \cos \Phi \cos \frac{\phi}{2} \left[ \sin 2\beta - \frac{\Delta\Omega}{\Omega} + \tan \Phi \tan \frac{\phi}{2} \left( 1 - \frac{\Delta\Omega}{\Omega} \sin 2\beta \right) + 2 \left( 1 - \frac{\Delta\Omega}{\Omega} \tan \Phi \tan \frac{\phi}{2} \right) \left( \theta \cos 2\beta - \theta^2 \sin 2\beta \right) \right] \quad (7)$$

where  $\alpha = \frac{\pi}{4} + \beta$

$$2\Omega = K_1 \sigma_1 k_1 + K_2 \sigma_2 k_2$$

$$2\Delta\Omega = K_1 \sigma_1 k_1 - K_2 \sigma_2 k_2$$

A similar expression is obtained for  $V(\alpha + \theta)$  except that  $\Delta\Omega$  and  $\Omega$  are interchanged. The system can generally be adjusted so that  $\beta$ ,  $\Delta\Omega/\Omega$ , and  $\Phi \ll 1$ . Equation (7) and the similar expression for  $V(\alpha + \theta)$  reduce to:

$$v_s(\alpha + \theta) \approx -I\Omega \cos \frac{\phi}{2} \left( 2\theta + 2\beta - \frac{\Delta\Omega}{\Omega} + \Phi \tan \frac{\phi}{2} \right) \quad (8)$$

$$V(\alpha + \theta) \approx -I\Omega \cos \frac{\phi}{2} \left[ 2\beta \frac{\Delta\Omega}{\Omega} - 1 + \Phi \tan \frac{\phi}{2} \left( \frac{\Delta\Omega}{\Omega} - 2\beta \right) + 2\theta \left( \frac{\Delta\Omega}{\Omega} - \Phi \tan \frac{\phi}{2} \right) \right] \quad (9)$$

where terms to third order in small quantities have been dropped and it has been assumed that  $\phi \leq \pi/2$ .

The Faraday rotation is obtained from the measured values of  $v_s$  and  $V$  by either of the following combinations:  $R_1 = (v_s^+ - v_s^-)/(V^+ + V^-)$  or  $R_2 = (v_s^+/2V^+) - (v_s^-/2V^-)$ , where the superscripts (+) and (-) indicate measurements made with forward and reversed magnetic fields, respectively. From equations (8) and (9), by dropping small quantities of third order,

$$R_1 = -\frac{I_v}{I_V} \left[ 2\theta \left( 1 + \frac{\Delta I_v}{I_v} \frac{\Delta H}{H} \right) + \left( 2\beta - \frac{\Delta\Omega}{\Omega} + \Phi \tan \frac{\phi}{2} \right) \frac{\Delta I_v}{I_v} \right] \quad (10)$$

$$R_2 = -\frac{I_v}{I_V} \left[ 2\theta \left( A + B \frac{\Delta H}{2H} \right) + \left( 2\beta - \frac{\Delta \Omega}{\Omega} + \phi \tan \frac{\phi}{2} \right) B \right] \quad (11)$$

where  $2\theta = \theta^+ - \theta^-$

$$2\Delta H = H^+ + H^-$$

$$2H = H^+ - H^-$$

$$2I_v = I_v^+ + I_v^-$$

$$2\Delta I_v = I_v^+ - I_v^-$$

with similar definitions for  $I_V$  and  $\Delta I_V$ , and

$$A = \left( 1 - \frac{\Delta I_v \Delta I_V}{I_v I_V} \right) \left[ 1 - \left( \frac{\Delta I_V}{I_V} \right)^2 \right]^{-1}$$

$$B = \left( \frac{\Delta I_v}{I_v} - \frac{\Delta I_V}{I_V} \right) \left[ 1 - \left( \frac{\Delta I_V}{I_V} \right)^2 \right]^{-1}$$

The subscripts  $v$  and  $V$  designate, respectively, the average value of the source intensity when either  $v_s$  or  $V$  is being measured, and  $H^+$  and  $H^-$  are the average values of the forward and reversed magnetic fields, respectively.

## DISCUSSION

Generally  $\theta$  is obtained from equation (10) or equation (11) by neglecting all unmeasured quantities; thus,  $\theta = R_1/2$  or  $\theta = R_2/2$ . In addition to this error of negligence, an error is introduced because of the error involved in measuring  $v_s$  and  $V$ . For the moment this error will be neglected. The value of  $\theta$  obtained in this way is the sum of the rotation  $\theta_s$  induced by transmission through the sample and the rotation  $\theta_m$  caused by reflection from mirrors located in the magnetic field. The mirrors are located in the magnetic field because the magnet used at NOLC does not have axial access. The value of  $\theta_m$  must be obtained from a separate measurement. For simplicity, consider equation (10); the treatment of equation (11) is similar. Equation (10) has the form

$$R = 2\theta(1 + p) + q \quad (12)$$

where  $\theta = \theta_s + \theta_m$ . A similar expression holds for the measurement of  $\theta_m$ ; thus

$$R_m = 2\theta_m(1 + p_m) + q_m \quad (13)$$

From equations (12) and (13), an expression for the error in the measured value of  $\theta_s$  can be obtained.

$$\theta_s - \left( \frac{R}{2} - \frac{R_m}{2} \right) = -p\theta_s + (p_m - p)\theta_m + \frac{1}{2}(q_m - q) \quad (14)$$

Because of the random nature of the quantities  $\Delta I_V/I_V$  and  $\Delta H/H$ , the factors  $p_m - p$  and  $q_m - q$  are not necessarily zero.

The first term of equation (14) is of the order of  $(\Delta H/H)(\Delta I_V/I_V)\theta_s$ , and the second term is of the order of  $(\Delta I_V/I_V)(\Delta H/H)\theta_m$ . The magnitude of the third term depends on the method used to balance the system. In principle, if the system is adjusted until  $v_s(a) = 0$ , then  $q = q_m = 0$  (see equation 8). The difficulty with this adjustment is that the magnetic field can cause a movement of the optical components and thus produce a displacement of the light beams with respect to the detectors, resulting in an imbalance,  $(\Delta\Omega/\Omega)_d$ , of the system. Since the imbalance does not depend on the direction of the magnetic field, it does not appear as a rotation, but only contributes to  $q_m - q$ . This contribution is of the order of  $(\Delta\Omega/\Omega)_d(\Delta I_V/I_V)$ . Alternatively, the system can be adjusted until the condition  $v_s^+ + v_s^- = 0$  holds. Under this condition  $q_m - q \sim (\theta_m + \theta_s)(\Delta I_V/I_V + \Delta H/H)\Delta I_V/I_V$ . The second balancing method generally gives the best results.

Instead of making fine adjustments in the system, an alternative procedure is available. If the electronics of the detection system can be arranged so that the measurements of  $v_s$  and  $V$  for a given field direction take place simultaneously, or nearly so, then equation (11) can be used virtually without error introduced by neglecting unmeasured quantities. This comes about because under this condition  $I_V \approx I_V$  and  $\Delta I_V \approx \Delta I_V$  so that  $B \approx 0$  and  $A \approx 1$ .

In contrast to phase detection, fine adjustment of the system is not possible with amplitude detection because, as can be seen from equation (5),  $v_s$  will be linear only if the system is unbalanced—for instance, by making  $\beta > \phi$ . This gives an error in  $\theta$  proportional to  $\phi\Delta I_V/I_V$ . However, the alternative procedure mentioned above is still available.

If the system is such that  $\Delta H/H \approx 0.01$ ,  $\Delta I_V/I_V \approx 0.1$ , and  $\theta_s \ll \theta_m$ , then the error of negligence will be of the order of  $\theta_m \times 10^{-3}$ . The polar Faraday rotation on the mirrors in a field of 20 kG is typically

less than 0.001 radian.<sup>4</sup> Thus the error in  $\theta$  will be of the order of  $10^{-6}$  radian. This error is of the same order as that introduced by errors in the measurement of  $v_s$  and  $V$ ; that is, under optimum conditions  $\Delta v_s/V \approx 10^{-6}$ , where  $\Delta v_s$ , the rms noise voltage in  $v_s$ , is typically of the order of a microvolt and  $V$  is typically of the order of a volt. The values of  $\Delta v_s$  and  $V$  quoted above are obtained by using PbS detectors, time constants of several seconds, and samples thin enough so that the transmitted intensity is about 0.3 of the incident intensity.

A severe restriction on this theoretical sensitivity of  $10^{-6}$  to  $10^{-5}$  radian arises if the apparatus is not mechanically stable. If the apparatus is rigidly constructed, with attention being paid to the isolation of the system from the surroundings, then movements of the optical components can be negligible. However, instabilities in the intensity distribution of the arc itself will still be present. Since such instabilities introduce an error into  $\theta$  of the order of  $\delta(\Delta\Omega)/\Omega$ , where  $\delta(\Delta\Omega)$  is the change in  $\Delta\Omega$  during the time interval between the measurements of  $v_s^+$  and  $v_s^-$ , the sensitivity can be reduced by several orders of magnitude. For this reason, the detectors should be positioned so that movement of the arc affects both detectors equally. Moreover, it is advantageous to sacrifice the signal-to-noise ratio of the detectors and to use detectors which are large enough for the beams to remain within the sensitive area for small movements of the arc.

## SUMMARY

It has been shown that the utilization of phase-sensitive detection with a double-beam null technique provides an increase in the linearity of the response of the system; moreover, that this increase in linearity allows the measurement of small values of Faraday rotation independent of phase imbalance of the bridge circuit, residual magnetization of the electromagnet, and source intensity fluctuations, provided these quantities are reasonably small. However, instabilities in the intensity distribution of the arc limit these advantages to such an extent that the detector signal-to-noise ratio should be sacrificed by using detectors large enough so that the beams remain within the sensitive areas for small movements of the arc. If, by the use of detectors other than PbS, the ratio  $\Delta v_s/V$  can be reduced to below  $10^{-6}$ , then the apparatus should be modified in order to fully utilize the detectors. The system should be so designed that no mirrors are located in the magnetic field and the ratio  $v_s/V$  is measured directly.

---

<sup>4</sup>E. A. Stern, J. C. McGroddy, and W. E. Harte, Phys. Rev., Vol. 135, p. A 1306 (1964); J. C. McGroddy, A. J. McAlister, and E. A. Stern, Phys. Rev., Vol. 139, p. A 1844 (1965).

# ELLIPTICITY IN MULTIPLY REFLECTED FARADAY ROTATION

by

C. J. Gabriel and H. Piller  
Infrared Division

## INTRODUCTION

The presence of multiple internal reflections can cause difficulty in the accurate measurement of Faraday rotation and ellipticity in slab-shaped samples of materials for which the product of the absorption coefficient  $\eta$  and the thickness  $d$  satisfies the condition  $\eta d \lesssim 1$ . In a previous report,<sup>5</sup> a model was discussed whereby multiply reflected Faraday rotation could be conveniently treated. In this report the model will be extended to include the effects of internal polar-reflected Faraday rotation. The primary purpose of the report, however, is to provide simple relationships between the observed rotation and ellipticity and the rotation produced by a single passage of the light beam through the sample. Two extreme cases will be considered: (1) that of precise coherence among the multiply reflected beams, and (2) that of complete incoherence among the multiply reflected beams. The first case is especially useful in the treatment of experiments that use a laser as a light source and thin, highly polished samples. The second case applies in low-resolution spectroscopy and in experiments utilizing samples that are rough compared to the wavelength of the light used.

## THE MODEL

The following model is used to discuss the effects of multiple reflections.

1. A collimated, linearly polarized light beam is normally incident upon a plane parallel slab.
2. The amplitude of the transmitted beam of light is the sum of the amplitudes of the light beams produced by partial internal reflection on the sample surfaces.
3. The effect of the magnetic field is introduced phenomenologically as a rotation of the plane of polarization upon each passage through

---

<sup>5</sup>H. Piller and C. J. Gabriel, NAVWEPS Report 8812, Quarterly Report: Foundational Research Projects, January-March 1965, p. 27.

the sample and upon each internal reflection from the surfaces. The ellipticity produced in a single passage through the sample is neglected.

Only a brief treatment of this model will be given here.

After passing through an analyzer rotated by an angle  $\alpha$  with respect to the polarizer, the amplitude of the  $q$  times reflected beam is given by

$$\tau_q = t_1 t_2 (-r_1 r_2)^q e^{-i(2q+1)\delta} \cos [(2q+1)\theta + 2q\phi + \phi' - \alpha] \quad (1)$$

where  $t_1$ ,  $t_2$ ,  $r_1$ , and  $r_2$  are the Fresnel coefficients for normal incidence:

$$\begin{aligned} r_1 &= \frac{1 - n + ik}{1 + n - ik} & r_2 &= \frac{n - 1 - ik}{1 + n - ik} \\ t_1 &= \frac{2}{n + 1 - ik} & t_2 &= \frac{2(n - ik)}{n + 1 - ik} \end{aligned} \quad (2)$$

in which  $n$  and  $k$  are the real and imaginary parts of the complex index of refraction of the sample, and  $n = 1$ ,  $k = 0$  in the surrounding medium. The complex phase shift  $\delta$  is given by  $\delta = 2\pi(n - ik)d/\lambda$ , where  $\lambda$  is the wavelength in vacuum. The factor  $\exp[-i(2q+1)\delta]$  in equation (1) takes into account the phase shift and absorption occurring in the bulk material. The angle  $\theta$  is the Faraday rotation for a single passage;  $\phi$  is the polar Faraday rotation that takes place upon each internal reflection; and  $\phi'$  is any magneto rotation that might take place on passage through both surfaces. Although  $\phi'$  is expected to be zero, it is included for completeness.

The intensity of the emerging beam will, in general, be a periodic function of the analyzer position  $\alpha$ . The value of  $\alpha$  for which the intensity is a relative maximum is the observed rotation and will be designated by  $\gamma$ . The ratio of the minimum intensity to the maximum intensity gives the ellipticity in the case of complete coherence, and a measure of the depolarization in the case of complete incoherence.

### COMPLETELY COHERENT BEAMS

The transmitted amplitude for coherent beams is given by the summation of the amplitudes obtained from equation (1). Hence,

$$\tau = \sum_{q=0}^{\infty} \tau_q = t_1 t_2 e^{-i\delta} \left[ \frac{\cos(\Theta - A) + r_1 r_2 e^{-2i\delta} \cos(\Theta + A)}{1 + 2r_1 r_2 e^{-2i\delta} \cos 2\Theta + (r_1 r_2)^2 e^{-4i\delta}} \right] \quad (3)$$

where  $\Theta = \theta + \phi$  and  $A = \alpha + \phi - \phi'$ . Utilizing equation (3) yields the transmitted intensity

$$\tau\tau^* = K [\cos^2(\Theta - A) + c_1 \cos(\Theta + A) \cos(\Theta - A) + c_2 \cos^2(\Theta + A)] \quad (4)$$

where  $c_1 = 2(a \cos \phi + b \sin \phi) \exp(-\eta d)$  and  $c_2 = R^2 \exp(-2\eta d)$ , in which

$$a = \frac{k^2 (6 - 2n^2 - k^2) - (n^2 - 1)^2}{[(1+n)^2 + k^2]^2} \quad (5)$$

$$b = \frac{4k(n^2 + k^2 - 1)}{[(1+n)^2 + k^2]^2} \quad (6)$$

$$\phi = \frac{4\pi n d}{\lambda} \quad (7)$$

$$\eta = \frac{4\pi k}{\lambda} \quad (8)$$

$$R^2 = a^2 + b^2 \quad (9)$$

with  $d$  the sample thickness and  $\lambda$  the wavelength. The quantities  $a$  and  $b$  are the real and imaginary parts, respectively, of  $r_1 r_2$ ;  $R$  is the reflectivity; and  $\eta$  is the absorption coefficient. The parameter  $K$  (see Appendix A) is independent of  $a$  and thus an explicit form is not necessary here.

The condition  $d(\tau\tau^*)/da = 0$  yields the expression

$$\tan 2\Gamma = \frac{(1 - c_2) \sin 2\Theta}{(1 + c_2) \cos 2\Theta + c_1} \quad (10)$$

where  $\Gamma = \gamma + \phi - \phi'$ . This expression relates the observed rotation  $\gamma$  to the Faraday rotation  $\Theta$  and the polar reflection Faraday rotation  $\phi$ , since  $\phi'$  can be expected to be zero. The partial inversion of equation (10) yields

$$\sin 2(\Theta - \xi) = \frac{c_1 \tan 2\Gamma}{[(1 - c_2)^2 + (1 + c_2)^2 \tan^2 2\Gamma]^{\frac{1}{2}}} \quad (11)$$

where  $\tan 2\xi = [(1 + c_2)/(1 - c_2)] \tan 2\Gamma$ .

The transmitted beam becomes elliptically polarized upon passing through the sample. The ellipticity arising in this model is, of course, not related to the intrinsic ellipticity, which has been neglected here, but is caused by the multiple reflections. The ellipticity  $\epsilon$  is defined by  $\epsilon^2 = I_{\min}/I_{\max}$ , where  $I_{\min}$  and  $I_{\max}$  are, respectively, the minimum and maximum intensities obtained from equation (4) as  $\alpha$  is varied through 180 degrees. Since  $I_{\max}$  occurs when  $A = \Gamma$ , then  $I_{\min}$  occurs when  $A = \Gamma + \pi/2$ . Hence, from equation (4)

$$\rho = \frac{\cos 2(\Theta - \Gamma) + c_1 \cos 2\Gamma + c_2 \cos 2(\Theta + \Gamma)}{1 + c_1 \cos 2\Theta + c_2} \quad (12)$$

where  $\rho = (1 - \epsilon^2)/(1 + \epsilon^2)$ . In principle, equations (12) and (10) can be used to obtain  $\theta$  and  $\phi$  from measured values of  $\epsilon^2$  and  $\gamma$  if the condition  $\phi' \approx 0$  holds.

By treating  $\sin 2\Theta$  and  $\cos 2\Theta$  as independent variables, equations (10) and (12) can be solved simultaneously, to yield

$$\sin 2\Theta = \frac{(1 + c_2)^2 - c_1^2}{1 - c_2} \frac{\rho \sin 2\Gamma}{1 + c_2 - \rho c_1 \cos 2\Gamma} \quad (13)$$

$$\cos 2\Theta = \frac{\rho(1 + c_2) \cos 2\Gamma - c_1}{1 + c_2 - \rho c_1 \cos 2\Gamma} \quad (14)$$

From the identity  $\sin^2 2\Theta + \cos^2 2\Theta = 1$ , it follows directly that

$$\rho = \left[ 1 + \frac{4c_2 - c_1^2}{(1 - c_2)^2} \sin^2 2\Gamma \right]^{-\frac{1}{2}} \quad (15)$$

Thus,  $\Gamma$  can be determined from the measured value of  $\rho$ . Then, using equation (10),  $\Theta$  can be obtained. If the conditions  $\phi \approx 0$  and  $\phi' \approx 0$  hold, then equation (15) can be used to check the validity of the model by relating the measured quantities  $\gamma$  and  $\rho$ .

## COMPLETELY INCOHERENT BEAMS

In the case of incoherent beams, the intensity of the transmitted beam is given by

$$\tau\tau^* = \sum_{q=0}^{\infty} \tau_q \tau_q^* \quad (16)$$

Evaluation of equation (16) yields

$$\tau\tau^* = K' \left\{ 1 + c_2^2 - 2c_2 \cos 4\Theta + (1 - c_2) [\cos 2(\Theta - A) - c_2 \cos 2(\Theta + A)] \right\} \quad (17)$$

where  $K'$  (see Appendix A) is independent of  $\alpha$ . The condition  $d(\tau\tau^*)/d\alpha = 0$  yields

$$\tan 2\Theta = \frac{1 - c_2}{1 + c_2} \tan 2\Gamma \quad (18)$$

This equation relates  $\theta$  and  $\phi$  to  $\gamma$  since the condition  $\phi' \approx 0$  is expected to hold.

The transmitted beam is not elliptically polarized but, rather, partially depolarized. The polarization factor  $(I_{\max} - I_{\min})/(I_{\max} + I_{\min})$  has the same form as the quantity  $\rho$  used above to describe the ellipticity. The same symbol,  $\rho$ , will be used for the polarization factor. From equation (17)

$$\rho = \frac{1 - c_2}{1 + c_2^2 - 2c_2 \cos 4\Theta} [\cos 2(\Theta - \Gamma) - c_2 \cos 2(\Theta + \Gamma)] \quad (19)$$

The insertion of equation (18) into equation (19) yields

$$\rho = \left[ 1 - \frac{4c_2}{(1 + c_2)^2} \sin^2 2\Gamma \right]^{\frac{1}{2}} \quad (20)$$

Equation (20) gives  $\Gamma$  in terms of the measured quantity  $\rho$ . This value of  $\Gamma$ , when substituted in equation (18), yields a value of  $\Theta$ . Thus, from the measured values of  $\rho$  and  $\gamma$ , both  $\theta$  and  $\phi$  can be obtained if the con-

dition of  $\phi' \approx 0$  holds. Under the conditions  $\phi \approx 0$  and  $\phi' \approx 0$ , the applicability of the model can be checked by using equation (20) to relate the measured values of  $\gamma$  and  $\rho$ .

## DISCUSSION

Although the rotation  $\theta$  can be determined from a measurement of  $\gamma$ , assuming  $\phi = \phi' = 0$ , photometric techniques generally do not measure  $\gamma$  independently of  $\rho$ , so either a measurement or calculation of  $\rho$  is necessary. For example, in a technique used at this Laboratory,<sup>6</sup> the transmitted light beam is split into two perpendicularly polarized components. When the system is properly balanced, the quantity that is measured is  $(I_1 - I_2)/(I_1 + I_2)$ , where  $I_1$  and  $I_2$  are the intensities of the two components of the light beam. Writing

$$I_1 = I_{\max} \cos^2(\alpha - \gamma) + I_{\min} \sin^2(\alpha - \gamma) \quad (21)$$

$$I_2 = I_{\max} \sin^2(\alpha - \gamma) + I_{\min} \cos^2(\alpha - \gamma) \quad (22)$$

gives

$$\frac{I_1 - I_2}{I_1 + I_2} = \rho \cos 2(\alpha - \gamma) \quad (23)$$

Generally, the system is adjusted so that  $\alpha = \pi/4$ . Under this condition  $(I_1 - I_2)/(I_1 + I_2) = \rho \sin 2\gamma$ . A separate measurement of  $\rho$  can be made if the system is adjusted until  $\alpha = \gamma$ , that is, for maximum  $I_1 - I_2$ ; then  $(I_1 - I_2)/(I_1 + I_2) = \rho$ . However, if  $\rho \approx 1$ , a measurement of  $\rho$  made in this way can be more inaccurate than simply to set  $\rho = 1$  initially and then make successive approximations until consistency is reached by using the relationships among  $\rho$ ,  $\gamma$ , and  $\theta$  and the measured value of  $\rho \sin 2\gamma$ . For small values of  $\theta$ , equations (15) and (20) indicate that  $\rho = 1$ , and  $\gamma$  is obtained directly from the measurement.

In order to use the expressions for the rotation and ellipticity, it is necessary to know the values of  $c_1$  and  $c_2$ . This requires the accurate knowledge of  $n$ ,  $k$ ,  $d$ , and  $\lambda$ , particularly if interference effects are observed. For example, suppose that  $\Phi$  is only known to within one percent; then  $\Delta\Phi$ , the error in  $\Phi$ , will be  $0.01(4\pi nd/\lambda) \approx 0.1nd/\lambda$ . Unless

<sup>6</sup>C. J. Gabriel, V. A. Patton, and H. Piller, NAVWEPS Report 8226, Quarterly Report: Foundational Research Projects, October-December 1964, p. 69.

$\lambda$  is large,  $nd/\lambda$  can be greater than one, so the condition  $\Delta\Phi \ll \pi$  does not hold, and  $c_1$  cannot be obtained accurately. When interference effects are not observed, the situation is improved since  $c_1$  does not appear in the expressions describing this case and  $c_2$  does not involve the phase  $\Phi$ .

Even if  $c_1$  and  $c_2$  are not known accurately, the expressions derived are still useful for the interpretation of experiments in which the rotation or the ellipticity is measured as a function of  $d$ ,  $\lambda$ , or the magnetic field. Moreover, by using these expressions, independent measurements of both  $\gamma$  and  $\rho$  provide a check on the consistency of the values of  $c_1$  and  $c_2$ , and thus a check on the accuracy of the correction necessary to obtain the intrinsic rotation.

#### APPENDIX A—VALUES OF $K$ AND $K'$

In order that equations (4) and (17) can be conveniently used for the interpretation of experiments involving the magneto-absorption of linearly polarized light, the explicit forms of  $K$  and  $K'$  are given here.

$$K = Te^{-\eta d} [1 + 2c_1(1 + c_2) \cos 2\Theta + c_1^2 + 2c_2 \cos 4\Theta + c_2^2]^{-1} \quad (24)$$

$$K' = Te^{-\eta d} [2(1 - c_2)(1 - 2c_2 \cos 4\Theta + c_2^2)]^{-1} \quad (25)$$

where  $T = |t_1 t_2|^2$ . From equation (2),  $\text{Im}(t_1 t_2) = b$  and

$$\text{Re}(t_1 t_2) = \frac{4\{n[(n+1)^2 + k^2] + 2k^2\}}{[(n+1)^2 + k^2]^2} \quad (26)$$

# OPTICAL CONSTANTS OF GERMANIUM IN SPECTRAL REGIONS FROM 0.5 TO 3.0 eV

by

R. F. Potter  
Infrared Division

## INTRODUCTION

The interaction of electromagnetic radiation with materials has long been recognized as a means of acquiring information on the basic properties of the materials. For those instances where the Maxwell theory of electromagnetism can be expected to hold, the measurements are usually presented in the form of optical (or dielectric) constants. The word constants would better be replaced with the term coefficients, inasmuch as the constants vary considerably as a function of wavelength, material source, and techniques of measurement. It is this variation, of course, which provides the spectroscopic information that is sought. The measurement of the optical properties of opaque but specular materials has had increased activity in recent years. The incentive has come mainly from the need for more experimental details on the band structure parameters of semiconductors.<sup>7</sup> Information concerning the band structures of the metals has also been gained from studies of the optical properties.<sup>8</sup>

Three principal techniques have been used for measuring the complex dielectric constants  $\epsilon = \epsilon_1 + i\epsilon_2$  in the near infrared, visible, and ultraviolet regions. The technique that has provided the most data in recent years has been the measurement of reflectance ( $R_0$ ) with the radiation incident nearly normal to the sample surface. Much of this work has been done without an absolute reflectance measurement but in arbitrary units. Interpretation of such spectra depends upon additional information as to whether the reflectance is dominated by the real or the imaginary part of the dielectric constant.

Using this technique, Tauc<sup>9</sup> and Cardona<sup>10</sup> have made considerable contributions, providing high resolution data over a wide spectral region.

---

<sup>7</sup>J. C. Phillips, Phys. Rev., Vol. 133, p. A 452 (1964).

<sup>8</sup>For a recent review, see M. Suffczyński, Phys. Stat. Sol., Vol. 4, p. 3 (1964).

<sup>9</sup>For a review, see J. Tauc, Proceedings of the International Conference on the Physics of Semiconductors, Exeter (1962), p. 333; also S. Lukeš and A. Schmidt, *op. cit.*, p. 389.

<sup>10</sup>M. Cardona, J. Appl. Phys., Vol. 32, p. 958 (1961).

Much of their work was concerned with spectral regions where  $\epsilon_2$ , the imaginary part of the dielectric constants, is dominant and thus  $R_0$  has spectral features similar to  $\epsilon_2$ . Consequently, from  $R_0$  one can gain an indication of the relative shape of the density-of-states function. This technique is not so suitable, however, in the regions where the dominance of either  $\epsilon_1$  or  $\epsilon_2$  is indeterminant.

The measurement of the absolute reflectance at normal incidence has been carried out by several workers. Philipp and Taft<sup>11</sup> applied the so-called Kramers-Kronig<sup>12</sup> analysis, which is applicable if sufficient spectral range has been covered. Given the reflectance over a sufficient spectral region, the real and imaginary parts of the dielectric constant can be calculated for that region. The principal requirement is to insure that all of the necessary information has been gathered.

The technique of ellipsometry, which also gives the real and imaginary parts of the dielectric constant, has been used to study germanium. Archer applied this technique to examine the optical properties of germanium in the visible region.<sup>13</sup> His results are in good agreement with those of Philipp and Taft and with more recent measurements by Philipp and Ehrenreich<sup>14</sup> which were obtained from the K-K approach. Archer's results are also in reasonable agreement with recent measurements by Marple and Ehrenreich,<sup>15</sup> who also applied ellipsometric techniques, although Archer's do not resolve certain spectral features.

Photometric techniques have also been used for determining the optical constants. Avery<sup>16</sup> and, more recently, Lindquist and Ewald<sup>17</sup> have devised techniques involving the measurement of the ratios of the parallel and perpendicular components of the reflectance. A different technique based on similar principles was described recently by the author.<sup>18</sup>

---

<sup>11</sup>H. R. Philipp and G. A. Taft, Phys. Rev., Vol. 113, p. 1002 (1959).

<sup>12</sup>For a discussion, see F. Stern in Solid State Physics, Vol. 15, ed. by F. Seitz and D. Turnbull, New York: Academic Press (1963), p. 300.

<sup>13</sup>R. J. Archer, Phys. Rev., Vol. 110, p. 354 (1958).

<sup>14</sup>H. R. Philipp and H. Ehrenreich, Phys. Rev., Vol. 129, p. 1550 (1963).

<sup>15</sup>D. T. F. Marple and H. Ehrenreich, Phys. Rev. Ltrs., Vol. 8, p. 87 (1962).

<sup>16</sup>D. G. Avery, Proc. Phys. Soc. (London), Vol. B 65, p. 425 (1952).

<sup>17</sup>R. E. Lindquist and A. W. Ewald, J. Opt. Soc. Am., Vol. 53, p. 247 (1963).

<sup>18</sup>R. F. Potter, J. Appl. Opt., Vol. 4, p. 53 (1965).

With this newer technique, a reflectometer was used to measure the optical constants of electropolished germanium samples in the spectral region from 0.5 to 3.0 eV at 300° and 120°K.

#### MEASUREMENT OF $X_n^2$ AND $\rho_n$ AND DETERMINATION OF THE OPTICAL CONSTANTS

The experimental technique, having been fully described,<sup>19</sup> will not be repeated here except to say that the spectral source is a high-intensity Bausch and Lomb monochromator with a tungsten lamp. Suitable Corning glass filters and interference filters are used for separating orders at the longer wavelengths. The polarizer is a Glan-Thompson prism; the detector, a lead sulfide photoconductor. The intrinsic germanium was kindly provided by T. Donovan of the Michelson Laboratory, Naval Ordnance Test Station, China Lake, and had been electropolished by him. The resolving power of the monochromator is between 60 and 200 over the spectral range given here.

The experiment is one of measuring, as functions of the radiation frequency, both the ratio  $\rho_n = R_{\parallel}/R_{\perp}$  at the pseudo-Brewster angle (i.e., that angle for which  $\rho$  is a minimum) and the pseudo-Brewster angle ( $\phi_B$ ) itself. The symbols  $R_{\parallel}$  and  $R_{\perp}$  designate the reflected intensity for the component having the electric vector parallel and perpendicular, respectively, to the plane of incidence; and the pseudo-Brewster angle is expressed in the quantity  $X_n^2 = \sin^2 \phi_B \tan^2 \phi_B$ . Figure 2 shows these two quantities over the spectral range at 300°K, and Figure 3 shows the same quantities at 120°K. The curves for  $\rho_n$  have been corrected by subtracting a quantity  $A(h\nu)^2$  where  $A = 4 \times 10^{-3}(\text{eV})^{-2}$ . This corresponds to an oxide layer, approximately 20 Å thick and having a refractive index of 2.0, on the surface of the sample.

An examination of Figures 2 and 3 demonstrates the power of this type of spectroscopy. One can see certain spectral features present in the raw data prior to any reduction to the optical quantities. The observed quantities have shifted both in temperature and in value. The quantity  $X_n^2$  shows five spectral features in this region, while  $\rho_n$  shows two. Their relationship to the optical constants will be explained.

It was shown by the author<sup>20</sup> that the quantities  $X_n^2$  and  $\rho_n$  (for the present range of values) can be related to each other through the quantities  $\alpha_0^2$ ,  $\beta_0^2$ , with an error of less than one percent, as expressed in equation (1).

---

<sup>19</sup> Ibid.

<sup>20</sup> Ibid.

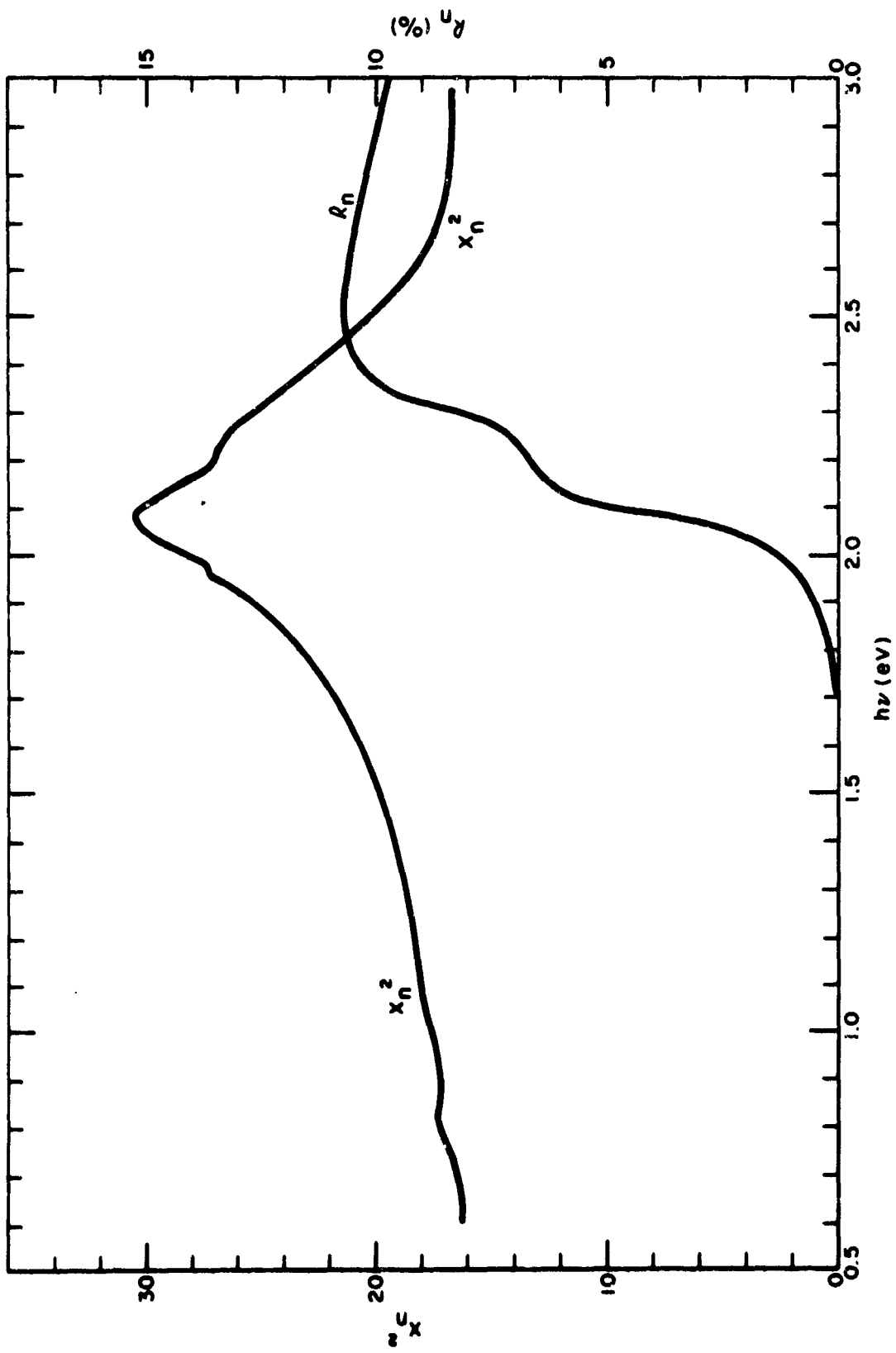


FIGURE 2. The Experimentally Determined Quantities  $X_n^2 = \sin^2 \phi_B \tan^2 \phi_B$  and  $R_n = R_{\parallel}/R_{\perp}$ , for Electropolished Germanium at 300°K

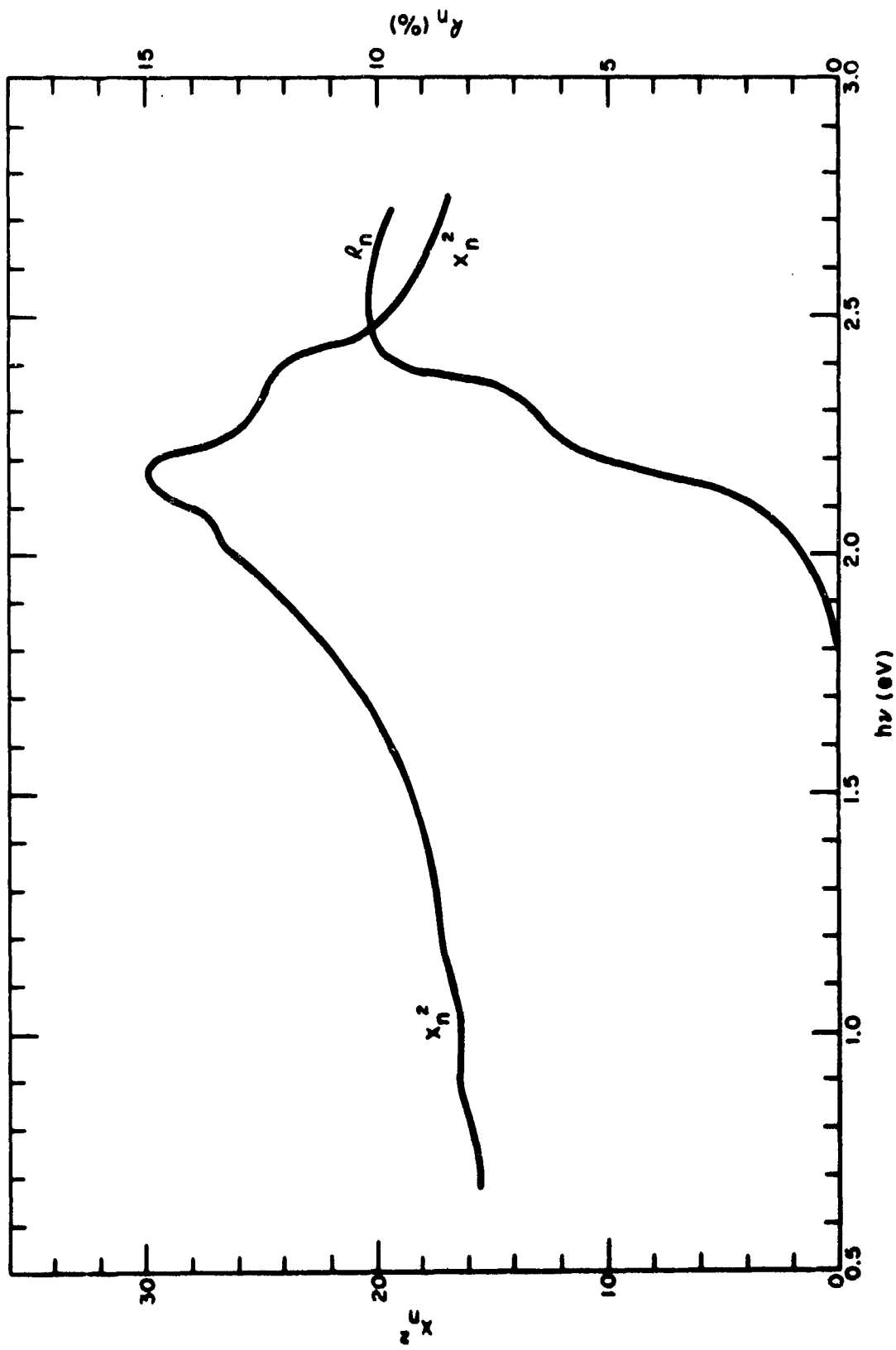


FIGURE 3. The Experimentally Determined Quantities  $X_n^2 = \sin^2 \phi_B \tan^2 \phi_B$  and  $R_n = R_{\parallel}/R_{\perp}$  for Electropolished Germanium at 120°K

$$a_0^2 = \left( \frac{1 - R_n}{1 + R_n} \right)^2 X_n^2 \quad \beta_0^2 = \frac{4R_n}{(1 + R_n)^2} X_n^2 \quad (1)$$

The quantities  $a_0^2$  and  $\beta_0^2$  are related to the dielectric constants  $\epsilon = \epsilon_1 + i\epsilon_2 = n^2 = (n^2 - k^2) + i2nk$ , according to equation (2).

$$a_0^2 - \beta_0^2 + \sin^2 \phi_B = \epsilon_1 = n^2 - k^2 \quad (2)$$

$$a_0^2 \beta_0^2 = \frac{\epsilon_2^2}{4} = n^2 k^2$$

The information in Figures 2 and 3 is sufficient to provide the direct determination of the optical constants in the given spectral region.

The quantities  $\epsilon_1$  and  $\epsilon_2$  for the same two temperatures are shown in Figures 4 and 5. One sees the marked degree of correspondence between  $X_n^2$  and the quantity  $\epsilon_1$ ;  $R_n$  and  $\epsilon_2$  are not so close in their correspondence, although similarities do exist. The quantity  $\epsilon_1$  shows small but quite definite spectral features in the vicinity of 0.80 and 1.10 eV at 300°K, and near 0.90 and 1.20 eV at 120°K. The basis for this structure is given in Figure 6, which shows the experimental determination of the quantity  $X_n^2$  in the energy region between 0.7 and 1.30 eV. The accuracy shown corresponds to a precision of measurement of the pseudo-Brewster angle  $\phi_B$  of approximately 5 minutes of arc or less. The features at 0.80 and 0.90 eV, as well as those at 1.10 and 1.20 eV, are quite real and give rise to those respective features in  $\epsilon_1$ . In Figure 7, the feature at 1.97 eV at 300°K and near 2.03 eV at 120°K has not been reported by other investigators. The two prominent features in  $\epsilon_2$  data  $2.1 < h\nu < 2.3$  eV correspond to the  $\Lambda$  doublet, which is a prominent feature observed in normal reflectance.<sup>21,22</sup>

## DISCUSSION

Figures 4 and 5 exhibit five spectral features, four of which have been reported by other investigators. In no single experiment have all five spectral features been observed. They are all attributed to various inter-band transitions between the valence band and the conduction band structure of the germanium crystal. The 0.80 eV transition is the well-known direct gap at the  $\Gamma$  point corresponding to the  $\Gamma_{25,3/2} - \Gamma_2$  transition,

<sup>21</sup>J. Tauc, op. cit.

<sup>22</sup>M. Cardona, op. cit.

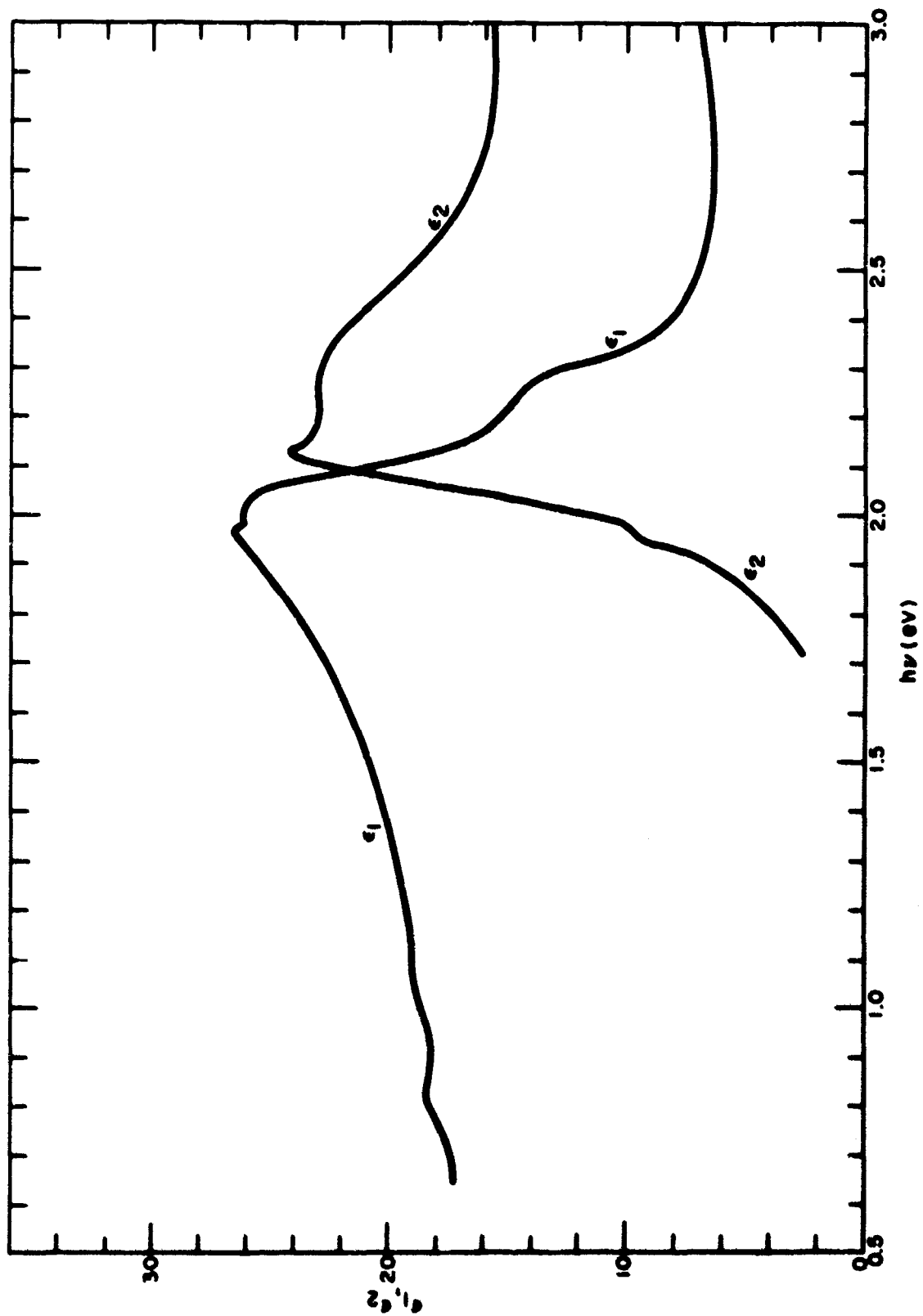


FIGURE 4. The Optical Constants for Electropolished Germanium at 300°K, Based on Data of Figure 2

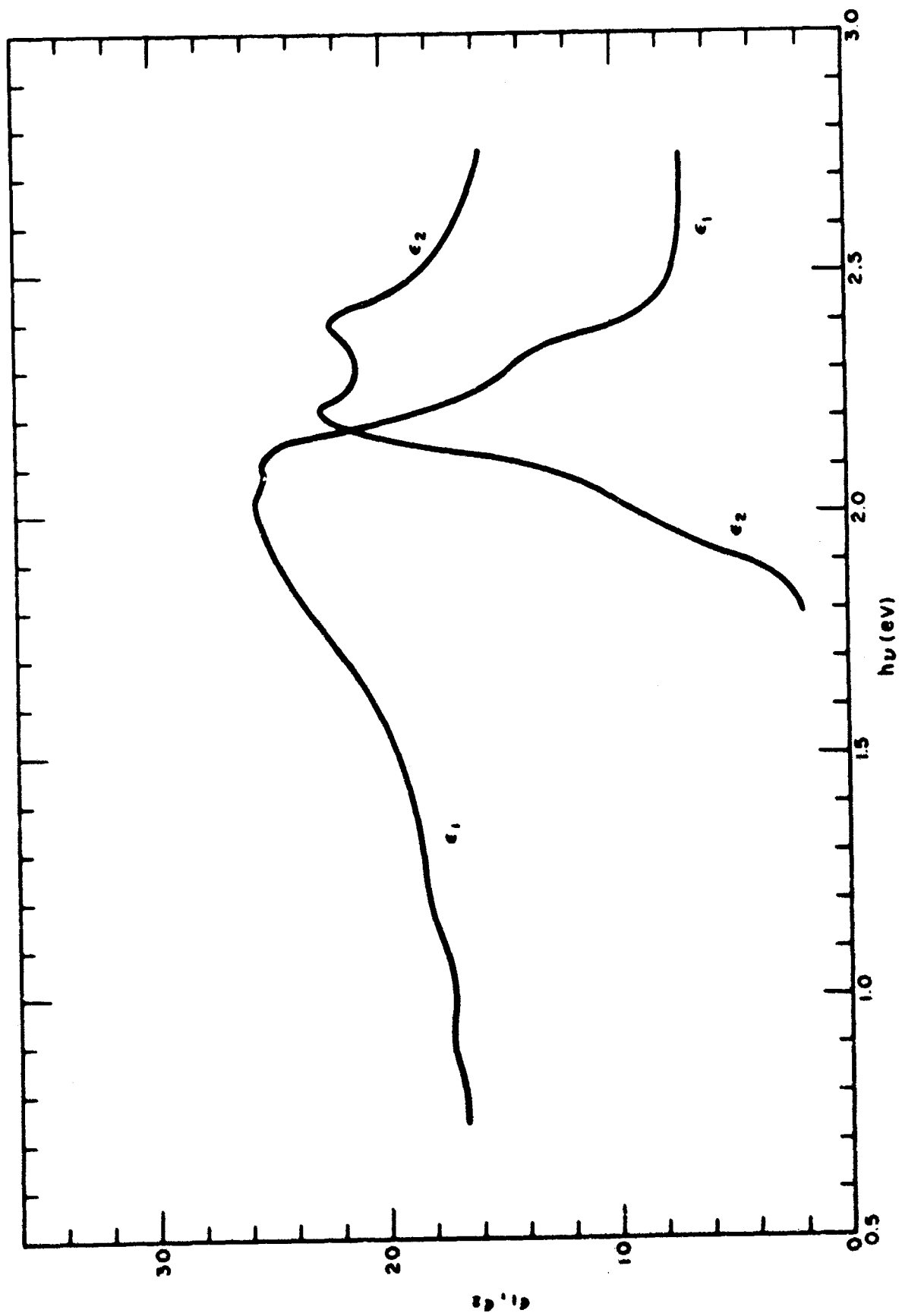
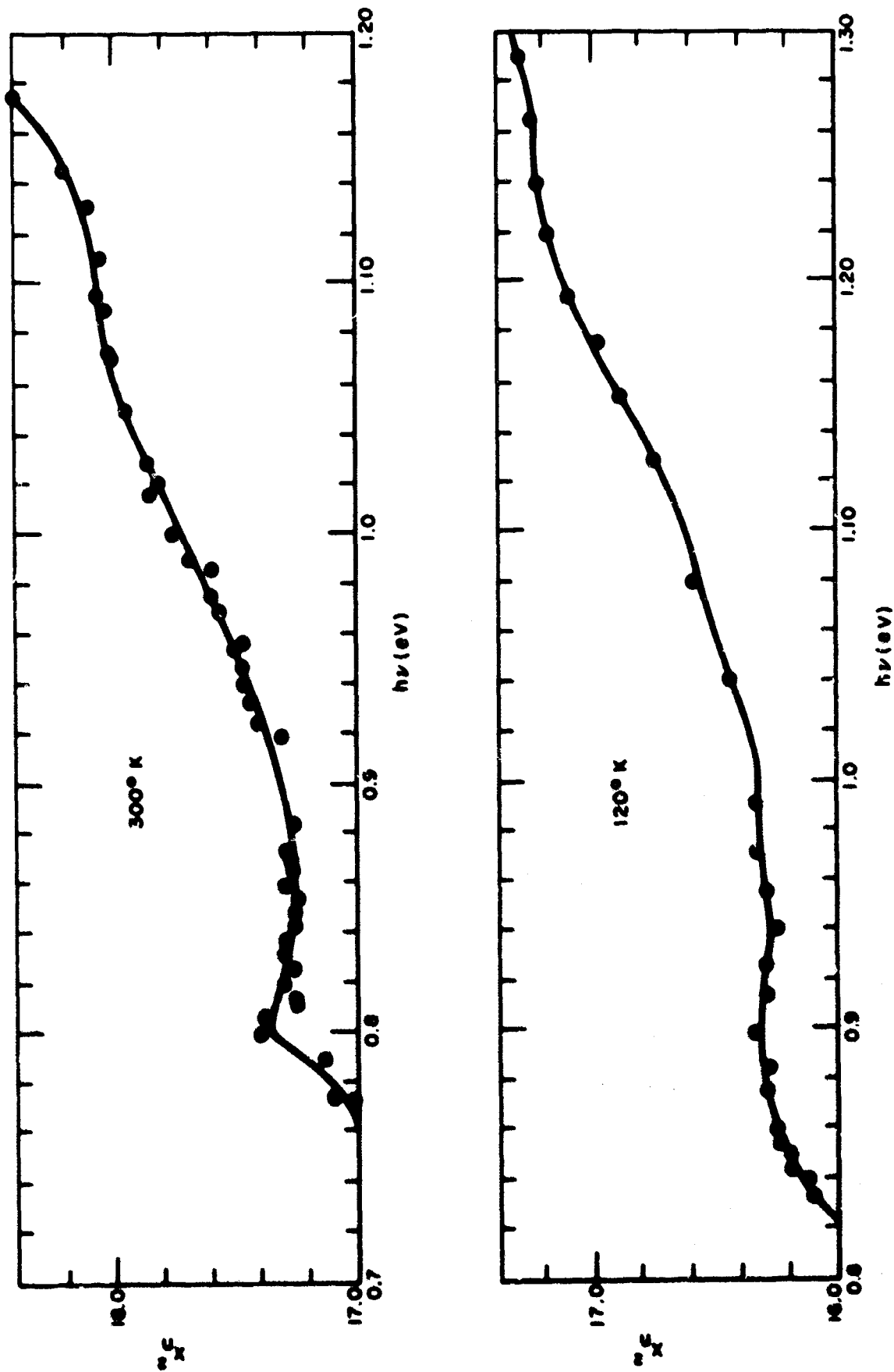


FIGURE 5. The Optical Constants for Electroplished Germanium at 120°K.  
Based on Data of Figure 3



**FIGURE 6.** Details of the Experimentally Determined Quantity  $X_n^2$  in the Spectral Region 0.70-1.30 eV. Each feature is preceded by a positive slope.

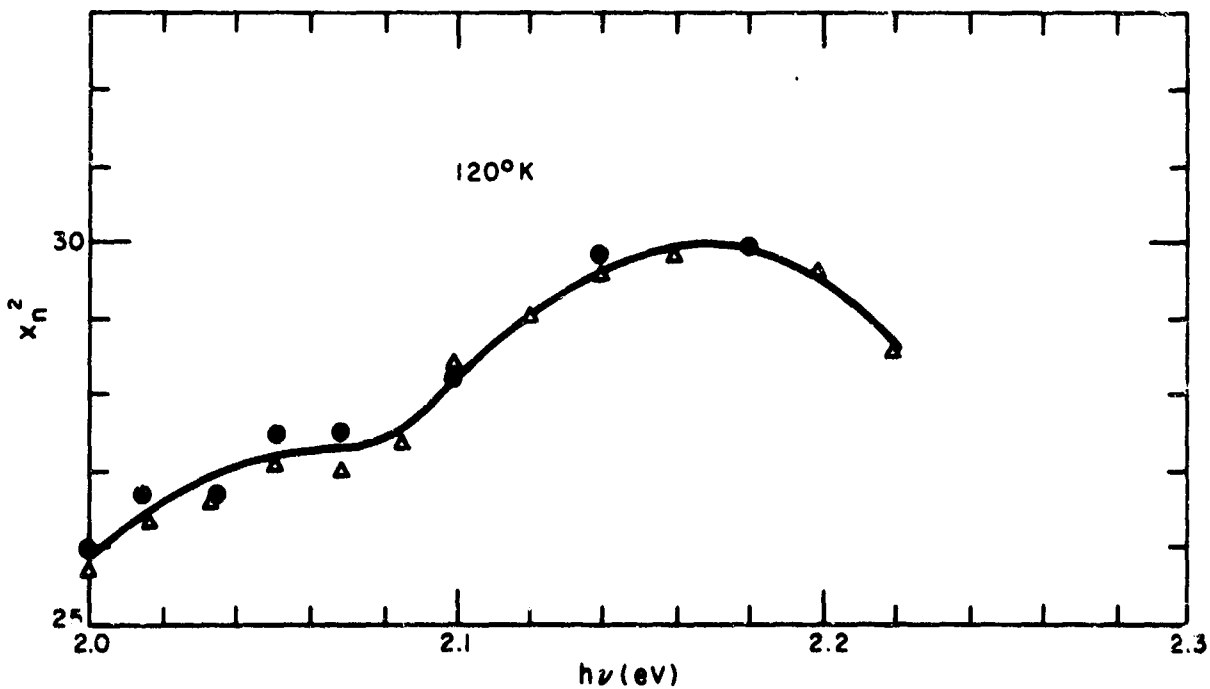
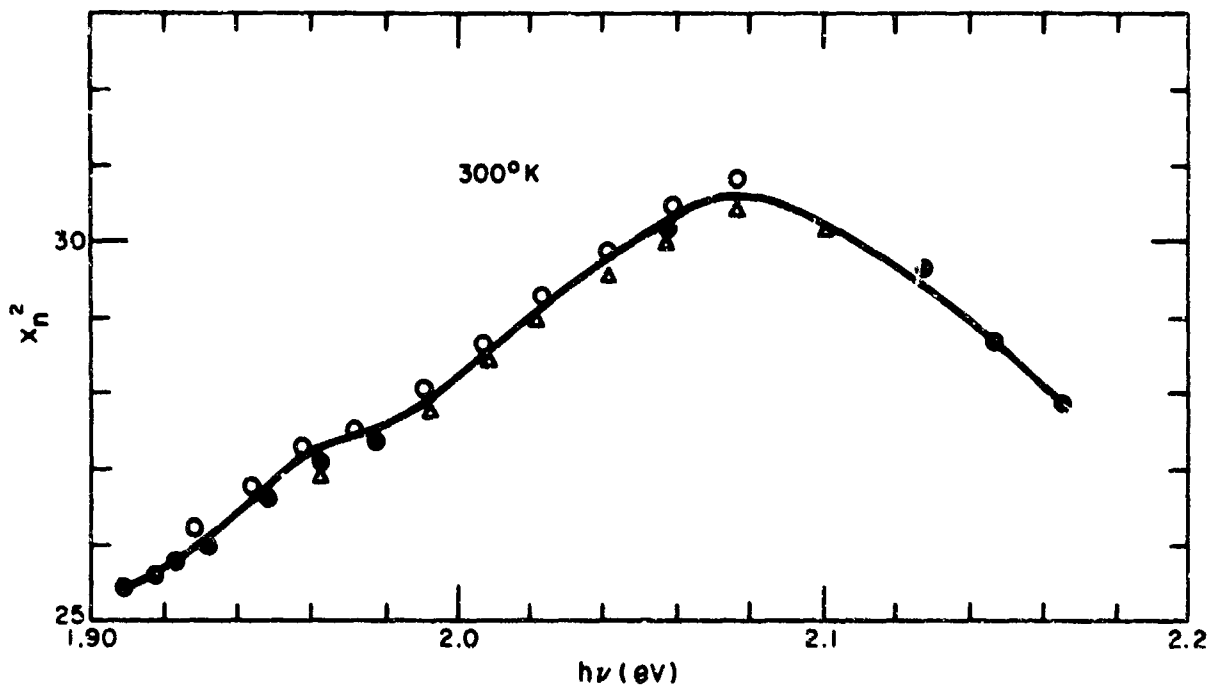


FIGURE 7. Detailed Plots of the Experimental Quantity  $X_n^2$  in the Vicinity of 2.0 eV. The symbols correspond to separate determinations and indicate the precision.

which has been observed in transmission measurements.<sup>23</sup> At 120°K the peak is approximately 0.38 eV, a shift of 0.08 eV. The next higher energy transition, appearing at approximately 1.095 eV at 300°K and at 1.22 eV at 120°K, is attributed to the transitions from the spin-orbit split band  $\Gamma_{25, \frac{1}{2}} - \Gamma_2$  transition, which has been observed by Hobden.<sup>24</sup> It would appear from Figure 6 that the direct edge has a smaller temperature coefficient than the split-off valence band transition.

The two principal features in  $\epsilon_2$  at 300°K, at approximately 2.1 and 2.3 eV (Figure 4), sharpen considerably at 120°K and shift to 2.2 and 2.4 eV (Figure 5). These two features have been observed in all normal reflectance measurements since they were first seen by Tauc. Initially they were attributed to direct transitions from the L point at the edge of the Brillouin zone, with the valence band splitting corresponding to a value between 0.18 and 0.20 eV. Detailed band calculation by Brust, Phillips, and Bassani<sup>25</sup> and by Brust<sup>26</sup> indicated that the joint density of states for transitions of this energy occur at the  $\Lambda$  direction, which is in the  $\langle 111 \rangle$  direction but not at the edge of the zone. Valence band splitting would still be of the order of 0.20 eV. Phillips,<sup>27</sup> in his analysis, indicates that this transition (to be classed  $M_1$ ) is associated with a saddle point giving a cusp in the joint density of states at the transition frequency.

All the transitions except the  $M_0$  transitions at the L point have been observed in other experiments, in particular in the Franz-Keldysh-Seraphin effect by Seraphin and coworkers.<sup>28</sup> The SKS effect—the application of an electric field and the observation of the induced changes in the band structure by reflectance techniques—was used in an effort to find  $M_0$  in a search from 1.8 to 2.0 eV. It is suggested that the effect of the  $\Lambda - M_1$  transition at 2.1 eV is so strong that the SKS observation of the  $M_0$  transition at 1.97 eV is obscured. The extreme precision of measuring  $X_n^2$ , it is believed, permits one to observe the spectral feature at 1.97 eV at 300°K and at 2.03 eV at 120°K (Figures 7 and 8).

---

<sup>23</sup>W. C. Dash and R. Newman, Phys. Rev., Vol. 99, p. 1151 (1955).

<sup>24</sup>M. V. Hobden, J. Phys. Chem. Solids, Vol. 23, p. 821 (1962).

<sup>25</sup>D. Brust, J. C. Phillips, and F. Bassani, Phys. Rev. Ltrs., Vol. 9, p. 94 (1962).

<sup>26</sup>D. Brust, Phys. Rev., Vol. 134, p. A 1337 (1964).

<sup>27</sup>J. C. Phillips, Phys. Rev., Vol. 133, p. A 452 (1964).

<sup>28</sup>B. O. Seraphin and R. B. Hess, Phys. Rev. Ltrs., Vol. 14, p. 138 (1965).

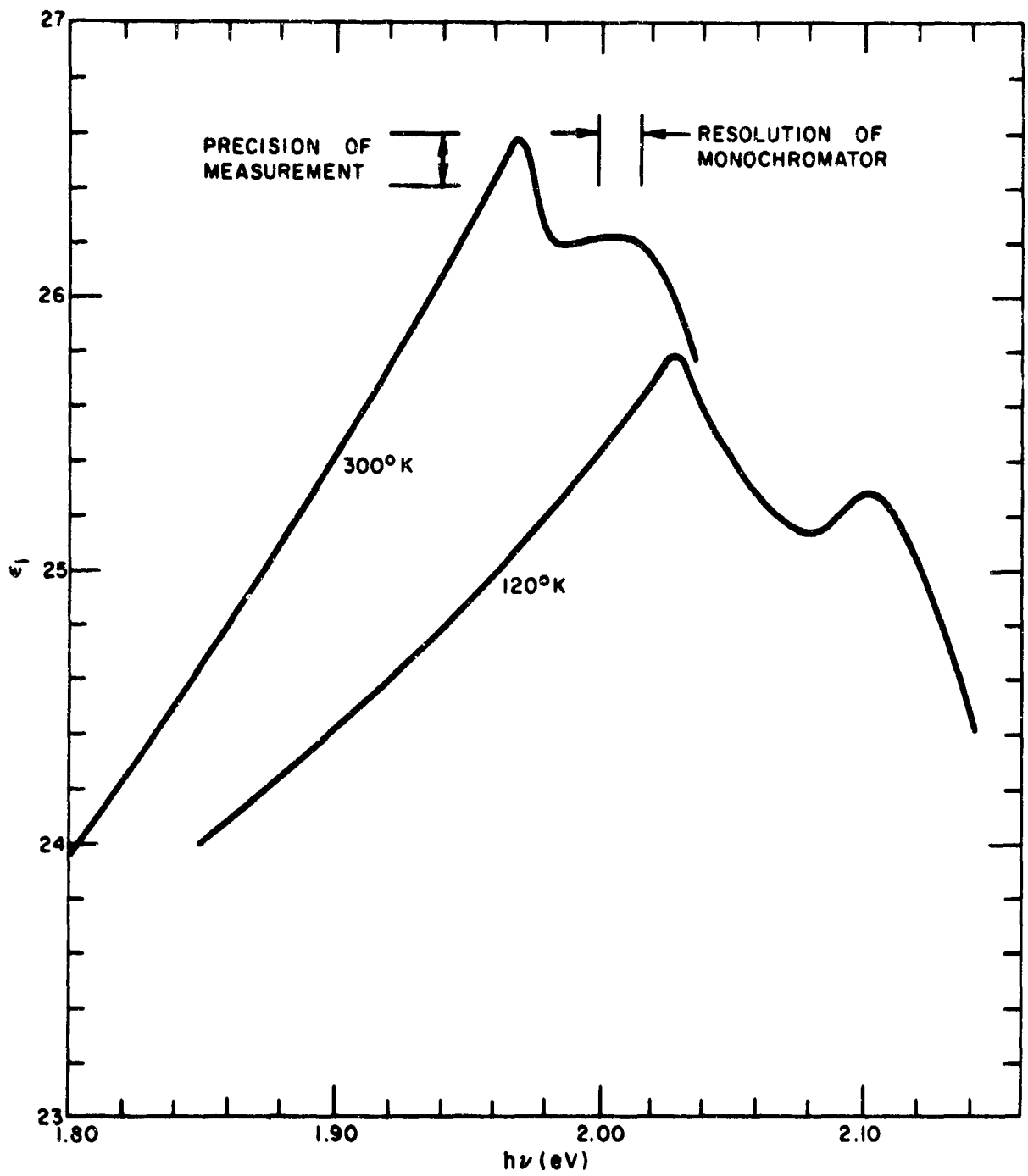


FIGURE 8. Real Part of the Dielectric Constant, Based on Data Shown in Figures 2, 3, and 7 in the Spectral Region 1.80-2.10 eV

The interband transitions occur at critical points in the Brillouin zone. These critical points (Van Hove singularities<sup>29</sup>) occur when the relation  $\sum_{ll'} \nabla_{\mathbf{k}}(E_{\mathbf{k}l} - E_{\mathbf{k}l'}) = 0$  is satisfied, as distinct changes in the joint density of states ( $J_{MS}$ ) occur at these points. Transitions where  $\nabla_{\mathbf{k}}E_{\mathbf{k}l} = \nabla_{\mathbf{k}}E_{\mathbf{k}l'} = 0$  and the difference  $E_{\mathbf{k}l} - E_{\mathbf{k}l'}$  is a minimum, are known as  $M_0$ -type. Such conditions occur for Ge at the center of the zone ( $\Gamma$  point) and at the  $\langle 111 \rangle$  edge (L point). A very large joint density of states maximum occurs between the valence and conduction bands of Ge in the  $\langle 111 \rangle$  direction ( $\Lambda$ ). The energy band difference is characterized as a saddle function of the type  $M_1$  (see D. Brust, footnote 26). The joint density of states has a maximum for the frequency  $E_{\mathbf{k}l} - E_{\mathbf{k}l'}$  at the saddle point.

Because the imaginary part of the dielectric constant is proportional to the joint density of states for a transition ( $\epsilon_2 \propto J_{MS}$ ), it is a very important band structure parameter. Brust has carried out a density of states determination for different types of Van Hove critical points.

In Figure 9 are illustrated the joint densities of states for two of the transition types. Figure 9a represents the case for minimum extrema in energy gap, i.e., at L or  $\Gamma$  points ( $M_0$ ), while Figure 9b represents the case for a saddle point ( $M_1$ ). The contributions  $\delta$  to the real and imaginary parts of the dielectric constant can be shown to be as follows:<sup>30</sup>

$$\delta\epsilon_1(\omega) = \frac{1}{\pi} \int_{\omega_c - \Delta}^{\omega_c + \Delta} \epsilon_2'(\omega') \ln |\omega'^2 - \omega^2| d\omega' \quad (3a)$$

$$\delta\epsilon_2(\omega) = -\frac{1}{\pi} \int_{\omega_c - \Delta}^{\omega_c + \Delta} \epsilon_1'(\omega') \ln \left| \frac{\omega' + \omega}{\omega' - \omega} \right| d\omega' \quad (3b)$$

where  $\omega_c$  corresponds to the transition frequency, and  $\omega_c + \Delta$  and  $\omega_c - \Delta$  give the frequency bounds outside of which the contributions  $\delta\epsilon_1$  and  $\delta\epsilon_2$  are negligible. Because the logarithms in the integrands are large at  $\omega \rightarrow \omega'$ , one expects principal changes in  $\epsilon_1(\omega)$  and  $\epsilon_2(\omega)$  when  $\epsilon_2'(\omega)$  and  $\epsilon_1'(\omega)$ , respectively, have large and abrupt changes.

From Figure 9c it is seen that  $\epsilon_2'(\omega)(M_0)$  has a discontinuity at  $\omega_c$ . Equation (3a) indicates that in this case  $\delta\epsilon_1(\omega)$  goes from a positive value at  $\omega < \omega_c$  to a maximum at  $\omega \gtrsim \omega_c$ . Figure 9d shows that  $\epsilon_2'(\omega)(M_1)$  also has a discontinuity at  $\omega_c$  but it goes from a positive value at  $\omega < \omega_c$  to a

<sup>29</sup> L. Van Hove, Phys. Rev., Vol. 89, p. 1189 (1953).

<sup>30</sup> F. Stern, op. cit., p. 332.

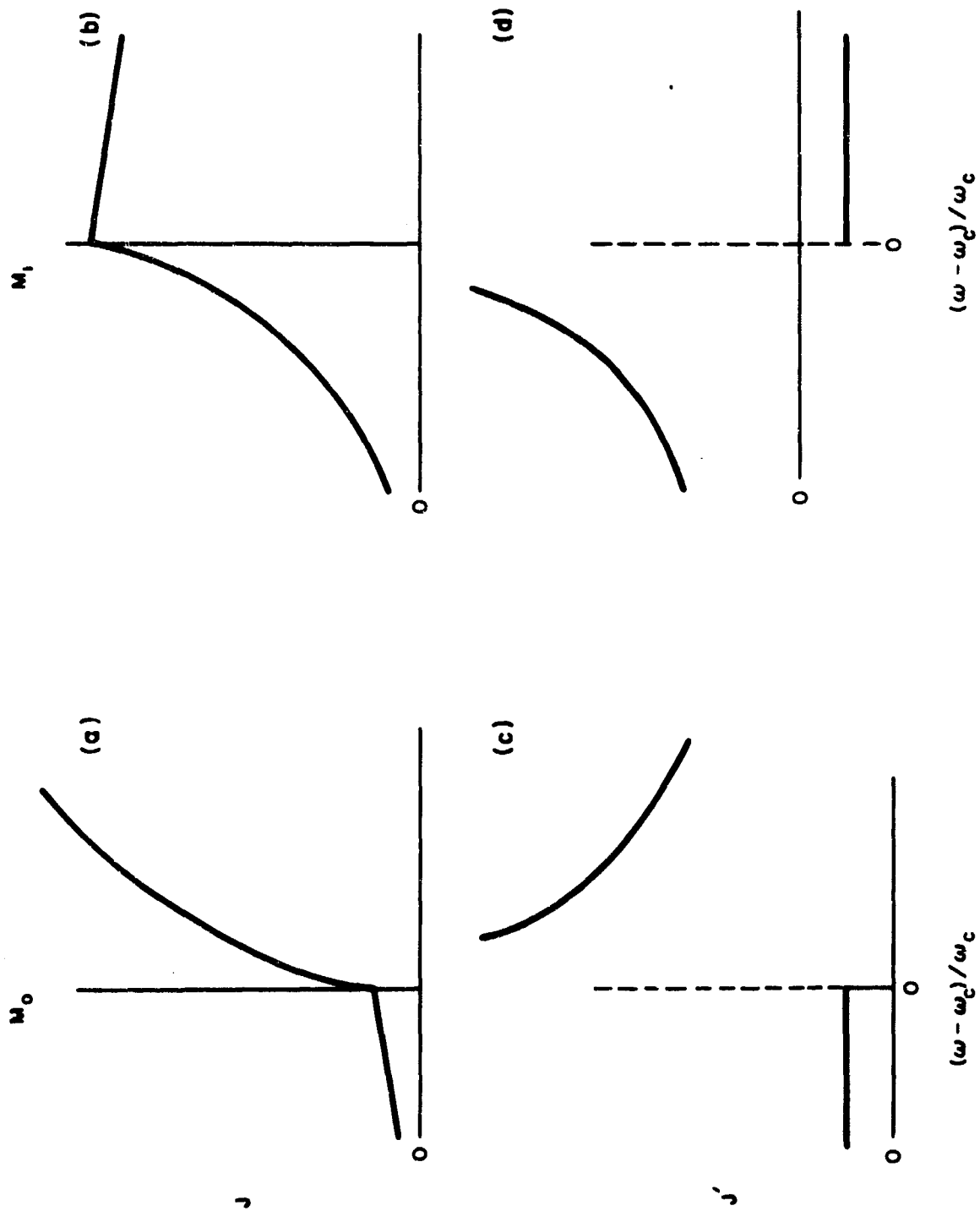


FIGURE 9. Schematic Representation of the Joint Densities of States and Their Derivatives for Two Types of Van Hove Critical Points. (a)  $J_{M_0}$ , (b)  $J_{M_1}$ , (c)  $dJ_{M_0}/d\omega$ , (d)  $dJ_{M_1}/d\omega$ .

negative constant at  $\omega > \omega_c$ . Equation (3a) indicates that, for negative  $\epsilon_2'$ ,  $\delta\epsilon_1(\omega)$  has a negative slope between a maximum value of  $\delta\epsilon_1$  at  $\omega \lesssim \omega_c$  and a minimum value at  $\omega \gtrsim \omega_c$ . Equation (3b) provides the corollary that a large negative slope in  $\epsilon_1$  corresponds to a positive extremum in  $\delta\epsilon_2$ . A positive slope in  $\delta\epsilon_1$  indicates that a sharp kink, if not a minimum, occurs in  $\delta\epsilon_2$  for the general case  $M_0$  (Figure 9a).

Although the slope for the 1.97 eV peak (300°K) in  $\epsilon_1$  is not clearly determined, it appears to be due to a weak transition, presumably at the L point; hence the maximum in  $\epsilon_1$  very nearly gives the  $L_3-L_1$  transition. The detailed data for this spectral region near 2.0 eV are shown in Figures 7 and 8. On the other hand, peaks at 0.80 and 1.09 eV appear to be preceded by positive slopes (Figure 6), with maxima in  $\delta\epsilon_1$  at energies very nearly equal to those for the assigned transitions. The negative slopes in  $\epsilon_1$  corresponding to peaks in  $\epsilon_2$  at 2.1 and 2.3 eV are strong indications that direct transitions take place at those frequencies of the  $M_1$  types, as indicated by Phillips<sup>31</sup> and Brust.<sup>32</sup> The assignments for the five spectral features are given in Table 1.

TABLE 1. Transition Assignments (eV)

Temperature (°K)	Type $M_0$			Type $M_1$	
	$\Gamma_{25'}^{3/2}-\Gamma_{2'}$	$\Gamma_{25'}^{1/2}-\Gamma_{2'}$	$L_{3'}-L_1$	$\Lambda_3^{3/2}-\Lambda_1$	$\Lambda_3^{1/2}-\Lambda_1$
300	0.80	1.09	1.97	2.11	2.29
120	0.88	1.24	2.03	2.22	2.41

It is of interest to compare the optical constants determined here with some very precise measurements of electropolished germanium reflectance made by Donovan, Ashley, and Bennett.<sup>33</sup> Their measurements were made at room temperature but with a precision of better than one-half of one-tenth of a percent in the spectral region from 1.2 to 4.7 eV. The data were tabulated and the results up to 3 eV are shown as open circles in Figure 10, along with the solid curve showing the calcu-

<sup>31</sup> J. C. Phillips, *op. cit.*

<sup>32</sup> D. Brust, Phys. Rev., Vol. 134, p. A 1337 (1964).

<sup>33</sup> T. M. Donovan, E. J. Ashley, and H. E. Bennett, J. Opt. Soc. Am., Vol. 53, p. 1403 (1963).

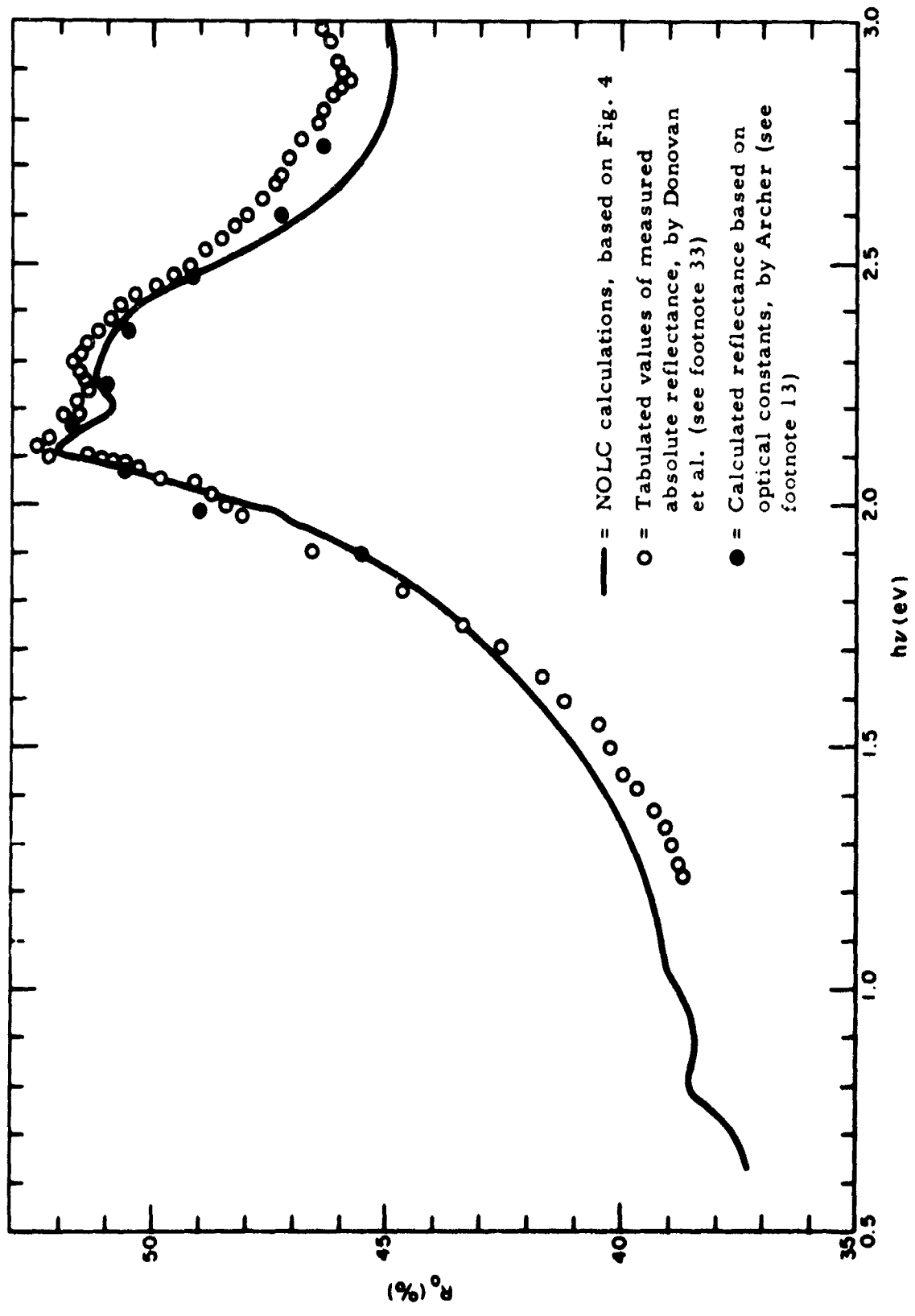


**FIGURE 10. Normal Reflectance for Electropolished Germanium at 300°K as Calculated From the Optical Constants, Shown in Comparison With Precise Reflective Measurements**

lated normal reflectance based on the NOLC data of Figure 4. Some selected points based on Archer's ellipsometric data,<sup>34</sup> which give values of the optical constants somewhat different from the present data, are also shown (closed circles) for comparison. One sees that the agreement is relatively good considering that Donovan et al. reported variations of as much as one-half of a percent between different runs. It is also seen that the use of normal reflectance to discern the  $M_0$  transition at 1.98 eV would be extremely difficult because of the enormously steep rise due to the  $M_1$  transition at 2.1 eV. Normal reflectance measurements of the  $M_0$  transition at 0.8 and 1.1 eV should be possible, given suitable care and precision such as that prescribed by Stern.

No absolute values of normal reflectances at low temperatures seem to be available, although Cardona and Sommers<sup>35</sup> show relative normal reflectance over the spectral region for two temperatures. The appearance of the peaks at 2.2 and 2.4 eV (Figure 11) are in good qualitative agreement with their curve for 90°K. It is evident that the  $M_0$  peak at 2.05 eV would still be relatively hard to see using normal reflectance. As mentioned above, the normal reflectance will usually be representative of either the real or imaginary part of the dielectric constant in most regions. But, as seen here, what goes on in the region between 1.5 and 2.0 eV is rather indeterminant. For that reason the optical constants directly determined with precision are useful quantities.

---

<sup>34</sup>R. J. Archer, op. cit.

<sup>35</sup>M. Cardona and H. S. Sommers, Jr., Phys. Rev., Vol. 122, p. 1382 (1961).

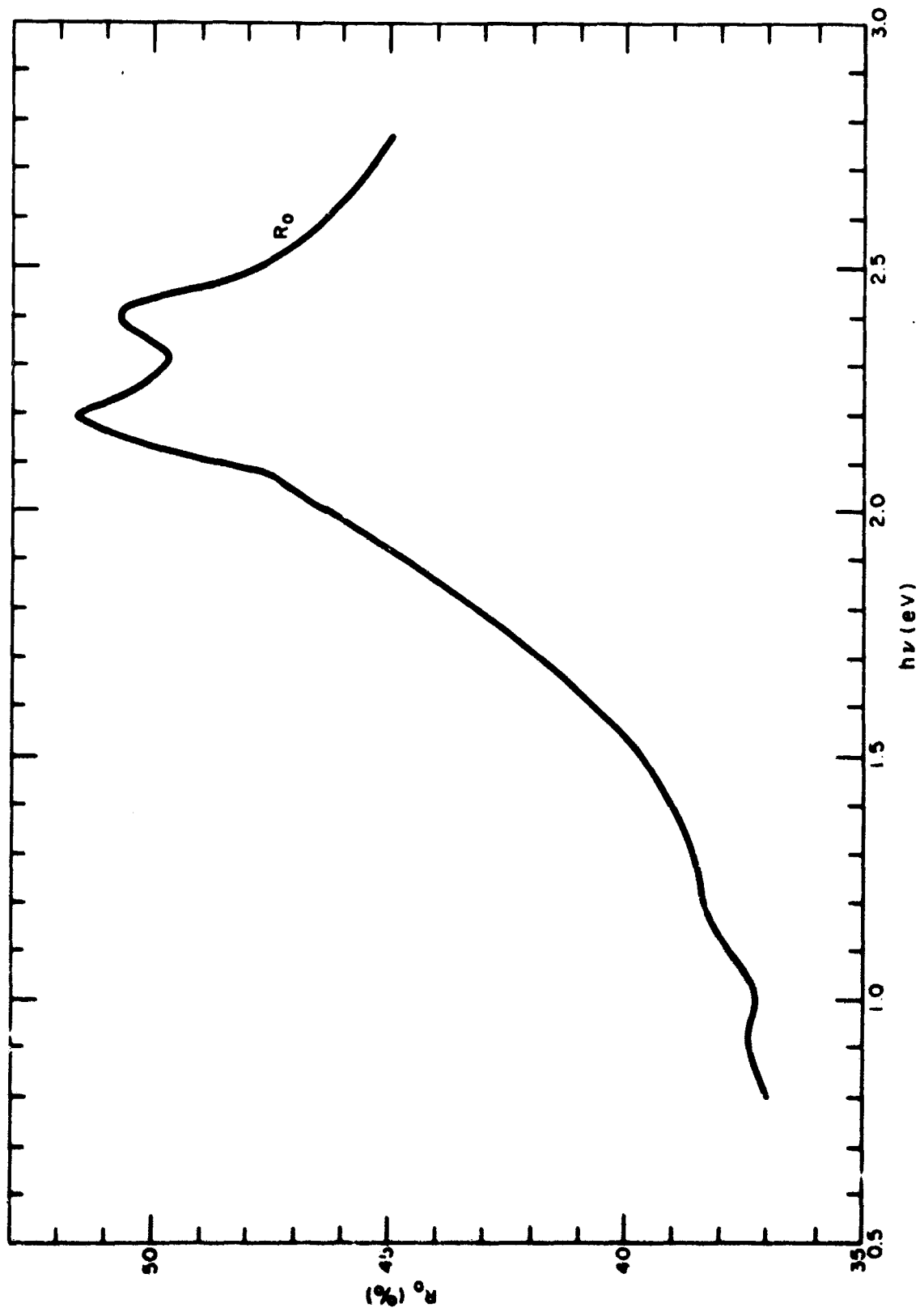


FIGURE 11. Normal Reflectance for Electropolished Germanium at 120°K as Calculated From the Optical Constants of Figure 5

# SOLID STATE SPECTROSCOPY

## CRYSTAL FIELD EFFECTS FOR $Ce^{3+}$ AND $Yb^{3+}$ IN THE GARNETS

by

G. F. Herrmann, J. J. Pearson, and K. A. Wickersheim  
Lockheed Missiles and Space Company  
Palo Alto, California

and

R. A. Buchanan  
Infrared Division, NOLC

The understanding of the anisotropy in the exchange interaction between the rare earth and iron ions in the garnets depends on detailed knowledge of the rare earth wave functions. Complete crystal field calculations have not been possible in the past because the available data did not suffice for a determination of all nine crystal field parameters in addition to the spin-orbit interaction. This lack necessitated the arbitrary suppression of a certain number of these parameters in the attempted calculations. The most systematic approach to date was applied by Hutchings and Wolf<sup>1</sup> (HW) to the spectrum of  $Yb^{3+}$  in a number of garnets. These workers used all nine crystal field parameters, imposing on them a set of constraints in which it was required that ratios among fourth- and among sixth-order parameters conform to those arising from a detailed point charge computation. By adjusting the five remaining parameters, Hutchings and Wolf were successful in obtaining a reasonable fit for the three  $J = 5/2$  levels and for two sets of g-factors.

Since the appearance of the above paper, the authors have obtained additional experimental data. These data include a new level of  $Yb^{3+}$  in yttrium gallium garnet (YGG) at  $\sim 900\text{ cm}^{-1}$ , a complete determination of the 4f energy levels for the electronically analogous ion  $Ce^{3+}$  (also in YGG), and the exchange splittings of certain levels of  $Ce^{3+}$  in YIG.<sup>2</sup> A program has been initiated that is designed to obtain as complete a

---

<sup>1</sup>M. T. Hutchings and W. P. Wolf, J. Chem. Phys., Vol. 41, p. 617 (1964).

<sup>2</sup>K. A. Wickersheim and R. A. Buchanan, Fifth Rare Earth Research Conference, Ames, Iowa, 30 August-1 September 1965. The majority of the data mentioned here were available at the time of the Ames presentation.

set as possible of crystal field and exchange parameters in the garnets and to uncover any systematic patterns in the behavior of the various rare earth ions.

As a first step, the analysis of  $Ce^{3+}$  has been undertaken with a view towards testing the applicability of the HW method, and an appropriate computer program has been formulated. To facilitate level identification it was found convenient to work from the outset with basis functions belonging to the irreducible representations of the octahedral group. In this form the non-cubicity of the calculated wave functions can be determined by inspection. As a check on the program, the spectrum of  $Yb^{3+}$  in YGG was recalculated using the HW parameters, and found to be in agreement with their results. The cubic parentage of the calculated wave functions was found to be clear-cut.<sup>3</sup> The corresponding cubic labeling, as given in Figure 1, follows a sequence  $\Gamma_7, \Gamma_6, \Gamma_8$  for the  $J = 7/2$  levels, rather than  $\Gamma_7, \Gamma_8, \Gamma_6$  as commonly assumed. It is felt that proper identification of the quartet ( $\Gamma_8$ ) parentage is a generally significant consequence of the re-examination of the HW calculation, as well as being of special importance in the analysis of the analogous (but inverted) level scheme for  $Ce^{3+}$ .

Next, a preliminary attempt was made to obtain a fit for the  $Ce^{3+}$  spectrum, utilizing the HW parameters for  $Yb^{3+}$  modified by three adjustable multiplicative factors which are applied, respectively, to the second-, fourth-, and sixth-order potentials. Implicit in this approach is the assumption that the difference in crystal fields in the two ions arises principally from differences in radial wave functions and isotropic shielding factors. The success of the procedure can be gauged from an inspection of Figure 2. The fit, while not perfect, is unmistakable. The parameters used (as defined by HW) are given by

$$\begin{aligned}
 A_2^0 &= -52, & A_2^2 &= 178, & A_4^0 &= -347, & A_4^2 &= 286, \\
 A_4^4 &= 963, & A_6^0 &= 101, & A_6^2 &= -321, & A_6^4 &= 1841, \\
 A_6^6 &= -326, & \text{and } 7/2\lambda &= 2157 \text{ cm}^{-1}
 \end{aligned}$$

The second-order coefficients differ from those of  $Yb^{3+}$  by a factor of  $\sim 0.6$ , the fourth-order by  $\sim 1.8$ , and the sixth-order by  $\sim 1.4$ . The agreement between calculated and observed levels greatly increases confidence

<sup>3</sup>Viewed in the framework of wave function space, the calculated functions deviate 20 degrees or less from the cubic basis functions.

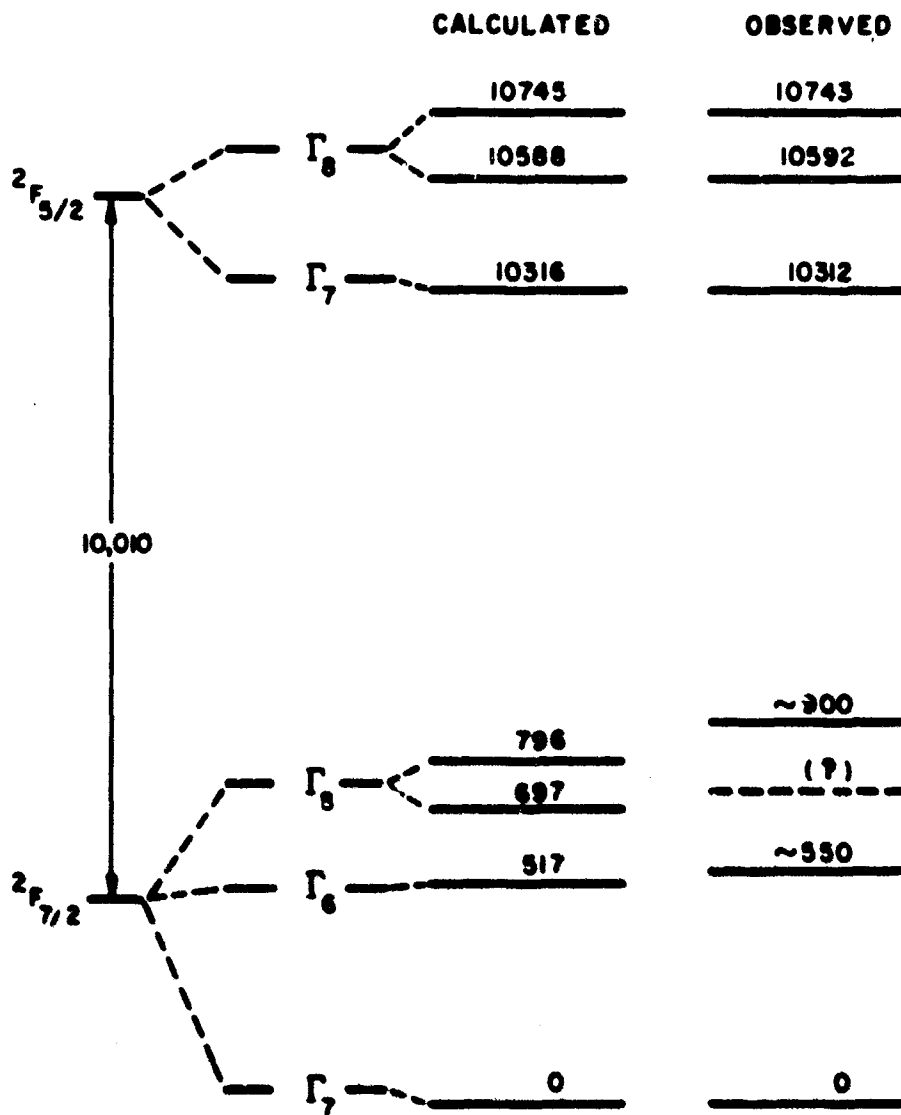


FIGURE 1. A Comparison of Calculated and Observed Levels, in  $\text{cm}^{-1}$ , for  $\text{Yb}^{3+}$  in Yttrium Gallium Garnet. Except for a readjustment of the spin-orbit parameter and the labeling of cubic parentages, the calculated results duplicate those of Hutchings and Wolf. The level near  $900 \text{ cm}^{-1}$  was observed in luminescence.

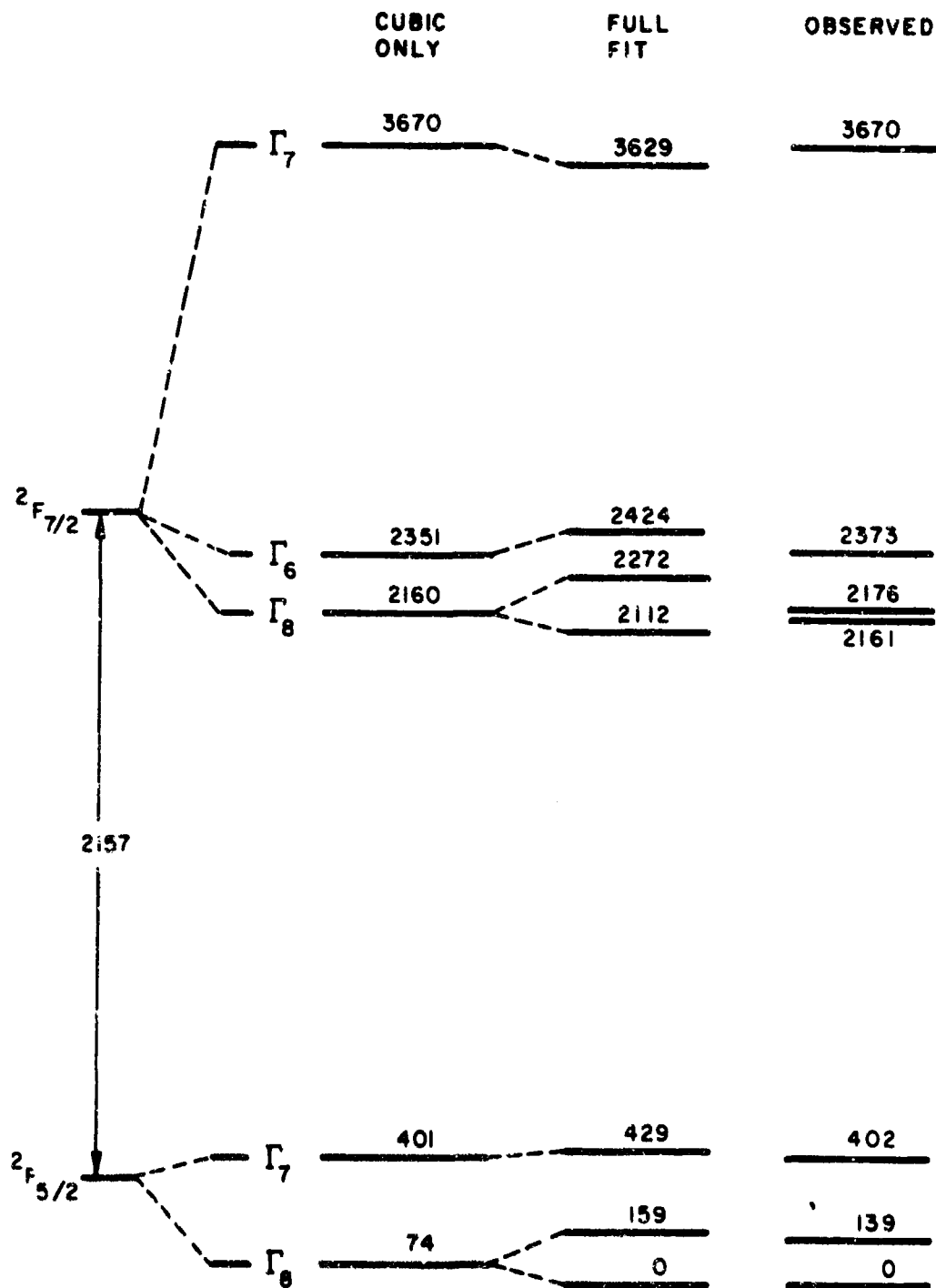


FIGURE 2. A Comparison of Calculated and Observed Energy Levels, in  $\text{cm}^{-1}$ , for  $\text{Ce}^{3+}$  in Yttrium Gallium Garnet. The cubic parameters used in the cubic-only fit are not identical with those used in the full fit. The level near  $402 \text{ cm}^{-1}$  was observed very recently in absorption.

in the present identification of the  $\text{Ce}^{3+}$  levels. It also reinforces belief in the approach used by Hutchings and Wolf, at least as a good first approximation, and at the same time confirms their interpretation of the optical spectrum of  $\text{Yb}^{3+}$  in the garnets.<sup>4</sup>

One should point out, on the other hand, that the energy levels are sensitive primarily to the predominant cubic terms in the potential, and it is therefore difficult to draw precise conclusions concerning the non-cubic terms without some knowledge of the eigenfunctions (e.g., from g-factors). In fact, the rather striking fit that is obtained with a strictly cubic potential to the  $\Gamma_6$ ,  $\Gamma_7$ , and the mean of the  $\Gamma_8$  components (see Figure 2) suggests that the immediate environment of  $\text{Ce}^{3+}$  is more nearly cubic than that of  $\text{Yb}^{3+}$ . This impression is reinforced by the relatively small splitting of the  $\Gamma_8$  quartets, and indirectly by the exchange splitting observed in the upper  $\Gamma_7$  level of  $\text{Ce}^{3+}$ , this splitting being far more isotropic than for the corresponding (ground) state of ytterbium.

Apart from the inversion of the energy level scheme, the most conspicuous differences in the spectra of  $\text{Ce}^{3+}$  and  $\text{Yb}^{3+}$  are caused by the fact that the ratio of crystal field to spin-orbit splitting is much larger in the former ion. In  $\text{Yb}^{3+}$  the 7/2 and 5/2 levels are well separated, and for most purposes can be regarded as uncoupled. This is not the case for  $\text{Ce}^{3+}$  where important contributions are made by matrix elements connecting 7/2 and 5/2 levels. There exists in particular a very large matrix element (predominantly of cubic origin) which connects the two  $\Gamma_7$  levels, causing a further shift (away from each other) of more than  $400 \text{ cm}^{-1}$ . This contributes to the very large separation between the upper  $\Gamma_7$  level and the remaining 7/2 levels as compared with the relatively small spacings between the 5/2 levels.

---

<sup>4</sup>The HW results indicate no electronic levels for  $\text{Yb}^{3+}$  between the ground state and  $517 \text{ cm}^{-1}$ , whereas D. L. Wood (J. Chem. Phys., Vol. 39, p. 1671, 1963) proposes two ytterbium levels in this range, and J. A. Koningstein proposes one (Solid-State Maser Research Report [Optical], Sixth Quarterly Report, dated 14 February 1965, U. S. Army Electronic Command Contract Number DA-36-039-AMC-02333E).

DOCUMENT CONTROL DATA - R&D		
<small>(Security classification of title, body of abstract and indexing annotation must be entered when the overall report is classified)</small>		
1 ORIGINATING ACTIVITY (Corporate author)		2a. REPORT SECURITY CLASSIFICATION
Naval Ordnance Laboratory Corona		UNCLASSIFIED
		2b. GROUP
3 REPORT TITLE		
QUARTERLY REPORT, FOUNDATIONAL RESEARCH PROJECTS, JULY-SEPTEMBER 1965		
4 DESCRIPTIVE NOTES (Type of report and inclusive dates)		
Progress		
5 AUTHOR(S) (Last name, first name, initial)		
6 REPORT DATE	7a. TOTAL NO. OF PAGES	7b. NO. OF REFS
15 December 1965	96	
8a. CONTRACT OR GRANT NO.	8c. ORIGINATOR'S REPORT NUMBER(S)	
b. PROJECT NO. WEPTASKS: R360-FR-104/211-1/R011-01-01 and c. RRMA-03-016/211-1/R007-03-01 d.	NAVWEPS Report 8833	
	8b. OTHER REPORT NO(S) (Any other numbers that may be assigned this report)	
10 AVAILABILITY/LIMITATION NOTICES		
Distribution of this document is unlimited.		
11. SUPPLEMENTARY NOTES	12. SPONSORING MILITARY ACTIVITY	
	Bureau of Naval Weapons (Navy Department)	
13. ABSTRACT		
<p>The following papers are presented on work performed under the Foundational Research Program: Condensation Reactions of Hexaphenyldichlorophosphonitrile Tetramer With Diols and Diamines; A Study of the Thermal Decomposition of Trans-2,6-Diazidohexaphenylcyclophosphonitrile Tetramer and Further Studies on the Solvent Polymerization of the Tetramer With Bisphosphines; The First Spectrum of Mercury in the 3.2- to 4.0-Micron Region; Note on Cesium I; Production of High Power Pulses by Magnetic Field Compression; Accurate Measurement of Small Rotary Dispersion; Ellipticity in Multiply Reflected Faraday Rotation; Optical Constants of Germanium in Spectral Regions From 0.5 to 3.0 eV; and Crystal Field Effects for Ce<sup>3+</sup> and Yb<sup>3+</sup> in the Garnets.</p>		